The Synergistic Influence of Chemical Composition and Industrial Annealing Processes on Lüders Bands Formation in Interstitial Free High Strength Steels

A Dissertation submitted

in partial fulfillment of the requirements
for the degree of

Master of Engineering

in

Production Engineering

by

Gurpreet Singh

Registration No.: 801585009

Under the Supervision of

Dr. Tarun Nanda
Associate Professor, MED,
Thapar University, Patiala

Dr. B. Ravi Kumar
Senior Principal Scientist, MTE
CSIR-NML, Jamshedpur

MECHANICAL ENGINEERING DEPARTMENT

THAPAR UNIVERSITY, PATIALA

July, 2017

CERTIFICATE

I hereby declare that the thesis entitled "**The synergistic influence of chemical composition and industrial annealing processes on the Lüders bands formation in interstitial free high strength steels**" is an authentic record of my work carried out as requirements for the award of the degree of **Master of Engineering** in **Production Engineering** at **Thapar University, Patiala** under the supervision of **Dr. Tarun Nanda**, Assistant Professor, Mechanical Engineering Department, Thapar university, Patiala and **Dr. B. Ravi Kumar**, Senior Principal Scientist, MTE Division, CSIR-NML, Jamshedpur during July, 2015 to July, 2017. No part of the matter embodied in this report has been submitted to any other university or institute for the award of any degree.

Gurpreet Singh

Date: 17/07/2017 Gurpreet Singh

It is certified that the above statement made by the student is correct to the best of our knowledge and belief.

Dr. Tarun Nanda
Associate Professor
Mechanical Engineering Department
Thapar University, Patiala - 147004

Dr. B. Ravi Kumar
Senior Principal Scientist
MTE Division
CSIR-NML, Jamshedpur - 831007

Dedicated to

MY GRANDPARENTS

LATE SH. SHER SINGH & LATE SMT. BHAJAN KAUR

Acknowledgement

Though this dissertation work belongs to me, but there are many people who effortlessly worked with me to complete this work. Now, I would like to thank all those people who made this possible.

First and foremost, I would like to express my deepest gratitude to my advisors, Dr. Tarun Nanda and Dr. B. Ravi Kumar, for their excellent guidance, motivation, immense knowledge, patience, and providing me with an excellent atmosphere for doing research. I would not have been able to finish my thesis writing without their help. They removed every obstacle which occurred in front of my research work. They shared their knowledge and experiences with me. I am grateful to have such advisors for my dissertation work. I wish to express my deepest gratitude to all members of CSIR-NML, Jamshedpur, who provided me the machines and equipment for testing purposes.

Next, I would like to thank to Mr. Sk. Jabed Miadad who helped in providing necessary literature and material. I would also like to thank Mr. Lalan Patro who helped me a lot in polishing of samples.

I would like to thank my parents, Sh. Kewal Singh and Smt. Karmjit Kaur, who gave me immense love and care. They motivated me to do masters after my graduation. So what I am today is only due to my parents. Further, I would to thank my brother Mr. Gursharn Singh, my sister Ms. Sukhmeet Kaur. They are my life and my love. They have supported me from my childhood.

At last but not the least, I want to thank my friends Mr. Ritiesh Kakas, Mr. Satyam Bhatia, Mr. Sahil Rai, Mr. Papalpreet Singh, Mr. Manpreet Singh, Mr. Nand Patel, Mr. Manish Kunj Panday, Mr. Jagjit Singh, Mr. Harsh Kansal, and Mr. Bhupinder Singh, who created a friendly environment around me and kept me motivated and helped me in my research work also.

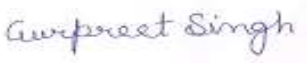

GURPREET SINGH

Abstract

The manufacturing of automobile components such as door inners, floor panels, bonnet linings etc. demand high formability and drawability. A type of low carbon steels called interstitial free steels (IF-steel) provide higher formability and drawability, which makes components manufacturing of these components easy. These steels consist of very low contents of carbon and nitrogen, typically < 0.0030 wt.% C and < 0.0040 wt.% N. In IF-steel, all the interstitial elements i.e. carbon (C) and nitrogen (N) etc. are removed from solid solution by forming precipitates with stabilizing elements viz. titanium (Ti), and niobium (Nb) etc. However, IF-steels have low yield strength. This limitation is removed by addition of solid solution strengtening elements like phosphorous (P), manganese (Mn) etc. to IF-steels. This new type of steel is known as Interstitial free high strength steel (IFHS steel).

The current research is mainly related to the industrial processing of interstitial free high strength steels. Literature reports that IFHS steels generally do not show Lüders bands formation due to absence of interstitial atoms in the solid solution. But, there were inputs from industry providing evidence regarding Lüders bands formation in case of IFHS steels also. This present work mainly investigates with the presence/absence of Lüders bands formation in typically four different types of IFHS steel compositions named as C1 (Ti-stabilized), C2 (Ti-Nb stabilized), C3 (low Ti-low Nb) and C4 (high Ti-low Nb). C4 composition (the high Ti-low Nb) also contained higher aluminium (Al) content than the other compositions. These steel compositions were subjected to the typical industrially followed batch as well as continuous annealing processes. This work presents the effect of chemical composition and annealing processing parameters on the formation of Lüders bands formation in IFHS steels. Lüders bands formation is an undesirable phenomenon, which tends to deteriorate the surface finish of material. Hence, the steel composition which shows Lüders band formation cannot be used for the manufacturing of automobile panels. Hence, the elimination of Lüders bands is a critical issue.

This research relates the formation of Lüders bands with the precipitation behaviour of specific IFHS steel composition subjected to a specific industrial annealing cycle. The results of the present work show that amount of stabilizing elements such as Ti and Nb in the chemical composition imposes restriction on the selection of batch or continuous annealing parameters. This is mainly due to the fact that the precipitation behaviour of these steels change with change in annealing parameters. Thus, inappropriate chemical composition and

annealing process parameters result in incomplete stabilization of carbon element. As a result carbon remains free in the solid solution and subsequently gives rise to Lüders bands formation. Hence, this study could be a very useful guide for the selection of appropriate chemical composition and annealing process parameters for industrial manufacturing of interstitial free high strength steels. C4 composition used in this research is considered as a good chemical composition for batch annealing cycles in the range of 680–730℃ due to absence of Lüders bands formation. Also the best combination of properties (YS= 190 MPa; $\bar{r}$-value= 1.57; Δr-value= 0.25) obtained from this composition after BAF process at 710 ℃ with heating rate of 60 ℃/h and cooling by furnace.

Key words: IF/IFHS steels; Yield point elongation; Lüders bands formation; Lüders strain; Stretcher strains; Formability; Drawability; Lankford parameter; Normal anisotropy; Planar anisotropy; Earing defect; Mechanical properties; Precipitation behaviour.

Contents

List of Figures

List of Tables

List of Acronyms and Symbols

List of Acronyms

ARB	Accumulative Roll-Bonding
BAF	Batch Annealing Furnace
CAL	Continuous Annealing Line
CGL	Continuous Galvanizing Line
CRM	Cold Rolling Mill
CWE	Cold Work Embrittlement
CT	Coiling Temperature
DIFT	Deformation Induced Ferrite Transformation
EDS	Energy Dispersive X-ray Spectroscopy
EBSD	Electron Back Scatter Diffraction
FE-SEM	Field Emission Scanning Electron Microscope
FRT	Finish Rolling Temperature
HSM	Hot Strip Mill
IF	Interstitial Free
IFHS	Interstitial Free High Strength
SANS	Small Angle Neutron Scattering
TEM	Transmission Electron Microscope
UTS	Ultimate Tensile Strength
YS	Yield Strength

List of Symbols

r	Plastic Strain Ratio
r_m	Normal Anisotropy
w_o	Initial Width
t_o	Initial Thickness
w	Final Width
t	Final Thickness
Δr	Planar Anisotropy

Chapter 1

Introduction

1.1 General

Steels have become an integral part of life in industrially developed countries. Low carbon steels, in which carbon content is of the order of 0.13% or less, are the most commonly used steels in the automotive industry. Interstitial free steels are generally known as IF-steels. These steels are included in the category of ultra-low carbon steels. These steels contain very low content of carbon typically in the range of 30–50 ppm [1]. These steels are extensively used to manufacture various components of an automobile body. These steels are highly formable, which is the principal requirement of deep drawing applications. High drawability of IF-steels makes them suitable for manufacturing of complex and intricate shaped components of an automobile. The relationship between strength and ductility for different grades of steel used in the manufacturing of automobile parts is shown in Fig. 1.1 [2]. The main applications of IF-steels in the automotive industry include rear floor pan, the spare wheel well, and the front and the rear inners of door (see Fig. 1.2a–c) [3–5].

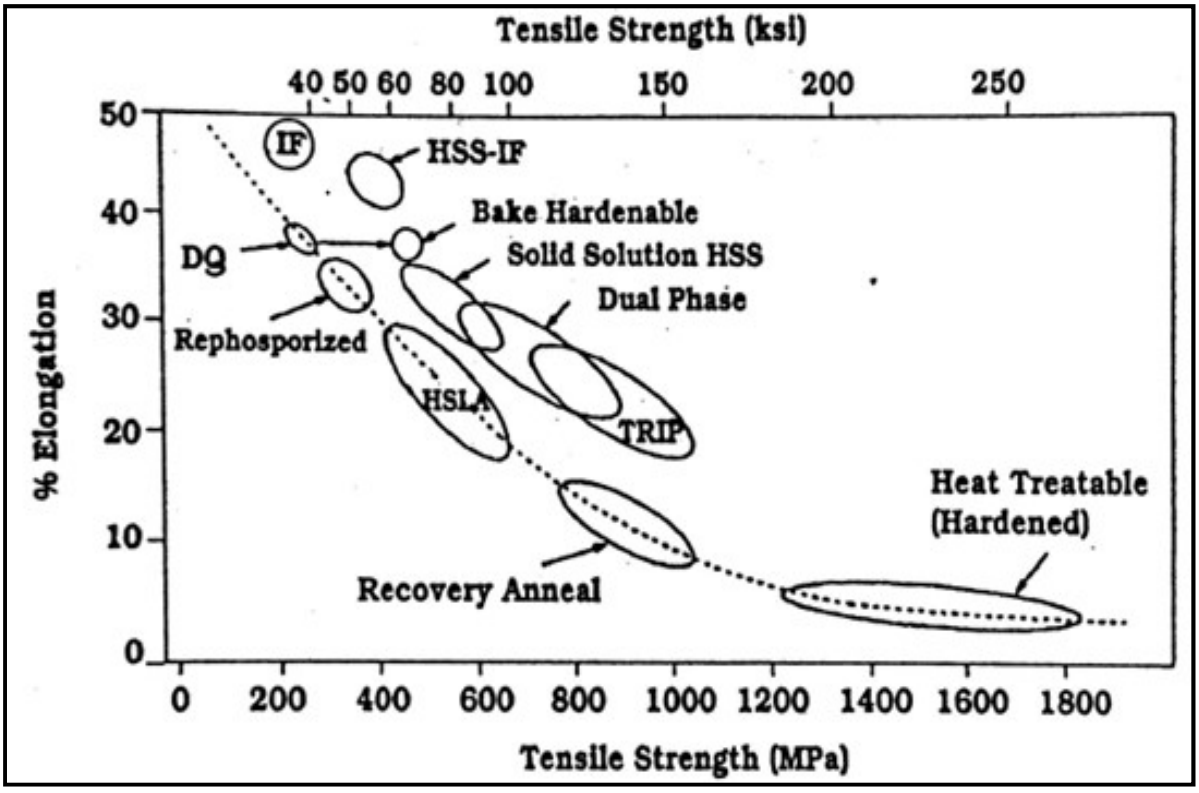

Figure 1.1: Strength-ductility relationship for various grades of steel [2].

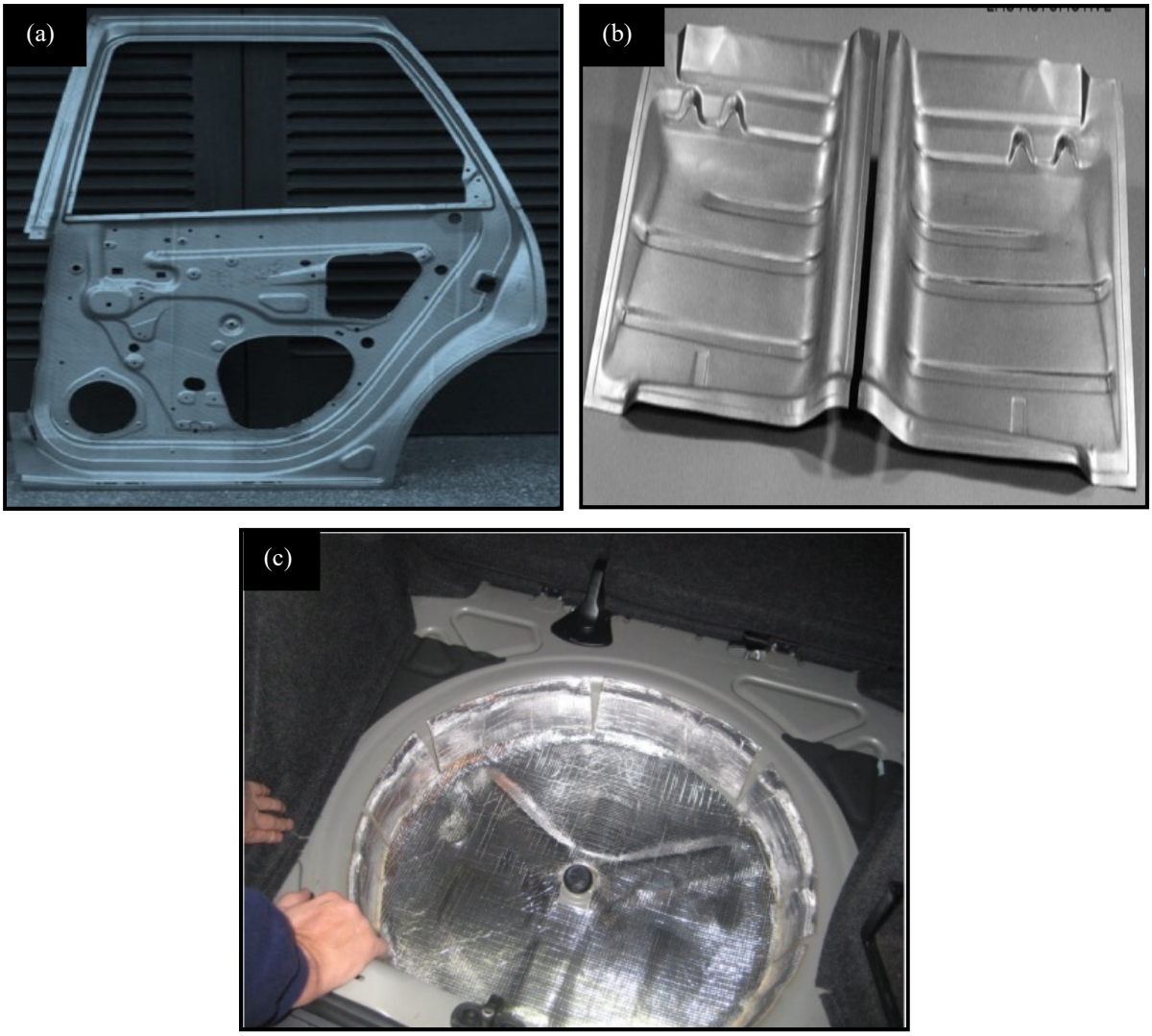

Figure 1.2: Applications of IF-steel in making parts of an automobile (a) door inner [3], (b) rear floor panel [4] , and (c) spare wheel [5] of an automobile made of IF-steel.

1.2 Interstitial free steels (IF-steels)

The term 'Interstitial free' refers to a unique condition in which the iron (Fe) matrix actually becomes free of interstitial solute atoms as shown in Fig. 1.3. Interstitial free steels consist of very low contents of carbon and nitrogen, typically < 0.0030 wt.% C and < 0.0040 wt.% N (all compositions are mentioned as weight percentage). Due to very low contents of C and N, these steels are highly formable but have low yield strength. These steels offers high resistance to thinning due to their high value of plastic anisotropy [2]. In interstitial free steels, titanium (Ti) and niobium (Nb) elements are present, which combine with the interstitial atoms (C and N) present in the steel and forms precipitates (like carbides and nitrides). As all interstitial atoms are stabilized in the interstitial steels, so these steels have no interstitial atom (or having negligible amount) in solid state in free form. Hence these steels get their name as interstitial free steels, as these steels are free from interstitial atoms [6].

These steels are different fron Al-killed steels grades which are also included in the low carbon steels. In the Al killed steel grades, Al usually fixes the N but C remains free in the solid solution. Due to presence of interstitial element C in the solid solution, these steels are prone to strain aging. But, in case of IF-steels, the interstitial elements are stabilized, so these steels are 'non-aging' type of steels [2].

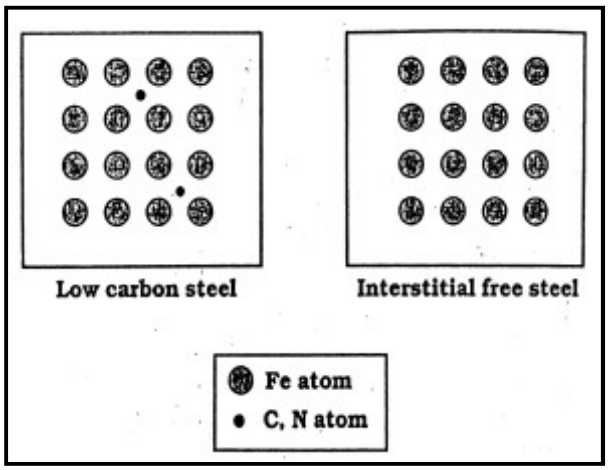

Figure 1.3: Fundamental concept of IF-steel [2].

1.3 Classification of IF-steels

There are three main categories of IF-steels–Ti stabilized IF-steels, Nb stabilized IF-steels and Ti-Nb stabilized IF-steels. In Ti stabilized IF-steels, Ti is the only element used for the stabilization of interstitials atoms in iron matrix. In Nb stabilized IF-steels, the stabilization of interstitial atoms is done by addition of Nb only. In Ti-Nb IF-steels, both Ti and Nb elements are added for the stabilization of interstitial atoms in the iron matrix [2].

1.4 Processing of IF-steels

The following steps are used for processing of IF-steels:

a) Steel making

The first step to make IF-steel is to produce an ultra low carbon steel composition. The hot metal is tapped from blast furnace and is converted into steel in LD converter by using oxygen blown steel making route. The decarburization process helps in removing the carbon in the form of carbon monoxide (CO) gas. The decarburization process is shown in Eq. (1.1) below in which the forward direction means decarburization.

$$C + O \rightarrow CO \text{ gas} \quad \ldots\ldots\ldots\ldots\ldots\ldots\ldots\ldots\ldots\ldots \quad (1.1)$$

This process lowers the content of carbon in steel to 0.02%. The liquid steel is treated further to produce ultra low carbon composition. This can be done through vacuum

degassing technique. The molten steel is then subjected to RH-vacuum degassing treatment. This process is a recirculation type of process, whose schematic diagram is shown in Fig. 1.4. In this process, the steel metal is present in ladle and a vacuum chamber is placed above the steel melt. The vacuum chamber is connected to steel melt through two snorkels. Argon gas is injected through various injection ports present on one of the snorkels. The function of argon gas is to locally reduce its density, due to which the melt rises through the snorkel and finally comes into vacuum chamber. Subsequently, the molten metal re-enters the ladle through another snorkel. In this way, the entire steel melt is subjected to a high level of vacuum through repeated circulation of this process. Decarburization reaction is reactivated again under vacuum during RH degassing. This lowers the content of carbon to 0.002%. Even 0.001% level can also be obtained with the help of suitable process control.

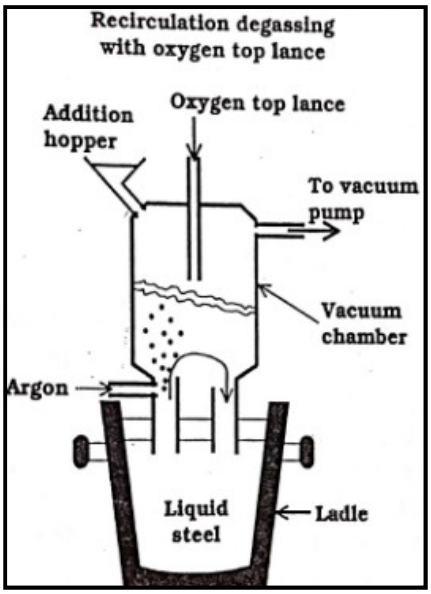

Figure 1.4: RH- vacuum degassing [2].

At the end of decarburization process, aluminium is added in the steel melt. This scavenges the remaining oxygen in the molten metal. This again increases the content of carbon in steel to some extent. Now at this stage Ti and/or Nb is/are added for the stabilization of interstitial elements (C and N). Manganese (Mn) and phosphorous (P) are also added to get high strength IF-steels. Nitrogen is also an interstitial element, and removal of N is also very important. The maximum removal of N takes place during oxygen steel making process. Vacuum degassing is not a effective process for the removal of further N due to already low driving force during vacuum degassing. Also

there is always a possibility of nitrogen pick up at various stages of processing due to contact of liquid steel with air [2].

b) Slab casting

After the steel making process, the liquid steel is passed from ladle to tundish. Tundish acts as a metal distributor to two or more casters. Also, it acts as a cleansing unit for the removal of inclusions. Then the liquid steel is passed to various casters. Fig. 1.5 shows the continuous casting process of IF-steel. After continuous casting, the solidified metal is cut in the form of slabs [7].

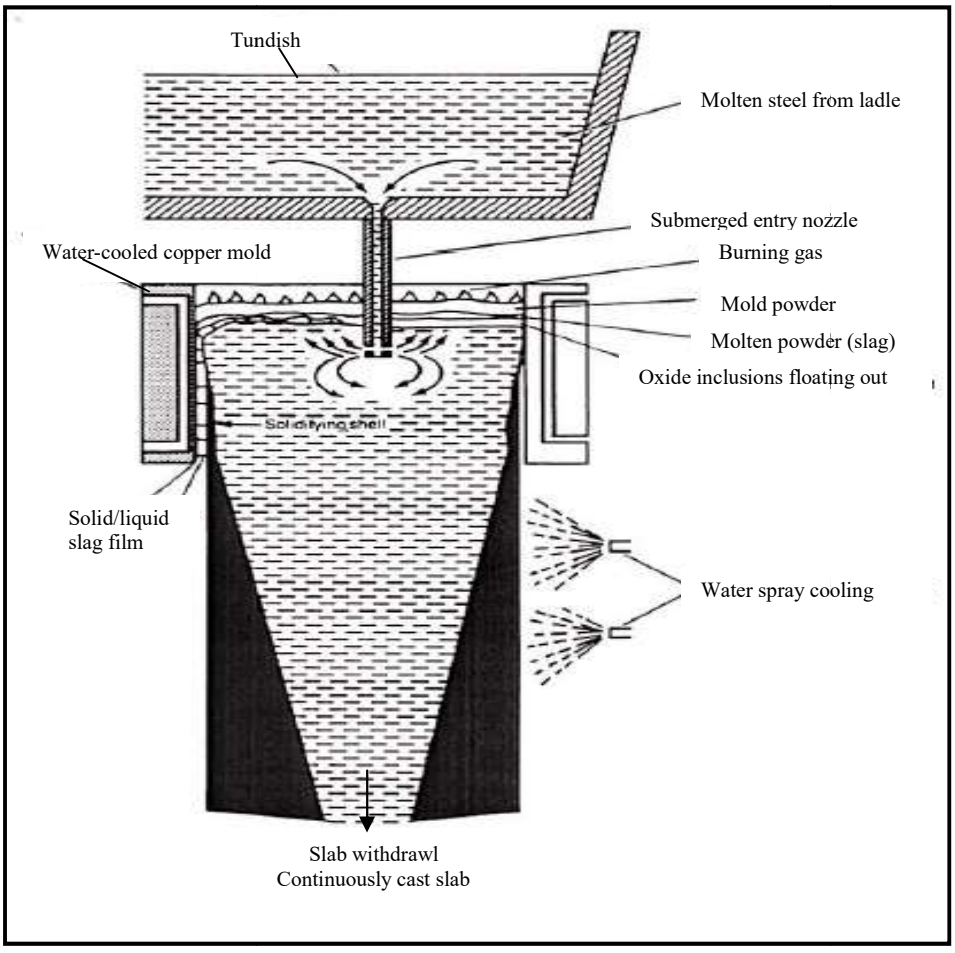

Figure 1.5: Continuous casting of IF-steel [7].

c) Hot rolling

After the slab casting process, the casted slab undergoes hot rolling process. The hot rolling process includes slab reheating, roughing, finish rolling, and coiling. During the hot rolling process, the dynamic recystallization occurs and the thickness of slab is reduced.

d) Cold rolling

There are two main purposes of cold rolling- one is to produce the required gauge for the customer and the other is to produce high energy deformed structure, so that recrystallized grains with preferred textures will be produced during annealing. Fig. 1.6 shows the difference in effect of hot and cold rolling on the grains [2].

e) Annealing

Annealing means heat treatment of cold-rolled sheets for the purpose of removal of internal stresses. The ductility also improves during annealing, thus actually makes the material 'usable'. But in case of IF-steels, annealing also plays a significant in developing the favourable texture component for deep drawing applications. Annealing also has direct effect on the various properties of IF-steel. Two types of annealing are generally used. One is batch annealing and the other is continuous annealing. The batch annealing process is very time consuming due to the low heating and cooling rates. But, continuous annealing process is very fast due to the high heating and cooling rates. Also, the highest temperature is more in case of continuous annealing.

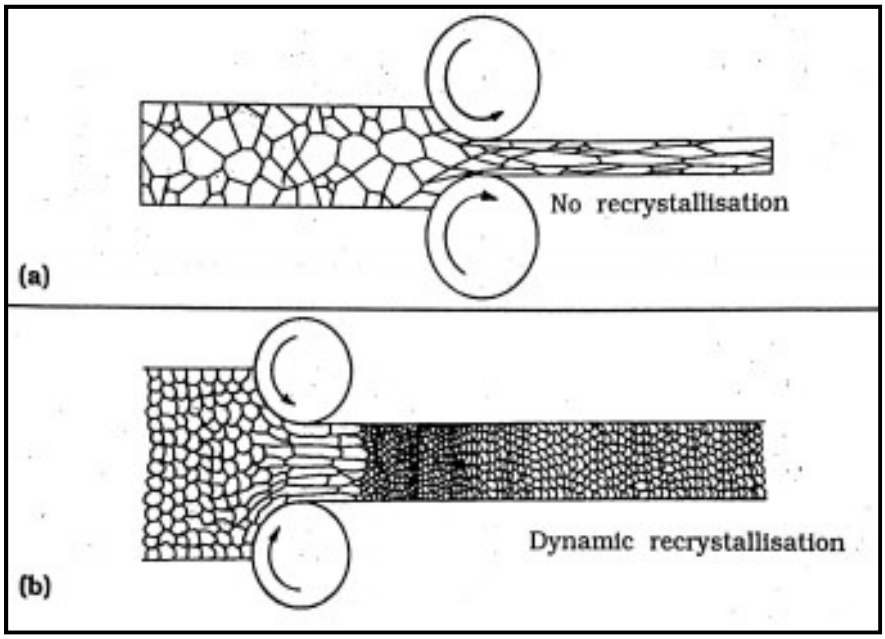

Figure 1.6: Effect of (a) hot rolling, (b) cold rolling on the grains [2].

1.5 Measurement of formability

The Lankford parameter commonly, known as r_m-value, is the measurement of formability or drawability and also the measurement of resistance to thinning. Lankford parameter is also known as normal anisotropy [2, 3]. For the calculation of Lankford parameter, first of all

there is a need to define the plastic strain ratio (r). In uniaxial tensile testing, the ratio of true width strain to true thickness strain gives the plastic strain ratio as given in Eq. (1.2) [2, 3, 8–10].

Therefore,

$$r = \frac{tru \quad width\ strain}{true\ thickness\ strain} = \frac{\varepsilon_w}{\varepsilon_t} = \frac{\ln\frac{w}{w_0}}{\ln\frac{t}{t_o}} \quad \ldots\ldots\ldots\ldots\ldots\ldots\ldots (1.2)$$

Where, w_o, t_o is the initial width and thickness respectively and w, t is the final width and thickness respectively.

Then r value should be measured in three directions with respect to rolling direction-rolling direction (r_0), transverse direction (r_{90}) and diagonal direction (r_{45}). Then normal anisotropy and planar anisotropy are given as Eq. (1.3) and Eq. (1.4) [2, 3, 8–10].

Normal anisotropy (Lankford Parameter) = $r_m = \frac{r_0+2r_{45}+r_{90}}{4}$ ..... (1.3)

Planar anisotropy= $\Delta r = \frac{r_0-2r_{45}+r_{90}}{2}$ ..... (1.4)

1.6 Interstitial free high strength steels (IFHS steels)

The main limitation of IF-steel is its low strength as compared to other types of steels. Due to this limitation, IF-steels are now replaced by IFHS steels in the automotive industry. IFHS steels offer greater strength than IF-steel without sacrificing too much of formability. Hence, IFHS offer good strength-ductility combination. In IFHS steel, the solid solution strengthening is achieved by addition of phosphorous (P) and manganese (Mn) elements [11, 12].

1.7 Lüders bands phenomenon

Yield point elongation (YPE) or Lüders band formation or Stretcher strains markings is a well estabilished phenomenon in low carbon steels. When a low carbon steel is strained under tensile deformation, a well defined sharp yield point is observed, followed by an adrupt drop in stress, and then an increase in strain at constant stress occurs. This increase in strain value at a constant stress is known as yield point elongation or Lüders band deformation phenomenon. The presence of Lüders bands on the surface of steel sheet deteriorates the surface finish [13]. Lüders band phenomena is usually caused by the release of dislocations which were locked in the Cottrell atmosphere (atmosphere of solute carbon atoms across dislocation) [14]. Lüders bands generally formed 45° to axis of tensile. Fig. 1.7a shows Lüders band formation on a tensile sample [15] and Fig. 1.7b shows yield point elongation in tensile stress-strain curve [16].

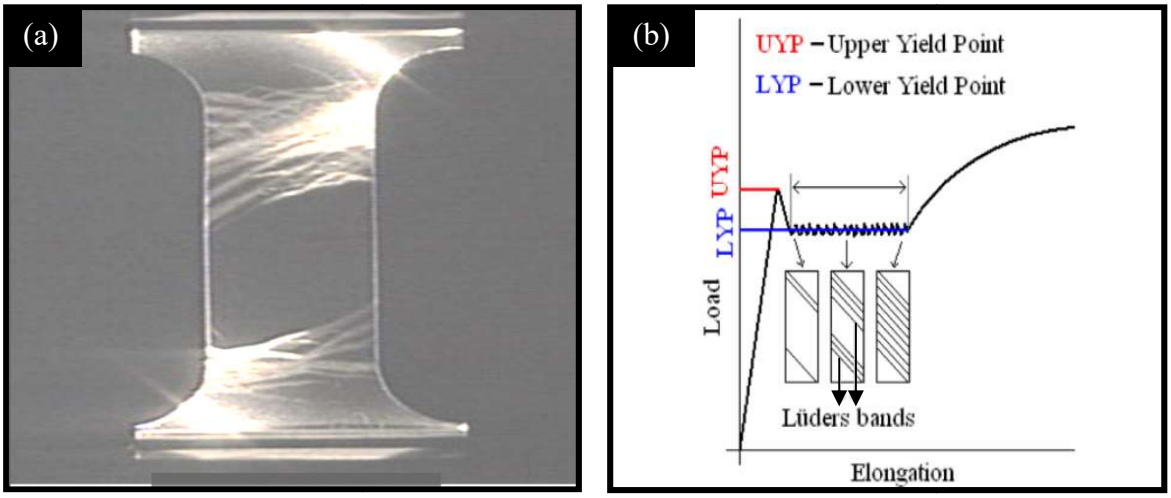

Figure 1.7: (a) Lüders bands formation in a tensile sample [15], (b) yield point elongation in tensile stress strain curve [16].

1.8 Summary of the chapter

Interstitial free steels are the steels in which interstitial atoms (C, N) are stabilized with the addition of some stabilizing elements like Ti and/or Nb. As these steels have no free interstitial atoms, so the formability of these steels is very high, but the strength of these steels is low. These steels are processed by conventional method of steel processing with an additional step of vacuum degasifying for the production of ultra low carbon steels. The limitation of low strength is removed by the addition of solid strengthening elements (P and/or Mn) to IF-steel, forming IFHS steels. IFHS steels have relatively higher strength and slightly reduced formability than IF-steels. IFHS steels have replaced IF-steel in automotive industry due to their superior properties. Lüders bands formation is one of the undesirable defects generally observed in low carbon steels. The main concern of this research is related to Lüders bands formation in IFHS steel compositions.

Chapter 2

Literature Review

2.1 General

In the present chapter, literature by various authors in the field of 'Interstitial free high strength steels' has been discussed. The work reported by various researchers has been summarized. In the last section, gaps in the existing literature have been discussed.

2.2 Literature summary

Shi and Cui [17] aimed to optimize the batch-annealing cycle to process IF-steels, which could save energy by reducing lead time, but maintains the necessary deep drawability. Two types of samples were used viz. Ti-IF sample and Ti-Nb IF sample. Table 2.1 shows the chemical composition of these samples.

Table 2.1: Chemical composition of steel used [17].

Steels	C (%)	N (%)	S (%)	Ti (%)	Mn (%)	P (%)	Nb (%)
Ti-IF	0.0035	0.0028	0.0041	0.076	0.17	0.01	<0.01
Ti-Nb IF	0.0031	0.0034	0.0054	0.076	0.14	0.007	0.017

The batch annealing cycle was performed in gas-protected furnace. The samples were heated to the several temperatures (650 ℃, 680 ℃, 710 ℃, 740 ℃, and 770 ℃) at the rate of 50 ℃/hr. The soaking times used were 5, 15, and 30 min, 1, 4, 6, 8, and 12 hr followed by furnace cooling. The r_m value (normal anisotropy) is calculated for the measurement of formability. When the samples were heated to different several temperatures with 4 hr soaking, then the r_m-value slightly increased from 1.92 to 2.08 with increase in temperature from 660 to 770 ℃ for Ti-IF-steels. But for Ti-Nb IF-steel, r_m-value increased in the range 1.9–2.16. So, r_m-value of Ti-Nb IF-steel was observed to be more sensitive to annealing temperature in comparison to that of Ti-IF-steel. This increase of r_m-value was due to increase in grain size and favourable annealing texture at higher annealing temperature. Now the samples of both steels were heated to annealing temperature of 710 ℃ and various soaking times were used. The influence of soaking time on r_m- value was observed to depend upon the annealing temperature. If the annealing temperature was low, where only partial recrystallization occurred, the lengthening of soaking time tend to increase in r_m value. If the

annealing temperature was high enough so that recrystallization occurred completely, then the lengthening of soaking time did not increase in r_m value. The new batch annealing cycle used 650 to 680 ℃ in place of 710 to 730 ℃. The cycle helped in saving time and energy consumption without much affecting the r_m-value and n- value (strain hardening exponent).

Jia *et al.* [18] investigated the effect of Ti content and process parameters on the precipitation characteristics of FeTiP in IFHS steel. Two compositions of IFHS steel were used viz. steel 1 and steel 2 as shown in Table 2.2. The slab from each composition was reheated to 1250 ℃ for 3 hr followed by hot rolling to 3 mm thickness with starting and finishing deformation temperatures of 1150 ℃ and 910 ℃. After this cold rolling was done upto 0.75 mm thickness followed by annealing at 810 ℃ and 840 ℃ respectively with holding time varying from 60 to 120 s for each case. The precipitates were observed under Transmission electron microscope (TEM) and the composition of precipitates was determined by using energy dispersive X-ray spectrometer (EDS).

Table 2.2: Chemical composition of steel used (in wt %) [18].

Material	C	N	Si	Mn	S	Ti	P
Steel 1	0.0018	0.0040	0.07	0.335	0.012	0.080	0.09
Steel 2	0.0018	0.0045	0.07	0.320	0.012	0.007	0.008

The samples from steel 1 showed few large sized TiN, TiS and MnS and fine TiC particles after annealing at 810 ℃ for 60 s as shown in Fig. 2.1a–b. With increase in holding time upto 90 s, few granular particles of TiC, large round shaped particles of $Ti_4C_2S_2$ (as shown in Fig. 2.1c) and complex sulphides (as shown in point 1 in Fig. 2.1d) was observed. With increase in holding time upto 120 s, large number of fine particles were observed as shown in Fig. 2.1e and also rod shaped particles of size 200 nm was observed as shown in point 3 in Fig. 2.1f. These rod-shaped particles were FeTiP and were confirmed by EDS shown as point 3. If the annealing temperature was taken to 840 ℃ followed by 60 s holding, then TiN, donut shaped sulfides and fine TiC particles was observed as shown in Fig. 2.2a–b. As holding time was increased to 90 s, the large sized sulfide complexes (such as MnS＋ TiS and MnS＋$Ti_4C_2S_2$), and fine $Ti_4C_2S_2$, TiC and FeTiP particles were observed as shown in Fig. 2.2c–d. After 120 s holding time, the large sized TiS, fine particles of TiC, $Ti_4C_2S_2$ and FeTiP, and some TiN particles were observed (see Fig.2.2e–f).

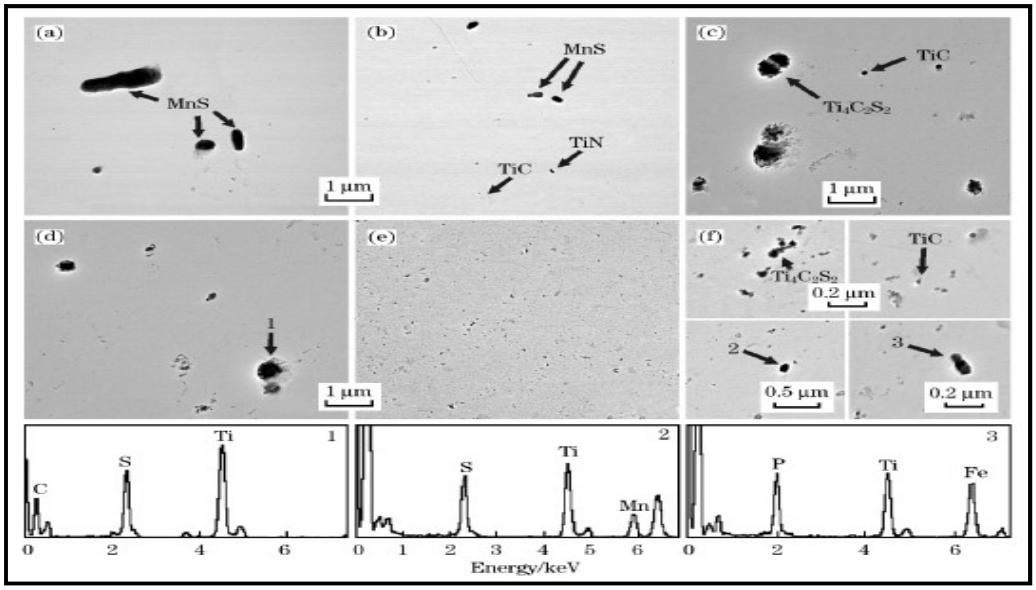

Figure 2.1: TEM micrographs of extraction replicas and corresponding EDS analysis results of samples annealed at 810 ℃ for 60 s (a, b), 90 s (c, d) and120 s (e, f) of steel 1 [18].

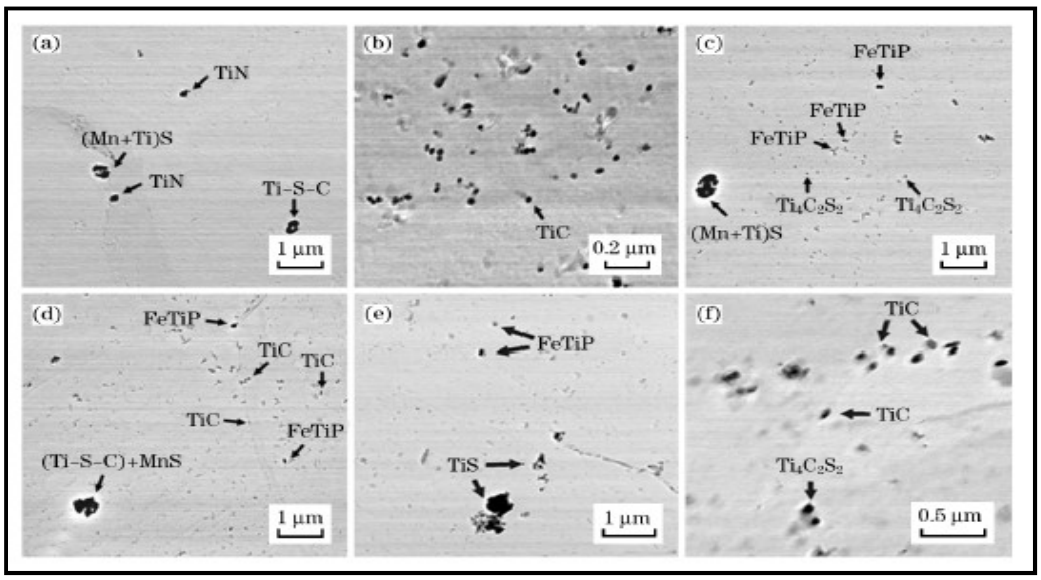

Figure 2.2: TEM micrographs of extraction replicas of samples annealed at 840 ℃ for 60 s (a, b), 90 s (c, d) and 120 s (e, f) of steel 1 [18].

Hence, it was observed that there was a critical time for the formation of FeTiP precipitates at a given temperature. Also, if the content of Ti is increased, there was less time needed for the formation of FeTiP precipitation. Hence FeTiP precipitates formed in two steps: the first step was formation of FeTi precursors which were dependent on Ti content and the second step was the diffusion of P, which was dependent on annealing temperature.

Kang *et al.* [19] studied the influence of addition of aluminium (Al) on the properties of Ti/Nb IFHS steel and aimed to develop IFHS steel with improved formability. Three samples

were taken with different contents of Al in them viz. M1, M2, and M3. Table 2.3 shows the chemical compositions of M1, M2, and M3 samples.

Table 2.3: Chemical composition of M1, M2, and M3 steel samples (in wt %) [19].

Name	C	Mn	P	S	Al	Ti	Nb	B	N
M1	0.0016	0.82	0.080	0.005	0.043	0.019	0.005	0.005	0.0019
M2	0.0020	0.84	0.081	0.006	0.130	0.025	0.006	0.007	0.0024
M3	0.0019	0.80	0.080	0.004	0.190	0.021	0.005	0.005	0.0020

The as-cast samples of above chemical compositions were hot rolled to a final thickness of 3.2 mm with finishing rolling temperature (FRT) of 910 ℃ and coiling temperature of 600 ℃. Then, the samples were 77.5% cold rolled followed by annealing. During annealing, the samples were heated to 830℃ at rate of 7℃/s, followed by 30 s and subsequently cooled to room temperature. Fig. 2.3 shows the schematic representation of processing of samples.

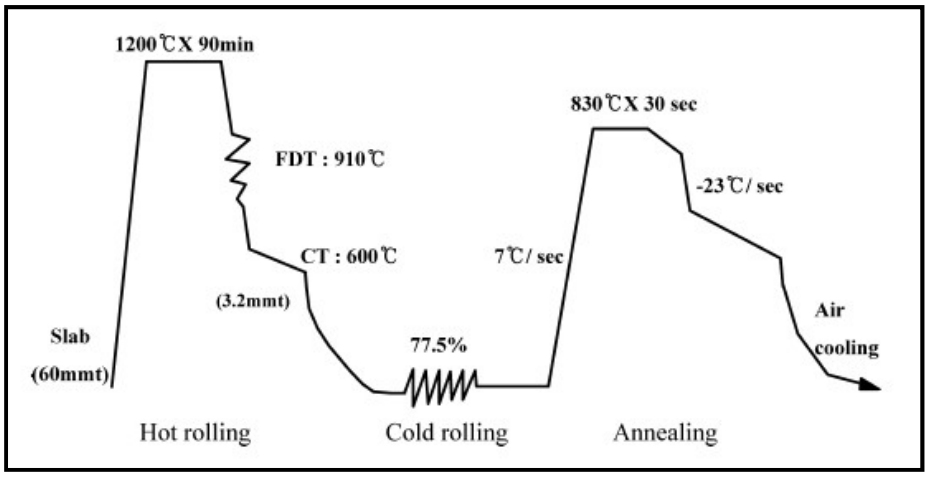

Figure 2.3: Schematic representation of processing of samples [19].

The tensile strength decreased, when the Al content increased (see Fig. 2.4a). But elongation values and r_m-value increased with increase in Al content (see Fig. 2.4b–c). The grain size of ferrite in M1 was about 18 μm and that of M3 was about 22 μm. This difference in ferrite grain size in three samples after annealing was the reason behind these observations. The recrystallization kinetics of ferrite was found to be faster in steels with more Al content than steels with less Al content. Also the favourable texture component {111}//ND got intensified and remaining texture component {110}//RD got weakened with increase in Al content, hence increased formability. Also, SANS (Small Angle Neutron Scattering) analysis showed

the larger sizes and less number of precipitates in the steel with more Al content that in the steel with less Al content (see as shown in Fig. 2.5a–b).

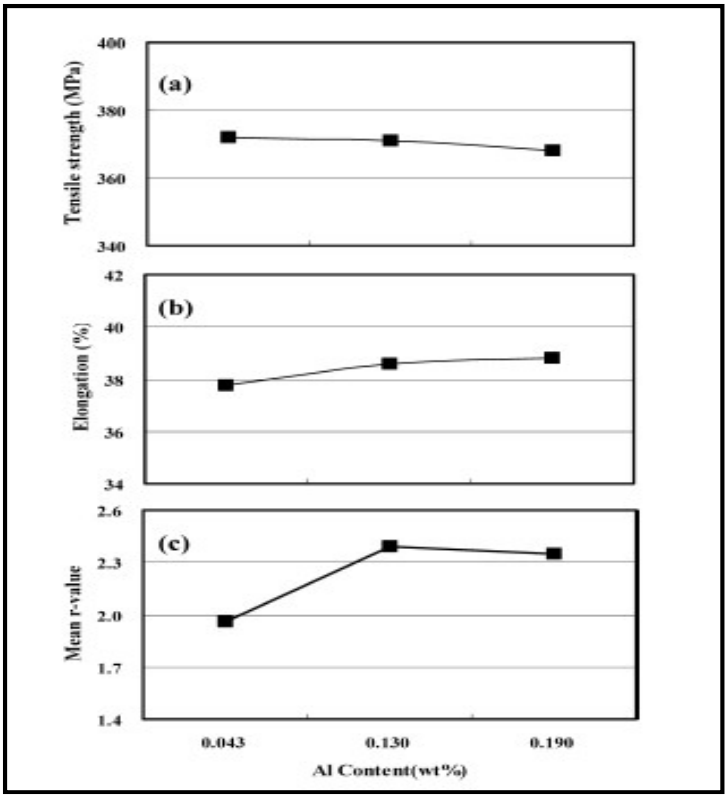

Figure 2.4: Influence of aluminum content on (a) tensile strength (MPa), (b) elongation values (%) and (c) mean *r*-value of IF-HSS containing Mn, P, Ti and Nb [19].

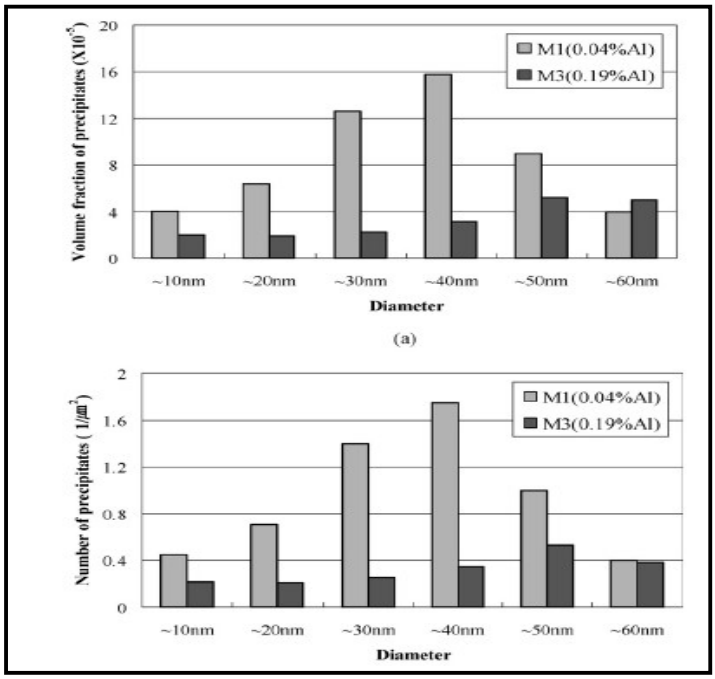

Figure 2.5: The results of SANS analysis in terms of (a) volume fraction of precipitates, (b) number of precipitates/mm^2 [19].

Nath *et al.* [20] investigated the effect of thermo-mechanical processing on the microstructure and properties of an IF-steel. The chemical composition of the sample used is given in Table 2.4.

Table 2.4: Chemical composition of the sample used (in wt %) [20].

C	Mn	Al	N	Ti	Nb	S	P	Si	Fe
0.003	0.10	0.041	0.003	0.062	0.010	0.009	0.011	0.012	99.69

The as-received sample of 4.28 mm was received after hot-rolling. Then it was cold-rolled to 80% followed by annealing at soaking temperature 680 ℃ for 10, 20, 30, and 40 min. The samples were given names of CR10, CR20, CR30, and CR40 according to their soaking time. The rate of cooling used was 7℃/min. Then, the samples were cleaned by using 200 and 400 grit size emery papers. After cold rolling with 80% reduction, the grains got elongated in the direction of rolling, thus lower ductility obtained made deep drawing difficult. Hence, annealing was done to get higher ductility. Now, the annealed samples at 680 ℃ for different soaking times did not exhibit yield point phenomena. This was the desirable condition, because yield point elongation can produce stretcher marks on the surface of specimen. The mechanical properties of studied IF-steel samples after annealing are given in Table 2.5.

Table 2.5: Mechanical properties of CR, CR10, CR20, CR30, CR40, and CR40 samples [20].

Sample	UTS (MPa)	Elongation (%)	Hardness (VHN)
CR	590	7.10	186
CR10	415	15	145
CR20	302	31	95
CR30	278	46	86
CR40	226	54	81

As the strength of CR sample was more and the elongation was less, so brittle fracture occurred in this case as shown in Fig. 2.6a. CR10 and CR30 showed mixed mode of fracture. Fig. 2.6b–c shows mixed mode of fracture with dimples and cleavage features. But CR30 and CR40 showed ductile fracture, which was desirable. Fig. 2.6c–d shows ductile fracture with dimples only. Due to very low strength of CR40, it was unacceptable in automotive application. But CR30 gave sufficient combination of strength and ductility. Hence the

optimum thermo-processing parameters for 80% cold reduction were soaking temperature of 680 ℃ and soaking time of 30 min.

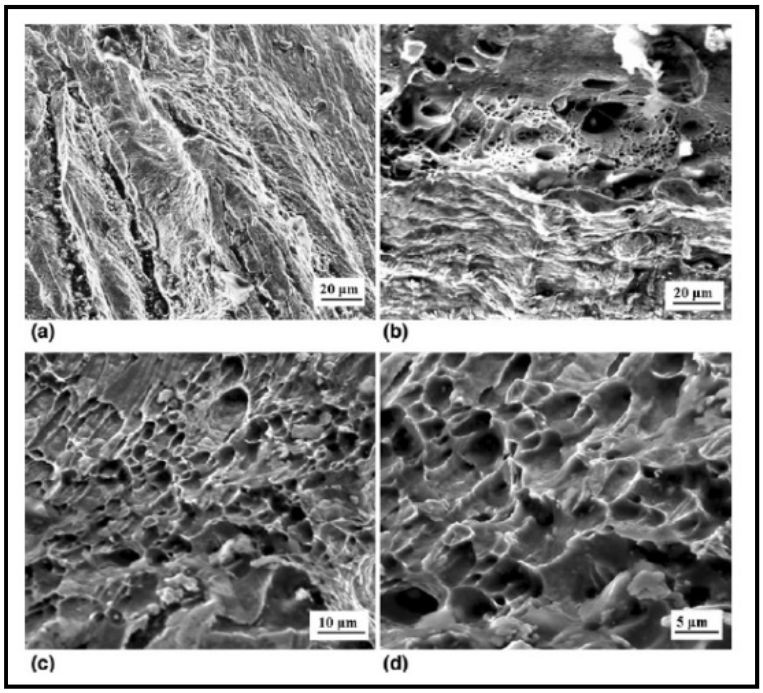

Figure 2.6: SEM fractographs showing fracture surfaces of (a) CR, (b) CR10, (c) CR20, and (d) CR30 tensile specimens [20].

Gao *et al.* [21] studied the effect of grain size on the yielding phenomenon and uniform elongation of IF-steel. Table 2.6 shows the chemical composition of IF-steel used.

Table 2.6: Chemical composition of IF-steel used (in wt %) [21].

C	N	Si	Mn	P	S	Al	Ti	Fe
0.002	0.0027	0.01	0.10	0.005	0.006	0.032	0.039	Bal.

The as-received material of 2 mm thickness had fully recrystallized structure with average grain size of about 30 μm. Then, the sample was rolled at 500 ℃ followed by five accumulative roll-bonding (ARB) cycles gave the total reduction in thickness of 98.4%. Then the samples were annealed at various temperatures in the range from 500–800 ℃ for the soaking time of 30 min followed by quenching in water in order to get different average grain sizes. The average grain size of ARB processed sample was found to be 0.45 μm. Similarly, average grain sizes of 0.65 μm, 0.85 μm, and 2.8 μm respectively was found in the samples annealed at 500 ℃ , 560 ℃ , and 600 ℃ with soaking time of 30 min respectively. As the grain size increased, the strength decreased and elongation increased. Also, the tensile testing

performed at room temperature after annealing revealed that the transition from continuous yielding to discontinuous yielding occurred, when average size of grains obtained was lowered to ultrafine range smaller than 1 μm as shown in Fig. 2.7. The stretcher strain markings occurred on the surface of samples due to discontinuous yielding is shown in Fig. 2.8.

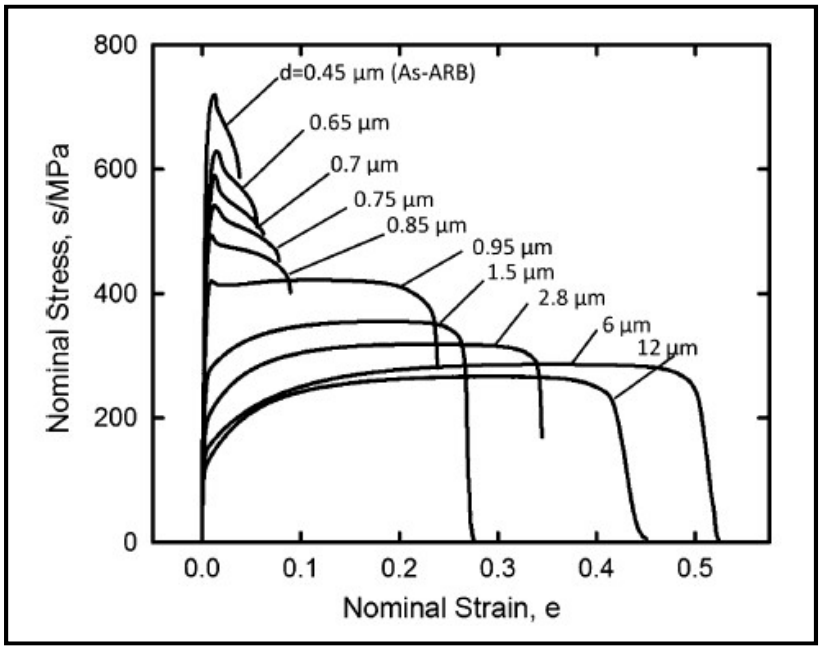

Figure 2.7: Nominal stress-strain curves of ARB processed and annealed samples of IF-steel with varying average sizes of grains [21].

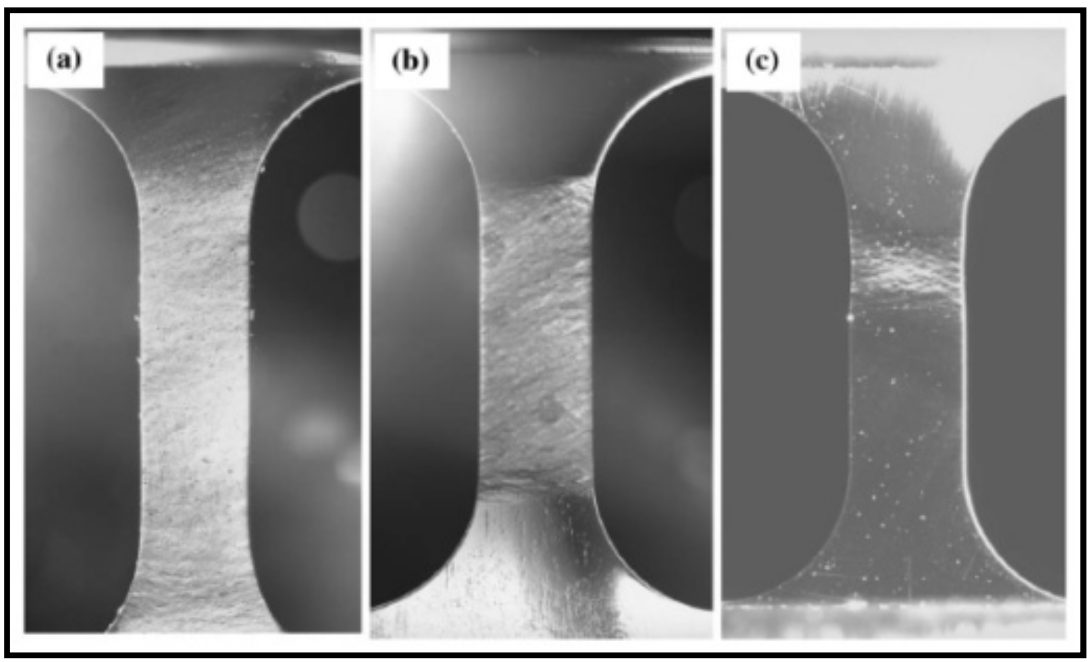

Figure 2.8: Surface appearances of the tensile samples with different mean grain size and different strain rates. (a) d =12 μm at ε= 0.25, (b) d=0.95 μm at ε=0.1, and (c) d= 0.75 μm at ε=0.03 [21].

As the Hall-Petch relation given in the Equation 5 gave the relationship between yield stress and average grain size.

$$\sigma_y = \sigma_0 + K_y d^{\frac{-1}{2}} \quad \text{.....(5)}$$

Where, 'σ_y' is the yield stress of material, 'σ_0' is the friction stress, 'K_y' is the slope of the equation, and finally 'd' is the average size of grains. Now distinct slopes were obtained with coarse grain size showing continuous yielding, and with fine grains showing discontinuous yielding as shown in Fig. 2.9. Also the dramatic drop was found in uniform elongation with the average grain size below 1.5 μm.

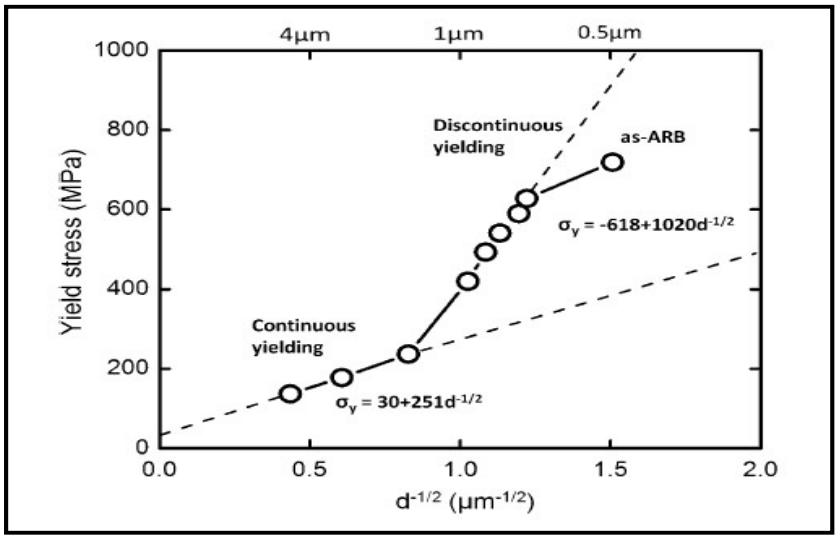

Figure 2.9: Dependence of yield strength on inverse of the square root of average size of grain of IF-steel specimen [21].

Akama *et al.* [22] investigated the effect of the addition of Ni on the yielding phenomenon of IF-steel. Three chemical compositions of IF-steels with varying amount of Ni were used. These were Fe–0.99Ni–0.081Ti, Fe–1.98Ni–0.048Ti, and Fe–3.02Ni–0.076Ti (wt. %). These three compositions were given names as 1Ni, 2Ni, and 3 Ni respectively. Ti was added in sufficient amount to each composition of steel to fix C and N as Ti(C, N). The as-received sample of 800 mm thickness was hot-rolled to 4 mm at 1493 K followed by 80% thickness reduction in cold rolling, and then annealed in the ferrite single phase region from 933 to 1098 K for 1.0 ks to control the size of grain. After this, the samples were again annealed at 873 K for 3.6 ks in order to ensure full precipitation of Ti as Ti(C, N). The friction stress in Hall-Petch relation increased linearly with increase in the content of Ni. This shows that the solid solution strengthening in the ferrite steel is directly proportional to the content of Ni in the range of 1–3%. Also the slope of Hell-Patch (k_Y) increased with increase in the Ni

content. In case of 3Ni, the value of k_Y was found to be 350 MPa $\mu m^{1/2}$ which was greater than the value of k_Y in case of IF-steel without Ni (k_Y= 150 MPa $\mu m^{1/2}$). Hence Ni also increased the grain refinement strengthening. So, the yield strength increased with increase in the Ni content and also in case Ni bearing IF-steels the well defined yield point was observed. In case of 3Ni, the yield point elongation was observed (see Fig. 2.10a). Also, Fig. 2.10b shows the result of aging index test (AI) for 3Ni. The results showed that there is no change in flow stress after aging. This shows that no free C and N were present in the steel. Hence discontinuous yielding was not caused by solute interstitial elements. So, interstitial elements are not always essential source of discontinuous yielding. Here the reason behind the yield point elongation was grain refinement strengthening.

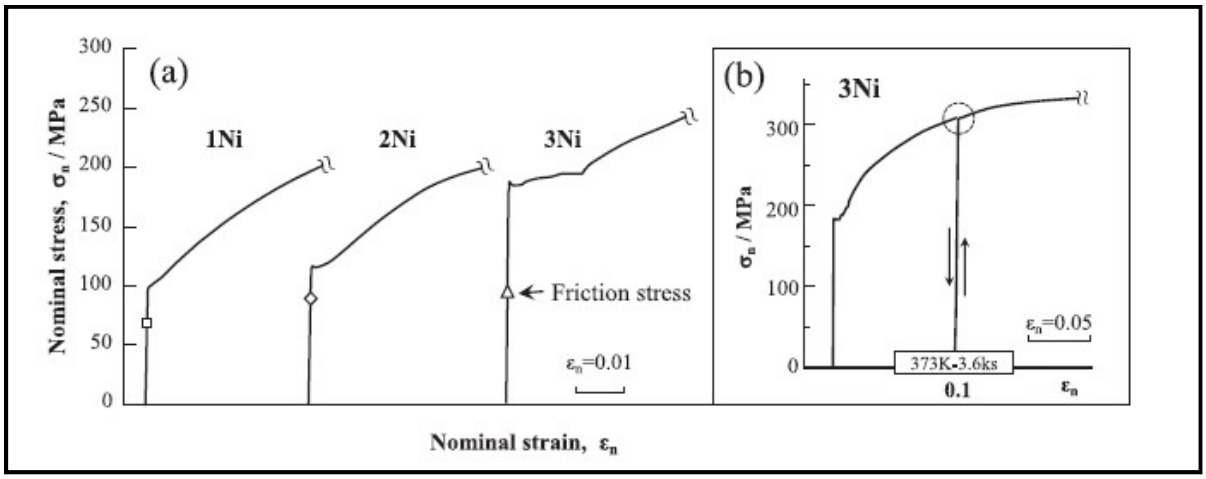

Figure 2.10: (a) Nominal stress–strain curves of Ni-bearing IF-steel, and (b) the result of the aging index test in 3Ni steel [22].

Bhagat *et al.* [23] aimed to develop a cold rolled IFHS steel for automotive applications with improved formability. Three ultra low carbon chemical compositions were used with varying amount of P, Ti, and Nb contents (see Table 2.7).

Table 2.7: Chemical compositions of various samples [23].

Steel	C	Mn	P	Al	Nb	Ti	N	B
1	≤0.0040	0.53	0.065	0.034	≤0.02	≥0.05	0.0038	0.001
2	≤0.0040	0.50	0.028	0.039	≤0.02	≥0.05	0.0031	0.0006
3	≤0.0040	0.54	0.046	0.023	≤0.015	≥0.02	0.0027	0.0006

The as-cast slabs were subjected to hot-rolling in a hot strip mill (HSM). The parameters for hot rolling were chosen in such a way, so that the microalloying elements make precipitates

during hot rolling process or coiling stage. Then these samples were subjected to cold-rolling in cold rolling mill (CRM) with 70–80% reduction in thickness followed by annealing cycle. Table 2.8 shows the properties of three samples after cold rolling followed by annealing process. Table 2.8 shows the range of YS from 193–237 MPa, UTS from 365–415 MPa, elongation from 37–42%, r_m-value from 1.5–1.8, and n-value from 0.22–0.26. Also steel 3 showed continuous yielding phenomena. If the steel 3 was annealed in continuous galvanizing line (CGL) after cold rolling, then YS, elongation values, and r_m-value remained unchanged, but the value of Δr increased when compared to the values obtained in batch annealing cycle as shown in Table 2.9.

Table 2.8: Mechanical properties of cold-rolled and annealed samples [23].

Steel	Yield strength (MPa)	Ultimate tensile strength (MPa)	Elongation (%)	r_m-value	Δr	n-value
1	237	415	37	1.5	+0.40	0.23
2	193	367	42	1.8	+0.35	0.25
3	226	365	41	1.8	+0.14	0.22

Steel 1 had huge Ti and P content, showed decreased formability with r_m-value of 1.5. Now reducing B and P contents as in case of steel 2 and steel 3 improved r_m-value to 1.8 but reduced strength. Also the steel containing lesser amounts of elements Ti, Nb, and 0.05% of P gave YS greater than 220 MPa, UTS greater than 350 MPa, r_m-value of 1.8, lowest n-value of 0.22, and lowest Δr value of 0.14. These excellent properties enabled the composition to manufacture those components of an automobile, which severely required forming operation.

Table 2.9: A comparison of mechanical properties of cold-rolled and annealed steel 3 processed through BAF and CGL [23].

Annealing cycle	YS (MPa)	UTS (MPa)	Elongation (%)	r_m value	Δr	n-value	BH (MPa)	Annealing temperature (°C)
BAF	226	365	41	1.8	+0.14	0.22	Nil	720
CGL	226	340	41	1.8	+0.63	0.19	24	890

Rana *et al.* [24] aimed to develop interstitial steel of high strength by hardening through copper precipitation. Three samples were used viz. IF-steel with Cu (IF-Cu), Ti stabilized IF-steel containing no Cu (IF-1), and Ti-Nb stabilized IF-steel containing no Cu (IF-2). Table

2.10 shows the compositions of the samples. Samples were subjected to hot-rolling process with finishing rolling temperature of 900 ℃ followed by 80% reduction in thickness by cold rolling and then annealed at 820 ℃ for 1 min. After continuous annealing, the samples were provided ageing at 550 ℃ in the bath of salt for 8 h. IF-Cu steel showed lower YS values, but comparable UTS and uniform elongation values as compared to IF-1 and IF-2 (see Table 2.11).

Table 2.10: Chemical composition of various samples used [24].

Steel	C	Mn	S	P	Si	Al	Cu	Ni	Nb	Ti	N
IF-Cu	0.002	0.08	0.007	0.012	0.023	0.011	1.18	0.013	—	0.043	0.00014
IF-1	0.004	0.57	0.005	0.031	0.01	0.042	0.015	0.023	0.0041	0.083	0.0017
IF-2	0.003	0.35	0.008	0.042	0.011	0.043	0.028	0.013	0.024	0.023	0.0026

The lower strength in case of IF-Cu was due to presence of lower amount of P and Mn, which were solid solution strengtheners.

Table 2.11: Mechanical properties of the continuous annealed samples [24].

Steel	YS (MPa)	UTS (MPa)	Elongation (%)	n-value	r_m-value	Δr
IF-Cu	186.3	365.8	23.2	0.27	1.4	−0.08
IF-1	214	354.3	24	0.22	1.77	−0.20
IF-2	238	373	23	0.20	1.57	+0.005

The strain hardening exponent value (n-value) of IF-Cu was higher than that of remaining two samples. This indicated the better stretchability of IF-Cu steel during forming operation. Also lower value of Δr in case of IF-Cu indicated lower probability of earing defect in it. But there was deterioration of r_m value in case of IF-Cu, which reflected lower deep drawability. But higher value could be achieved in this case by annealing at slightly higher temperature say 850 ℃. The higher strain hardening exponent value in case of IF-Cu was caused by the existence of Cu in the solid solution, whose effect was to increase capability of steel to possess high dislocations density due to strong interaction between atoms of Cu element and dislocations present in solid solution. Now ageing treatment was provided to the continuous annealed Cu containing sample (IF-Cu) sample at 550 ℃, then YS and UTS increased. IF-Cu samples assumed its peak strength after 1.5 h of ageing at 550 ℃. After 1.5 hr to 8 hr, the strength remained constant (see Fig. 2.11). The obtained yield strength and ultimate tensile strength in peak aged IF-Cu sample were 456 and 556 MPa respectively. Hence in peak aged

IF-Cu sample, the increase in YS was 270 MPa (147%) and in UTS was 200 MPa (54%). It is not possible to obtain such a large increment in YS and UTS by any other method. This strengthening was done by copper precipitation.

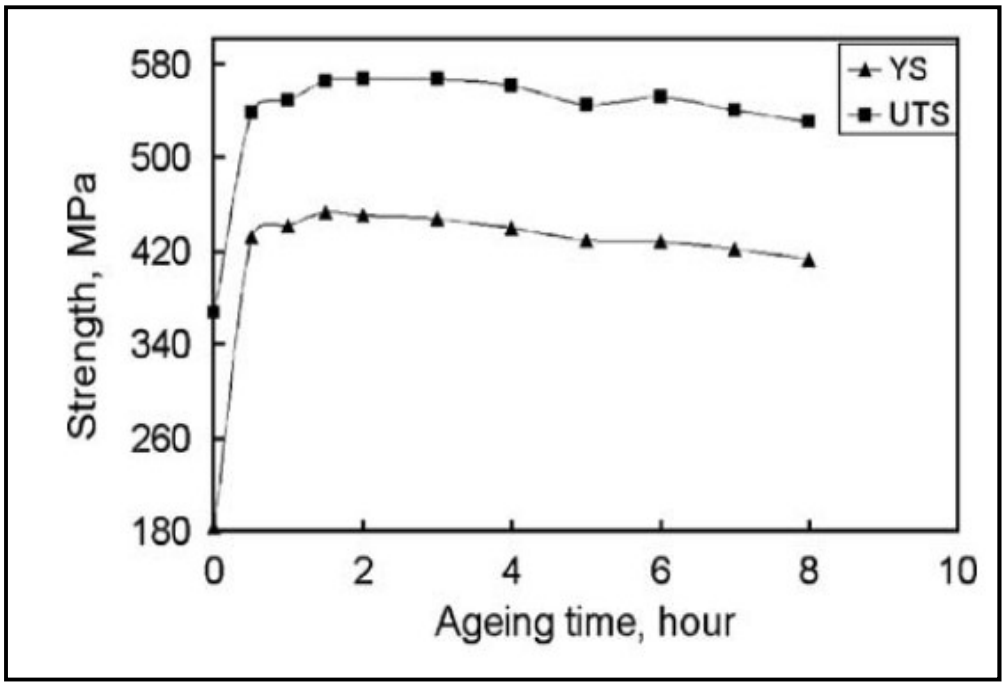

Figure 2.11: Age hardening curves of the IF-Cu steel [24].

Rege *et al.* [25] investigated the segregation behavior of P in Ti and Ti/Nb stabilized IF-steels. Five different samples were used, whose compositions are shown in Table 2.12.

Table 2.12: Chemical compositions of various samples [25].

Steels	C	N	Mn	S	P	Ti	Nb
0.06Ti	0.0036	0.0035	0.16	0.008	0.014	0.06	0.0
0.03Ti-Nb	0.0033	0.0037	0.16	0.009	0.014	0.03	0.03
0.06Ti-P	0.0035	0.0031	0.16	0.008	0.06	0.06	0.0
0.03Ti-Nb-P	0.0038	0.0030	0.16	0.007	0.06	0.03	0.03
0.06Ti-Nb-P	0.0036	0.0035	0.16	0.008	0.06	0.06	0.03

Samples were homogenized at 1300 ℃ for 1 hr followed by water quenching. Then hot deformation was done. The finish rolling temperature was 920 ℃ followed by coiling at 704 ℃ and then 80% reduction in thickness was taken during cold-rolling process as shown in Fig. 2.12. Then 0.03Ti-Nb-P and 0.06Ti-Nb-P were given annealing at 860 ℃ with 80 s soaking time and the remaining samples were given annealing at 840 ℃ with 80 s soaking

time, so that full recrystallization of samples occurred. The segregation behavior of P in Ti and Ti-Nb stabilized IF-steels were studied during various processing stages (a) after hot rolling process prior to cold rolling, (b) after coiling stage, and (c) after cold rolling process and annealing process. In case of 0.06Ti-P IF-steel, there was no segregation on the ferrite grain boundaries before coiling condition. But the segregation occurred around the $Ti_4C_2S_2$ precipitates. Fig. 2.13 shows the TEM micrograph from the $Ti_4C_2S_2$ precipitate, where no peak of P was observed. But, Fig. 2.14 shows the TEM micrograph around the region of $Ti_4C_2S_2$ precipitate, where the P peak was observed additionally. After coiling, the segregation of phosphorous (P) around $Ti_4C_2S_2$ precipitate disappeared, but segregation was observed at ferrite grain boundaries. Hence there was diffusion of P from $Ti_4C_2S_2$ precipitate to ferrite grain boundaries during coiling process. After cold rolling and annealing processes, the precipitates occurred at grain boundaries of ferrite and also in ferrite matrix.

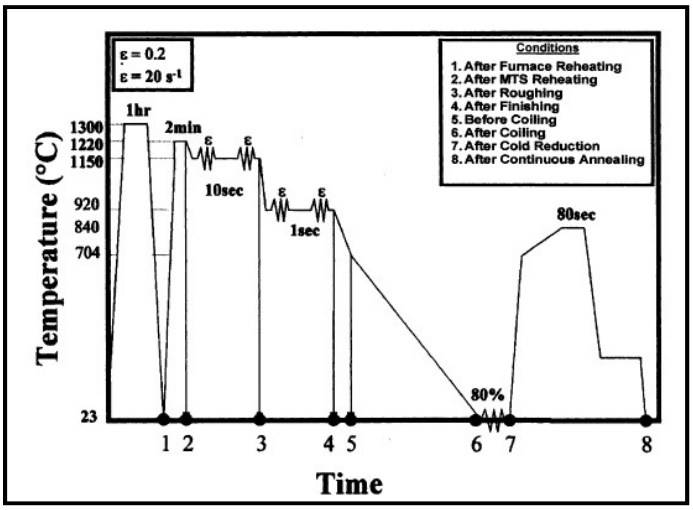

Figure 2.12: Schematic representation of different processing stages of IF-steels [25].

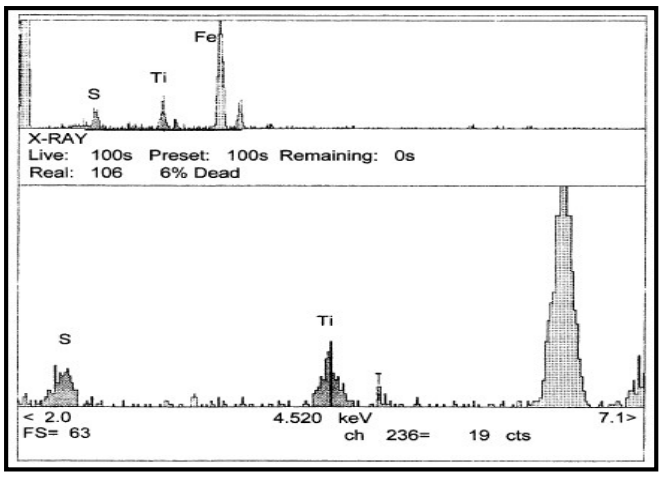

Figure 2.13: TEM micrographs from typical $Ti_4C_2S_2$ precipitate in 0.06Ti-IF-steel [25].

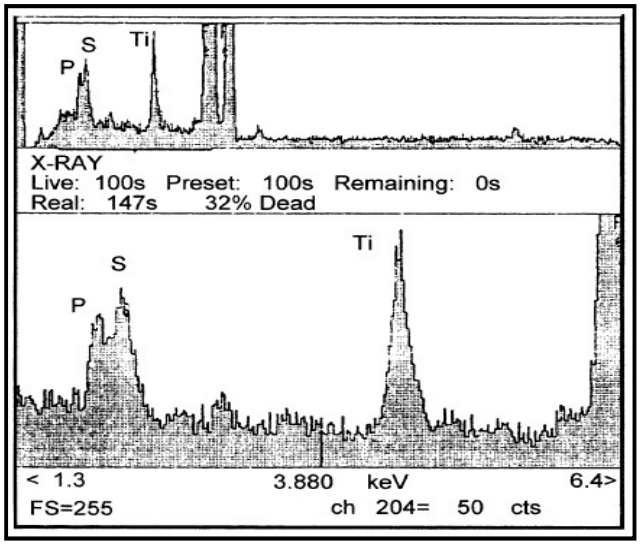

Figure 2.14: TEM micrographs from the region around the $Ti_4C_2S_2$ precipitate 0.06Ti-IF-steel [25].

The segregation behavior of phosphorous (P) element during different stages of processing in 0.06Ti–P steel is shown in Fig. 2.15.

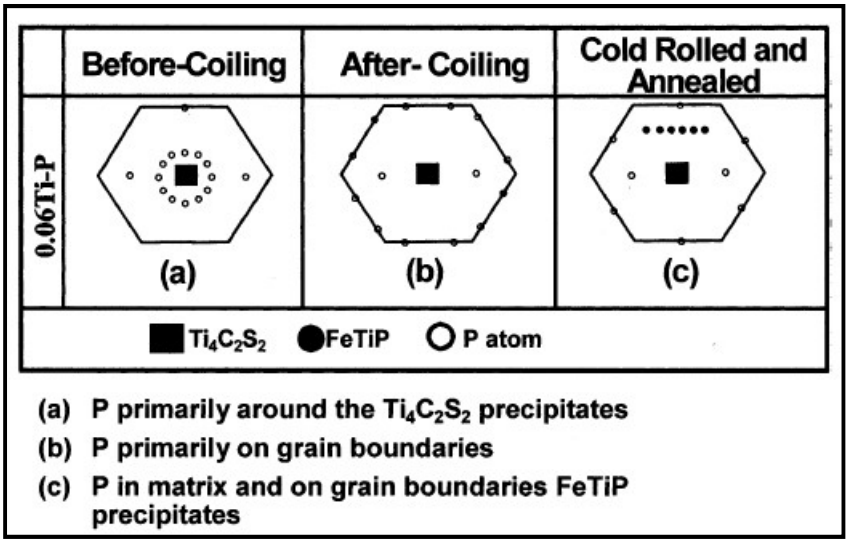

Figure 2.15: Schematic representation of the segregation behavior of Phosphorous (P) during different stages of processing in 0.06Ti–P steel [25].

Now, in case of 0.03Ti-Nb-P and 0.06Ti-Nb-P IF-steels, the segregation of phosphorous (P) around $(Ti,Nb)_4C_2S_2$ precipitate before coiling. But after coiling, the segregation of P was observed around precipitate and also on the grain boundaries. But Nb addition decreased the segregation on grain boundaries in as-coiled condition. But after cold rolling and annealing, the segregation of P was observed on grain boundaries of ferrite. The segregation behavior of phosphorous (P) during different stages of processing in 0.03Ti-Nb–P, and 0.06Ti–Nb–P steels is shown in Fig. 2.16.

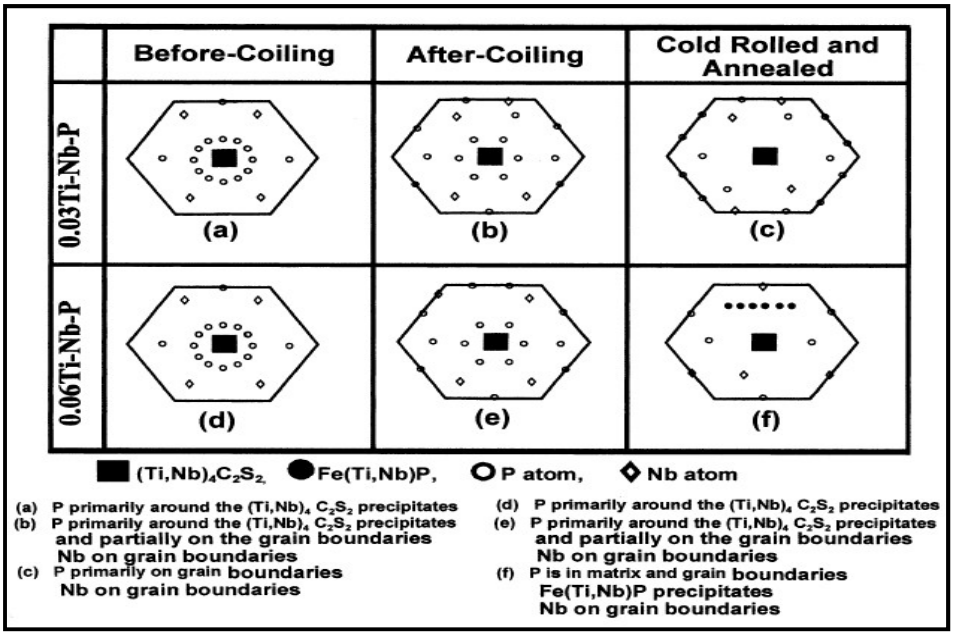

Figure 2.16: Schematic representation of the segregation behavior of phosphorous (P) during different stages of processing in 0.03Ti-Nb–P (a–c), and 0.06Ti–Nb–P steels (d–f) [25].

Both solutes, Nb and enough Ti in IF-steels could form Fe(Ti,Nb)P precipitates, which could decline the segregation of phosphorous (P) on the boundaries of ferrite grains. Steels having high content of P showed cold work embrittlement (CWE). The presence of niobium (Nb) on the boundaries of grains reduced segregation of P on grain boundaries and helped in improving cold work embrittlement resistance.

Ghosh *et al.* [26] studied different types of precipitates formed during processing of IFHS steels and their effects on the final properties. Batch annealed IFHS steels (BA-IFHS) and continuous annealed IFHS steels (CA-IFHS) were used for the study of precipitates in various samples. Various types of precipitates were formed during various stages of processing of IFHS steels. These were: TiN, CuS, TiS , TiC, $Ti_4C_2S_2$, Fe(Ti+Nb)P/FeTiP, MnS, and FeTi. The precipitate TiN was formed during steel solidification and continuous casting. This precipitate was very stable having FCC structure. TiS precipitates formed during later stages of steel making and continuous casting. These sulphides dissolved during hot rolling process (900 ℃< T< 1200 ℃) and during coiling stage (600 ℃< T <700 ℃). Hence this rhombohedral TiS precipitate was observed rarely in BA-IFHS steel, rather it transformed into MnS and very often formed (Ti+Mn)S. But in CA-IFHS steel, free stable TiS precipitates were observed. The precipitate CuS usually formed in combination with other precipitates. $Ti_4C_2S_2$ precipitates were also observed in some cases having hexagonal structure. When the steels were reheated above 1200 ℃, these carbosulphides got dissolved in

the solution. There was always a competition between TiC (having face centred cubic (FCC) structure) and FeTiP (having orthorhombic crystal structure) precipitates during batch annealing process. Depending upon the amount of Ti and P in the IFHS steel, FeTiP became more stable than TiC and deteriorated the deep drawability of IFHS steel. The Nb content improved the stability of TiS. TiS might form without MnS in CA-IFHS in the presence of Nb.

Ghosh *et al.* [27] aimed to achieve a better strength–formability combination along with improved resistance to corrosion of Ti/Nb stabilized IF-steel through grain refinement by using controlled thermo-mechanical rolling route. The composition of Ti/Nb stabilized specimen included 0.0026% C, 0.14% Mn, 0.008% S, 0.031% P, 0.007%Si, 0.052% Al, 0.012% Nb, 0.042% Ti, 0.0021% N, and 99.7% Fe. The critical temperatures such as ferrite to austenite transformation start temperatutre (A_{r_1}) and ferrite to autenite transformation finish temperature (A_{r_3}) was obtained by using dilatometery tests in Gleeble-3800 thermomechanical simulator and found to be 974 K and 1133 K respectively. The recrystallization stop temperature (T_{nr}) was found to be 1243 K by using Boratto equation ($T_{nr} = 887 + 464C + (6445Nb - 644\sqrt{Nb}) + (732V - 230\sqrt{V}) + 890Ti + 363Al - 357Si$). Sample of dimension 30×24×10 mm was used for thermomechanically controlled rolling. The samples were homogenized at 1473 K for 1 h in order to dissolve all existing precipitates of Ti and Nb. Then multi-pass rolling (up to 50% and 80% total reduction in area (RA) obtained) was performed in three different regions- below A_{r_3} (at 923 K), between A_{r_1} and A_{r_3} (at 1073 K) and above T_{nr} (at 1323 K) as shown in Fig. 2.17. The samples rolled at 923 K were further annealed at 1123 K for 100 s to attain partially recrystallized grains of ferrite from highly deformed microstructure. The controlled rolling above A_{r_3} at 1323 K led to refinement in size of grain by fast recrystallization from deformed austenite and after that austenite to ferrite transition formed fine grains of average size of 32–37 μm. The rolling at 1073 K (where no recrystallization took place) formed fine grains ($\sim$5 μm) by austenite to ferrite transformation by cooling. The rolling at 973 K produced ultrafine grains because of deformation induced ferrite transformation (DIFT) and the formation of micro-shear bands. Also it was seen that the 80% rolled sample at 923 K temperature showed yield strength of 427 MPa and 27% elongation, while the 80% rolled sample at 1073 K produced 350 MPa yield strength and 30% elongation, and the 80% rolled sample at 1323 K produced 300 MPa yield strength and 33% elongation. The region behind it was that the ultrafine grains helps in

increasing yield strength but larger sized grains helps in increase in ductility. The controlled rolling at 923 K temperature provided increase in strength but decrease in formability. So, after rolling the annealing of sample at 1123 K temperature was done followed by 100 s soaking and then air cooling. With this annealing treatment, Fe(Ti+Nb)P precipitates dissolved, which deteriorates formability. Hence, this annealing treatment recovered formability without much sacrificing in strength. Also the same rolling route provided good corrosion resistance due to highly dense oxide film formation on the surface. Hence, rolling below Ar_1 temperature followed by short annealing treatment provided good combination of strength, ductility, formability combination along with improved corrosion resistance.

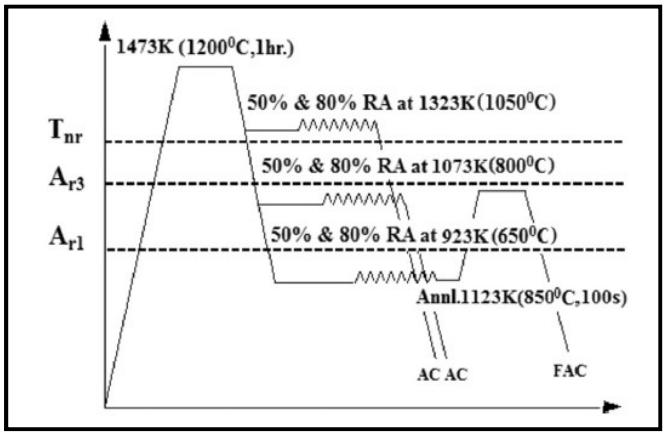

Figure 2.17: Schematic design of thermomechanical controlled rolling routes [27].

Zheng *et al.* [28] studied the influence of rate of cooling on the mechanical properties, microstructure, and crystallographic texture of continuously annealed IFHS steel. The chemical composition of the specimen used included 0.0015% C, 0.022% Si, 0.09% Mn, 0.0061 S, 0.015% P, 0.072% Ti, and 0.012% Nb. The continuous annealing cycles were performed which included heating the sample to 810℃, hold there for 180 s, followed by cooling to ambient temperature at different cooling rates (5, 50, 200, 500, and 1000 ℃/s) and then again heating to 240 ℃ and hold there for 120 s and then cooling by air to surrounding temperature (see Fig. 2.18). The yield strength (YS), r_m-value and Δr- value were greatly influenced by different cooling rates, while ultimate tensile strength (UTS), n-value, and elongation values were found to be little changed with change in cooling rates (see Fig. 2.19). YS increased with increase in cooling rates in the range of 5–1000 ℃/s. This was mainly due to the fact that the grain size decreased with increase in cooling rates. With decrease in grain size, YS increases according to Hall-Petch equation (see Eq. 5). The value also increased with increase in cooling rates except 500 ℃/s. At 500 ℃/s cooling rates, the lowest r_m-value

and Δr- value was achieved. This was due to the presence of different texture components in samples at different cooling rates.

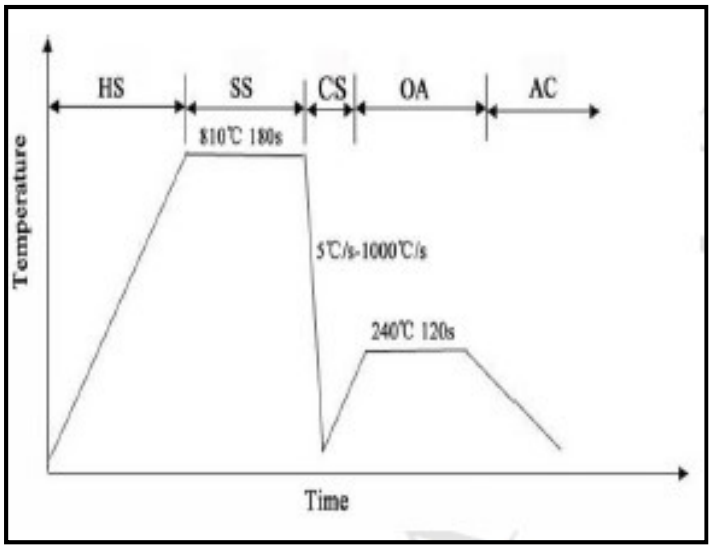

Figure 2.18: Continuous annealing cycle performed on IF-steel. (HS: heating section, SS: soaking section, CS: cooling section, OA: overageing section, and AC: Air cooling) [28].

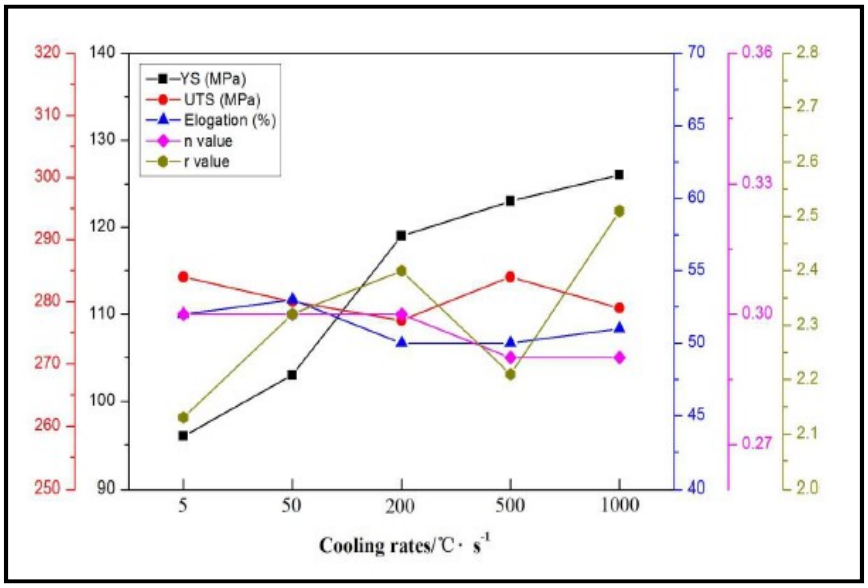

Figure 2.19: The influence of rates of cooling on the mechanical properties of IF-steel [28].

The main three textures components {111} <110>, {111} <112> and {011} <001> helps in increasing formability (r_m-value). But the texture component {011} <001> also increase earing defect (Δr- value), while other two had no effect on Δr- value. The intensity of texture component {111} <110> increased and the intensity of texture component {011} <001> decreased with increase in cooling rate from 5–1000 ℃/s. Also with the cooling rate of 5 ℃/s, the FeTiP precipitate formed, which deteriorate formability by reducing intensity of {111}

<110>, {111} <112> textures components. Hence sample with 5℃/s had low r_m-value. With higher cooling rates, the tendency to form FeTiP precipitates reduced, hence r_m-value increase with increase in cooling rates. But at 500 ℃/s, the sample had lower intensity of {011} <001> texture component. Hence, r_m-value was found to be lowest for cooling rate of 500 ℃/s. Then at 1000 ℃/s cooling rate the transition of {111} <112> to {111} <110> texture components again increased r_m-value.

Guo *et al.* [29] studied the influence of addition of phosphorus (P) on the properties of warm-rolled sheets of IF-steel. Two chemical compositions were taken viz Ti-IF composition (included 0.002% C, 0.008% Si, 0.16% Mn, 0.002% P, 0.004% S, 0.019% Al, 0.0029% N, 0.072% Ti) and Ti+P-IF composition (included 0.002% C, 0.005% Si, 0.16% Mn, 0.085% P, 0.0026% S, 0.023% Al, 0.0021% N, 0.065% Ti). The samples were initially austenized at 1050 ℃ for 2 hours followed by air cooling to 700 ℃ and then 90% total reduction in thickness was obtained by four passes during warm rolling in ferrite region. The finish rolling temperature of warm rolling was 560 ℃ and then air cooling of samples was done. After warm rooling, the samples were annealed at 750 ℃ for the soaking time of 3 hr. After annealing, it was found that both YS and UTS of Ti+P-IF-steel were increased, while elongation value, r-value and n-value decreased as compared to Ti-IF-steel as shown in Table 2.13.

Table 2.13: Mechanical properties of Ti-IF & Ti+P-IF-steel [29].

Steel	YS (MPa)	UTS (MPa)	Elonagtion (%)	n-value	r-value
Ti-IF	105	245	50	0.31	1.75
Ti+P-IF	165	325	40	0.25	1.38

The addition of P in the steel provided solid solution strengthening. Hence YS and UTS increased with the addition of P. But the decrease in formability (r-value), n-value and elongation was due to the fact that the adding P raised recrystallization temperature of the steel. Hence, in case of Ti+P-IF-steel, the recrystallization was not complete and resulted in long and narrow grains after annealing (see Fig. 2.20b). But Ti-IF-steel exihibited proper recrystallized grains in its microstructure (see Fig. 2.20a). Also the formation of FeTiP in Ti+P-IF-steel deteriorates formability and elongation values of steel by reducing the intensity of {111} texture component essential for better formability. Fig. 2.21a–b showed TEM micrograph EDS analysis of FeTiP in Ti+P-IF-steel.

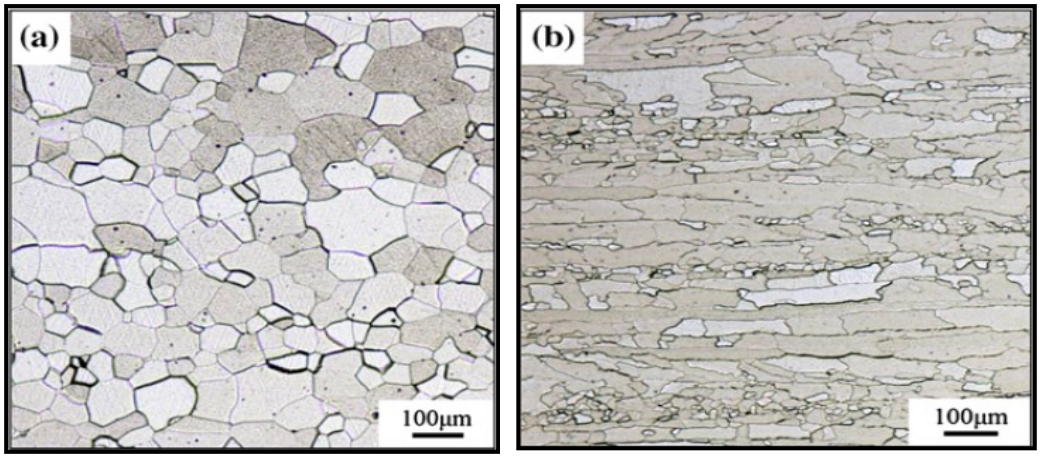

Figure 2.20: Microstructures of annealed samples of (a) Ti-IF-steel (b) Ti+P-IF-steel [29].

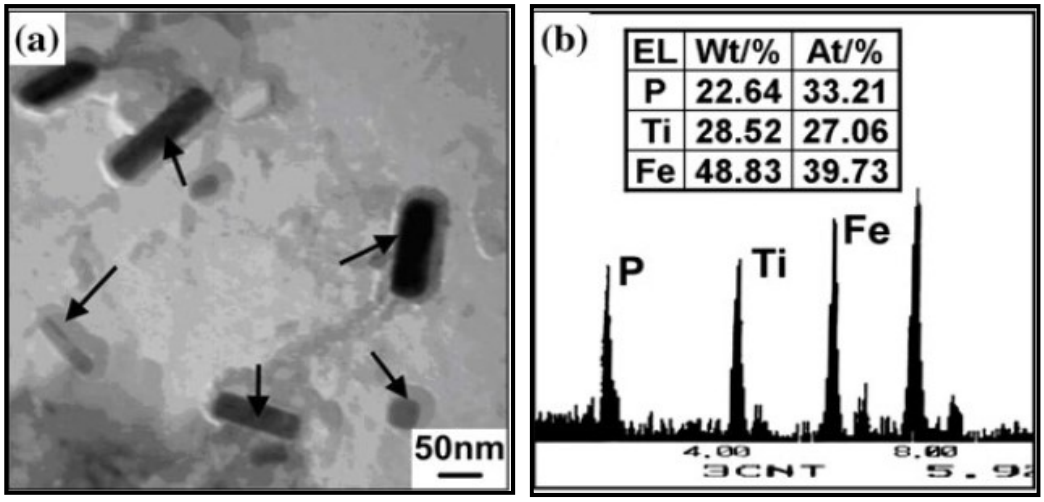

Figure 2.21: (a) TEM micrograph showing FeTiP precipitate in Ti+P-IF-steel (b) EDS analysis confirms the peaks of Fe, Ti, and P in the precipitate [29].

Majumdar *et al.* [30] investigated the mechanism of fatigue failure in IF and IFHS steel sheets. Two chemical compositions were taken for the study viz IF (contained 0.0035% C, 0.079% Mn, 0.0089% S, 0.0109% P, 0.006% Si, 0.0359% Al, 0.067% Ti, 0.003% N) and IFHS (0.004% C, 0.58% Mn, 0.007% S, 0.053% P, 0.008% Si, 0.026% Al, 0.055% Ti, 0.022%Nb,0.0008–0.0010% B, 0.003% N). Then fatigue tests were performed by taking the stress amplitudes below and above the endurance limits of steels (143 and 173 MPa for IF and IFHS steel respectively). It was found that below endurance limit, microcracks initiated only at inclusions for both steels, while above endurance tests, these cracks were initiated at ferrite grain boundaries and within slip bands along with at inclusions. The extent of microcracks was found to be different in both steels. For IF-steel, the abundance of microcracks were found at grain boundaries above endurance limit, while in case of IFHS

steel, only few isolated microcracks were found. Also in case of IF-steel, the fatigue cracks were initiated and propagated largely through grain boundaries due to the lesser cohesive strength of grain boundaries due to depletion caused by interstitial atoms. In case of IFHS steel, the fatigue failure occurred from microcracks present within slip bands. The propagation of fatigue cracks was found to be intergranular in case of IF-steels and transgranular in case of IFHS steel (see Fig. 2.22a–b). In IFHS steel, boron (B) and niobium (Nb) segregated at grain boundaries reduced the tendency of failure at grain boundaries.

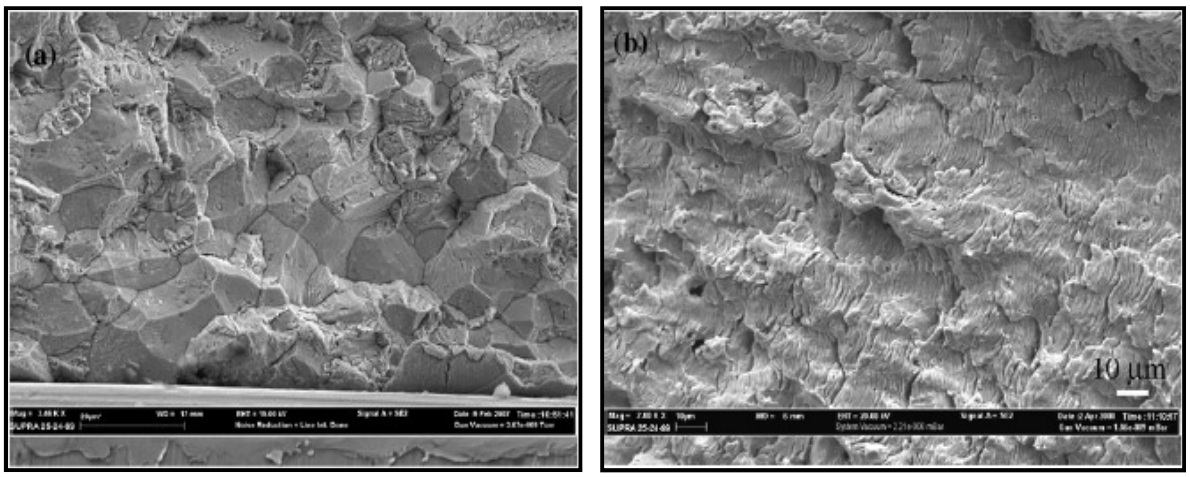

Figure 2.22: Fatigue failure in (a) IF, (b) IFHS steel [30].

Ghosh *et al.* [31] determined the crystal structure of precipitate FeTiP in a few interstitial free high strength steels. Three chemical compositions were taken for the study- among them two were Ti-Nb stabilized compositions and the third was Ti-stabilized composition. Table 2.14 shows the chemical compositions.

Table 2.14: Chemical composition of Ti-Nb and Ti-stabilized steels used [31].

Steel	C	Mn	P	Ti	S	Nb	N
Ti + Nb-IFHS steel 1	0.004	0.84	0.091	0.07	0.007	0.03	0.003
Ti + Nb-IFHS steel 2	0.004	0.50	0.058	0.041	0.007	0.018	0.0038
Ti-IFHS	0.002	0.39	0.040	0.041	0.007	–	0.0036

Ti-Nb stabilized compositions were given batch annealing cycle which included heating the sample to 700 ℃ followed by soaking of 20 h and then furnace cooling to room temperature. But Ti-stabilized composition was annealed at 700 ℃ for 15 min. Then after annealing the study of precipitates was done in Philips 200 TEM and EDS was carried out for all the

precipitates to find the composition of precipitates. The study of FeTiP- type precipitates was done in this paper. Fig.2.23a–b and 2.24a–b shows TEM and EDS analysis indicating the presence of Fe(Ti+Nb) precipiate in Ti+Nb stabilized steel 1 and steel 2 composition. The presence of FeTiP in Ti-stabilized steel is shown in Fig. 2.25a–b. Both precipitates Fe(Ti+Nb) and FeTiP were found to be orthorhombic in structure. The unit cell dimensions for FeTiP precipitate was– a = 5.816–5.821 Å, b = 3.731–3.745 Å and c = 6.554–6.569 Å.

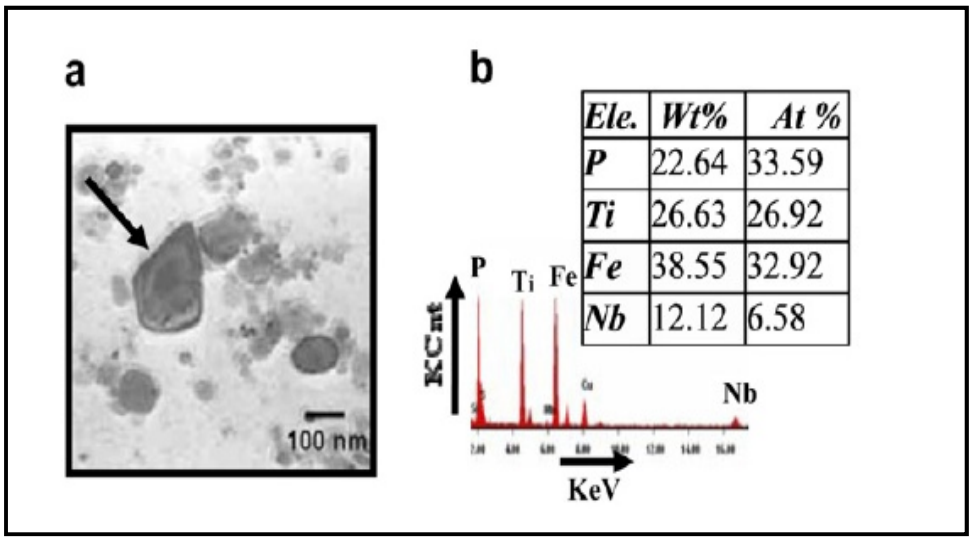

Ele.	Wt%	At %
P	22.64	33.59
Ti	26.63	26.92
Fe	38.55	32.92
Nb	12.12	6.58

Figure 2.23: (a) TEM characterization shows Fe(Ti + Nb)P precipitate in Ti + Nb-IFHS steel 1, (b) EDS analysis confirms the precipiate [31].

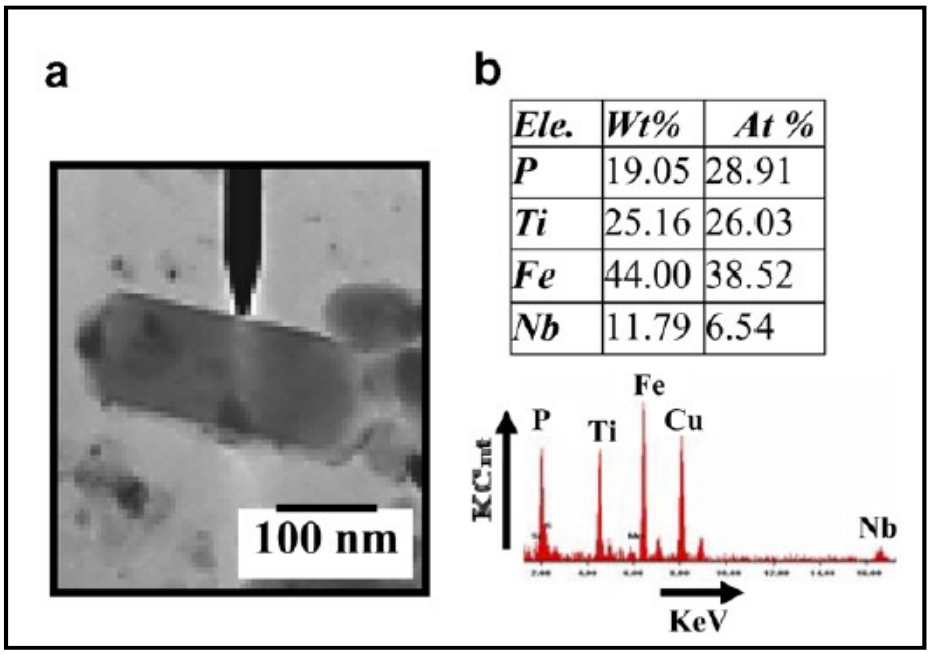

Ele.	Wt%	At %
P	19.05	28.91
Ti	25.16	26.03
Fe	44.00	38.52
Nb	11.79	6.54

Figure 2.24: (a) TEM characterization shows Fe(Ti + Nb)P precipitate in Ti + Nb-IFHS steel 1, (b) EDS analysis confirms the precipiatate [31].

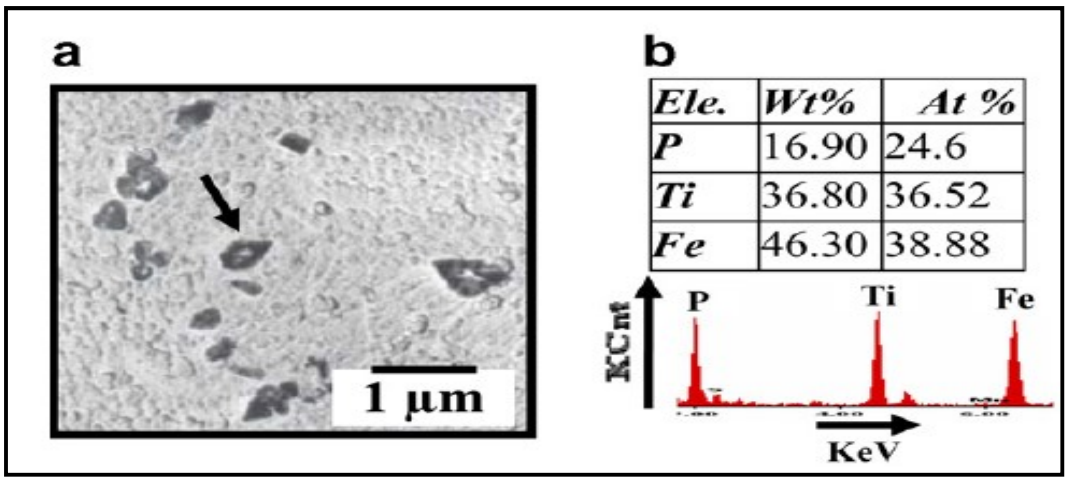

Figure 2.25: (a) TEM characterization shows FeTiP precipitate in Ti-IFHS steel annealed at 700°C with soaking time of 15 min, (b) EDS analysis confirms the precipitate [31].

Nb in FeTiP precipitate did not affect the crystal structure, but it tended to increment in the unit cell dimensions, as the unit cell dimensions for Fe(Ti-Nb) precipitate was– a = 5.939–6.105 Å, b = 3.800–3.817 Å and c =7.151–7.171 Å.

Ghosh *et al.* [32] investigated the precipitation formation characteristics and formation of texture in continuously annealed IFHS steel compositions. Two chemical compositions were used for the study viz Ti-stabilized composition (included 0.0040% C, 0.38% Mn, 0.009% Si, 0.007% S, 0.048% P, 0.043% Al, 0.035% Ti, 0.001% Nb, and 0.0028% N) and Ti-Nb-stabilized composition (included 0.0035% C, 0.37% Mn, 0.011% Si, 0.007% S, 0.048% P, 0.044% Al, 0.040% Ti, 0.046% Nb, and 0.0030% N). Ti-stabilized steel was hot rolled with finishing rolling temperature (FRL) of 892 ℃ and coiling temperature (CT) of 572 ℃ followed by cold rolling and annealing at 833 ℃. Ti-Nb stabilized sample was hot rolled with FRL of 887 ℃ and CT of 570 ℃ followed by cold rolling and annealing at 828 ℃. After annealing the study of precipitates was done on TEM and EDS. TiN, TiS, and TiC were the main precipitates in both compositions. But the large sized and less frequent TiN precipitates were found in case of Ti-Nb steel as compared to Ti- steel. This was mainly due to Nb element in the Ti-Nb composition, which increased the effective solute concentration of Ti in the solid solution, and hence TiN observed during initial steel making stages and got coarsened in later stages. MnS precipitates were also found in case of Ti-steel, but not in Ti-Nb steel. Because Nb promoted the formation of TiS precipitate over MnS precipitate. The precipitates of Nb found sometimes along with Ti precipitates in small amounts, remaining Nb remained in the solid solution. Nb helped in coarsens the carbides precipitates also. Nb

did not helped in improvement of r_m-value. But the absence of Nb produced many finer carbides precipitates. Hence, many nucleation sites available for (111)<110>oriented grains in the texture improved r_m-value.

Saha *et al.* [33] investigated the effect of double cold rolling and annealing on the formation of texture and properties of Ti/Nb stabilized IF-steel. The chemical composition of Ti/Nb steel included 0.003% C, 0.36% Mn, 0.006% S, 0.014% P, 0.012% Si, 0.047% Al, 0.0033% N, 0.011% Nb, and 0.05% Ti. The steel was subjected to hot rolling up to 80% reduction by continuous passes with FRL of 964 ℃, followed by 90% cold rolled and then annealed at 720 ℃ for 27 h. Then after annealing, again 65% cold rolling was done followed by annealing at 650 ℃ for 90 min. After first cold rolling, the textures contained γ-fibres, α-fibres, and rotated cube component {100}<011>. Then after first annealing, γ-fibres got sharpened and rotated cube component disappeared. But γ-fibres were not uniform in this annealed sample. Then again intensity of γ-fibre was increased by second cold rooling, but non-uniformity was still present there. But after second annealing, very sharp and uniform γ-fibres were found and no α-fibre or other component present in it. The uniformity in γ-fibres was mainly due to uniform grain size distribution and very high low-angle grain boundary fraction. The presence of highly intense and uniform γ-fibres helped in increasing the deep drawability of Ti-Nb steel and made steel free from earing defect.

Capdevila [34] studied the influence of microalloyed elements (Ti and Nb) on the recrystallization texture of warm-rolled IF-steels. Three warm rolled IF-steels were taken viz Ti-stabilized IF (IF-Ti), Ti and Nb stabilized IF (IF-TiNb), and high strength IF (IF-HR). Table 2.15 shows the chemical compositions of these steels.

Table 2.15: Chemical composition of studied steels [25].

Steel	C	Mn	P	Ti	S	Nb	N	Al
IF-Ti	0.0039	0.009	0.007	0.079	0.006	0.001	0.0043	0.028
IF-TiNb	0.0018	0.014	0.012	0.014	0.01	0.017	0.0021	0.027
IF-HR	0.0077	0.409	0.031	0.118	0.015	0.001	0.0026	0.044

The hot rolling pilot was used for thermomechanical simulation. The samples were reheated to 1373 K in austenitic region, then two roughing routes were performed-one is at 1373 K and another is at 1323 K with the deformation level of 35%. After this 40% deformation was given in austenitic domain (at 1273 K) followed by ferritic rolling was performed at 973K

with deformation level of 53%. After this steel was reheated at 1023 K, then recrystallization was observed by interrupted cooling cycles with time in the range of 30–5400 s. In IF-Ti steel, TiC and $Ti_4C_2S_2$ precipitates were observed, while in IF-TiNb steel, precipitates (Ti+Nb)(C,N) and Fe(Ti+Nb)P and in case of IF-HR, FeTiP precipitates were observed. As the microalloying content increased, the delay in the kinetics of recrystallization increased. This was mainly due to solute drag phenomena. Hence IF-Ti steel had faster kinetics of recrystallization, after this IF-TiNb and at last IF-HR steel. EBSD (Electron backscatter diffraction) analysis showed the presence of sub-grains in the warm-rolled IF and IF-HR steels. This indicated that the recovery process occurred during warm-rolling process was dynamic. Fig. 2.26a–d shows the EBSD analysis of IF-HR sample shows the sub-grains presence, sizes of sub-grains, boundaries of sub-grains, and histogram showing misorientation in the as-quenched structure.

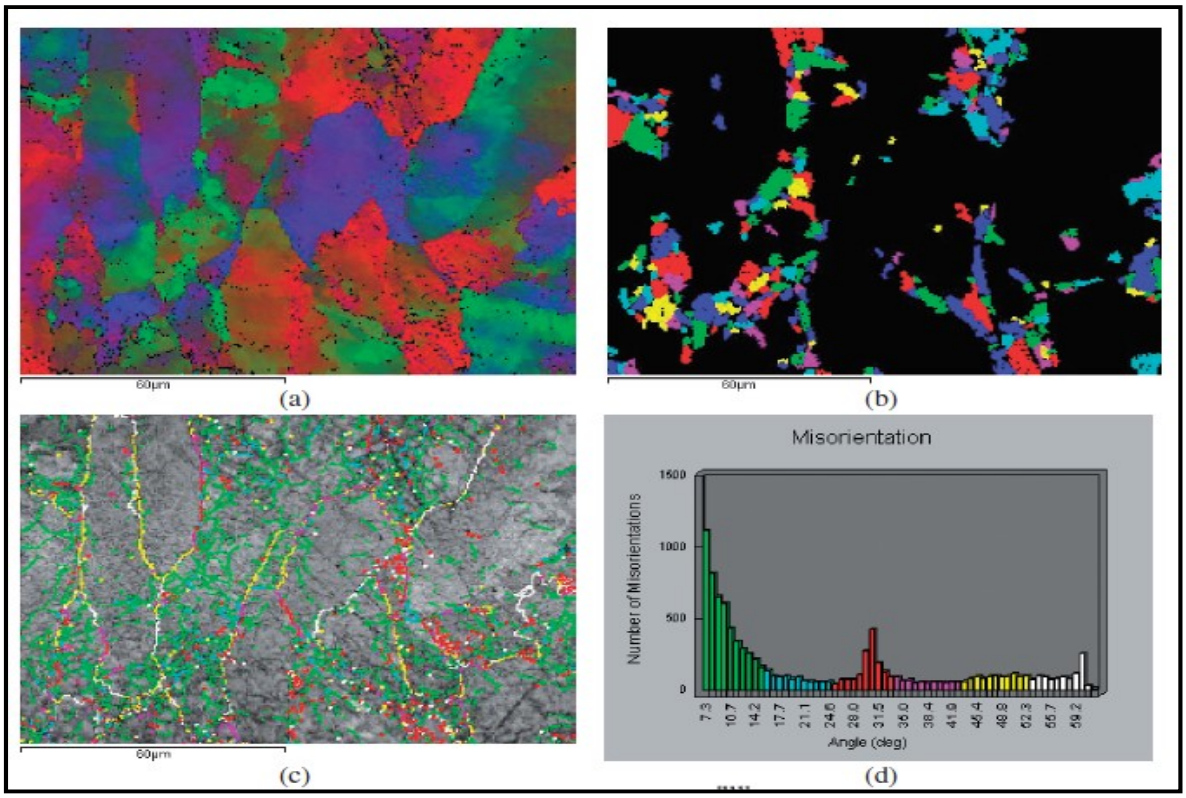

Figure 2.26: EBSD analysis shows (a) presence of sub-grains, (b) sizes of sub-grains, (c) boundaries of sub-grains and (d) histogram regarding misorientation in as-quenced microstructure of IF-HR sample [34].

The recrystallization mechanism for IF-HR steel was found to be grain-boundary nucleation, while in case of IF-Ti and IF-TiNb samples, continuous recrystallization of grains occurred in shear bands was the recrystallization mechanism. The formation of FeTiP precipitate in case

of IF-HR degrades the {111} texture gave rise to poor texture and deteriorates both strength and formability. This was due to the fact that removal of some P from the matrix as FeTiP reduced the solid solution strengthening effect. Also, FeTiP precipitate scavanged Ti, so less Ti atoms were left for stabilization of interstitial elements (C, N), and hence reduced formability

Choi *et al.* [35] investigated the influence of precipitation on the recrystallization behaviour of extra low carbon steels. Two low carbon steel compositions was used differ mainly in Ti content. These were steel A (consisted of 0.0068% C, 0.099% Mn, <0.001% P, 0.013% S, 0.038% Al, 0.026% Ti, and 0.0008% N) and steel 2 (consisted of 0.0070% C, 0.10% Mn, <0.001% P, 0.013% S, 0.053% Al, 0.082% Ti, and 0.0010% N). The samples were hot rolled with FRL of 930 ℃ up to 3 mm thickness and then cold rolled to a 0.8 mm final thickness. Then the samples were given recrystallization annealing in the range of 500–800 ℃ for 120 s in the salt bath and then water quenched. The recrystallization behaviour of two steels was found to be different. The recrystallization temperature of Steel B was found to be higher than that of steel A, as steel B had more Ti content. Because in case of steel B, precipitation of fine TiC precipitates were not found to be in equilibrium, especially in the region of ferrite and rest of Ti solute got precipitated during recrystallization annealing process. The recovery of dislocations dynamically interacted with the precipitation of fine TiC particeles and retarded the recrystallization of steel B. But in case of steel A, no addition TiC was found, which retards the recrystallization process. Hence steel B had higher recrystallization temperature than steel A.

Song *et al.* [36] investigated the influence of grain boundaries segregation of phosphorous (P) on the mechanical properties of titanium stabilized IF-steel after annealing. Ti-stabilized IF-steel was used for the study which consisted of 0.0028% C, 0.08% Si, 0.34% Mn, 0.04% P, 0.005% S, and 0.04% Ti. The samples were received in cold-rolled condition and then annealed at 810 ℃ for 90–600 s in the atmosphere of 80% N_2 and 20% H_2 followed by air cooling. It was found that the recrystallization was completed only after annealing at 810 ℃ for 180 s. The recystallisation process was not complteted in the samples with holding time in the range of 90–180 s. With the increase in holding time from 180 to 600 s, the yield strength decreased from 158.1 to 141 MPa, the tensile strength decreased from 354.9 to 322.7 MPa, and also $\bar{r}$ decreased from 2.098 to 1.688, while there was increase in n value from 0.2376 to 0.3046. These observations was only due to the fact that number of phosphorous atoms

segregated at grain boundaries increased with increase in holding time (see Fig. 2.27). When the content of P increased at grain boundaries, then it became easier for P to react with Ti and Fe to form FeTiP, which reduced strength and ductility. Also, fine Fe_3P precipitates found in the matrix, which delayed the process of recrystallization and reduced the intensity of {111} texture, as a result of which $\bar{r}$ value got lowered.

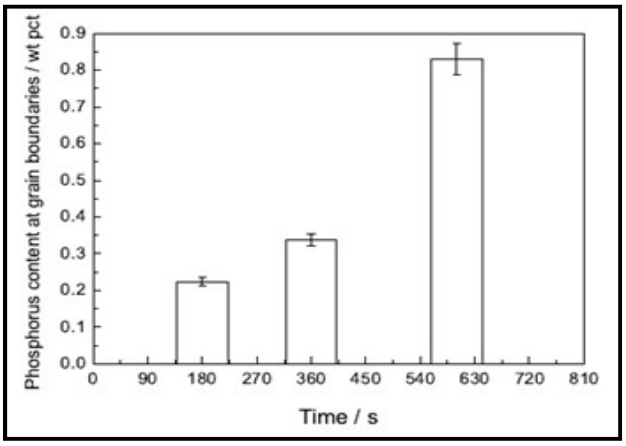

Figure 2.27: Phosphorous content at grain boundaries for sample annealed for different time [36].

2.3 Summary of the reviewed literature

This chapter reviewed the work done by various researchers in the field of interstitial free (IF) and interstitial free high strength (IFHS) steels.

- Several authors have worked to determine the effect of processing parameters on the precipitation behavior of IF and IFHS steels. TiC, TiN, MnS, TiS, FeTiP, and NbC are reported to be the main precipitates observed in IF and IFHS steels. The authors have mainly investigated the formation of FeTiP precipitates in IFHS steels as its formation deteriorates the formability of IFHS steels [9, 16, 17, 19, 20, 22–27].
- Several authors have worked to improve upon the mechanical properties of IF and IFHS steels (especially formability characteristics) by varying the processing parameters i.e. rolling parameters, annealing temperature, soaking time, heating and cooling rates [8, 11, 14, 18, 19, 24].
- A few authors have reported about discontinuous yielding phenomenon in tensile stress-strain curves of IF and IFHS steels. The authors have reported that the size of grains has a profound effect on the yielding phenomenon of IF and IFHS steels [12, 13].
- Some authors have investigated the influence of micro-alloying additions (Ti, Nb, Cu, Ni, Al, P etc.) on the precipitation behavior and resulting properties of IF and IFHS steels [9, 10, 13, 15, 16, 20, 25, 27].

2.4 Gaps in the existing literature

A lot of work has been done on IF and IFHS steels by various researchers to improve their properties. However, there are still some areas where further work needs to be done. These gaps in literature are given below:

- Though efforts have been done by researchers to enhance the strength of IF/IFHS-steels along with good formability, but strength levels beyond 500 MPa have not been achieved yet in this category of steels. Further, any improvement achieved in strength by various researchers has come at the expense of deterioration in formability. As a result, there is a need to optimize the various processing parameters during thermo-mechanical processing and/or alloy additions in such a way that higher strength levels can be achieved without much loss in formability.
- The addition of Ti and Nb in sufficient amount in IFHS steels makes their processing costly. There is a need to work on steel compositions containing low Ti and low Nb and to optimize their annealing cycles in such a manner that properties do not deteriorate.
- Efforts have been done by authors to enhance the strength levels of IF-steels through addition of phosphorous. However, addition of phosphorous can raise the ductile-brittle transition temperature resulting in cold work embrittlement (CWE). To reduce this tendency of CWE in presence of phosphorous, authors have used alloy additions of niobium, boron etc. in IFHS steels. Addition of these alloying elements viz. niobium, boron etc. impairs cost-effectiveness. Also, it is reported that addition of boron, can result in yield point elongation and thus presence of stretcher marks on the surface of steel. Work is not reported on thermo-mechanical processing routes to eliminate these problems.
- Most of the literature reported on stabilization of interstitial elements (C, N) pertains to the addition of Ti and Nb elements. The role of other elements like Al etc. addition on the stabilization has not been reported much.
- Most of the authors have reported occurrence of continuous yielding behaviour in IF/IFHS steels during tensile testing. A few authors have discussed about the discontinuous yielding behaviour in these steels during tensile testing. However, despite discontinuous yielding behaviour, these authors have not reported about presence/absence of Lüders bands formation (stretcher strains marks) in IF/IFHS steels. Further investigations with regards to this aspect are required.

Chapter 3

Design of the Study

3.1 General

This chapter presents the formation of research objective in the light of limitations in the existing literature. The chapter also discusses the details of starting materials to be used for the research work, the key issues, and general methodology. In addition to this, the details of equipment and machines used for research work have been provided.

3.2 Establishment of the objective function

IF/IFHS-steels generally shows continuous yielding phenomenon during tensile deformation because of the absence of free interstitial elements (C and N) in solid solution [23, 37, 38]. A few authors have reported that grain refinement strengthening in IF and IFHS steels may cause discontinuous yielding during tensile deformation, but no literature has been presented regarding yield point elongation or Lüders band formation in IF and IFHS compositions [21, 38–42]. Further, the effect of stabilizing elements (Ti, Nb, and Al) and annealing parameters on the formation/absence of Lüders bands in IFHS composition have not been reported. The amount of precipitates of stabilizing elements (Ti, Nb and Al) formed with interstitial elements (C and N) mainly depends on the amount of stabilizing elements in the composition and also on the annealing parameters. Hence, chemical composition and annealing parameters are the main factors that decide if there will be any free interstitial elements remaining in the solid solution or not, which ultimately affects the yielding phenomenon (continuous or discontinuous) of IF and IFHS steels. The present study investigates the influence of chemical composition and annealing parameters on the precipitation behaviour during processing of IFHS steels and then correlates it with Lüders band formation in IFHS composition.

3.3 Objective function

The overall objective of the present research was investigating "*the synergistic influence of chemical composition and industrial annealing processes on Lüders bands formation in interstitial free high strength steel*."

The present work aims to work on the following key issues:

- Investigating the effect of industrial annealing processes, (i) batch annealing furnace (BAF), and (ii) continuous annealing line (CAL) on the stabilization of interstitial elements (C and N) by stabilizing elements (Ti, Nb, Al).
- Investigating the relation between the precipitation behaviour and Lüders bands formation in IFHS compositions.
- Investigating the average sizes and shapes of precipitates formed during various annealing processes.
- Investigating the amount of Lüders strain (yield point elongation) present in tensile stress-strain curves of each chemical composition subjected to various annealing processes.
- Investigating the mechanical properties (YS, $\bar{r}$-value, Δr value) of chemical composition showing no Lüders band formation during tensile deformation after subjected to some optimum annealing process.

3.4 Experimental procedure

The experimental procedure used in the present work is shown in Fig. 3.1.

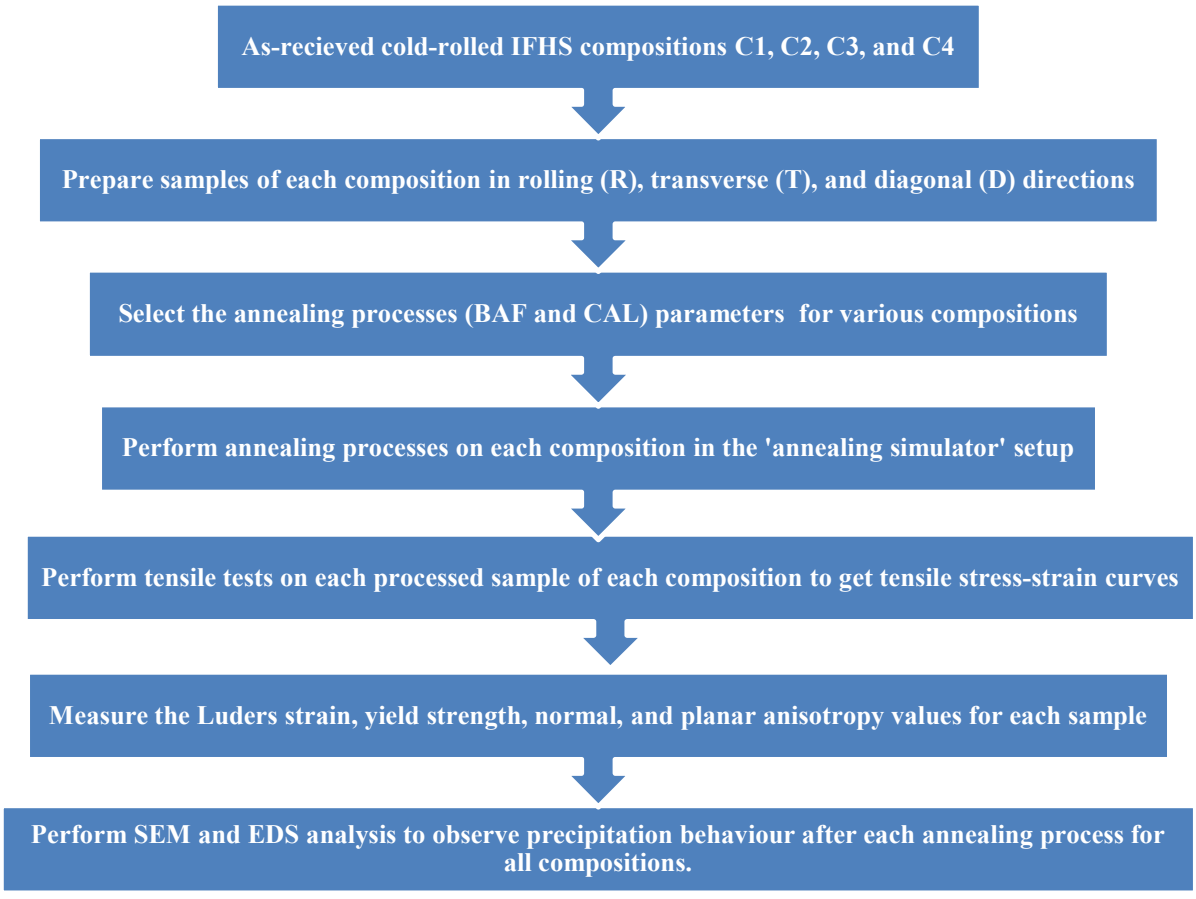

Figure 3.1: Experimental procedure used in the present research.

3.5 Materials selection

Industrially processed cold rolled IFHS steel sheets of compositions as shown in Table 3.1 were received with 67% thickness reduction and the final finished thickness of 0.78 mm. Four different IFHS compositions were used in this study to understand the role of various stabilising elements (viz. Ti, Nb, and Al) on the stabilization of interstitial elements (viz. C, N, and S) present in the given steels. The various chemical compositions included Ti-stabilized IFHS, Ti-Nb stabilized IFHS, low Ti-low Nb IFHS, and high Ti-low Nb IFHS. These steel compositions were designated as C1, C2, C3, and C4 respectively (see Table 3.1). Composition C4 (the high Ti-low Nb) also contained higher aluminium content than the other compositions. The critical (minimum) amount of Ti and Nb required for complete stabilization of all interstitial elements can be estimated empirically as given in Eqs. 3.1–3.2 [43–45].

$$\mathrm{Ti(stab)} = 3.42\mathrm{N} + 1.5\mathrm{S} + 4\mathrm{C} \quad \text{.....(3.1)}$$

$$\mathrm{Nb(stab)} = 7.74\mathrm{C} \quad \text{.....(3.2)}$$

Further, the excess/deficient amount of Ti and Nb (refered here as Ti* and Nb*) in any composition for complete stabilization of interstitial atoms is given as Eqs. 3.4–3.5 respectively [43–45].

$$\mathrm{Ti^*} = \mathrm{Ti_{total}} - \mathrm{Ti(stab)} \quad \text{.....(3.4)}$$

$$\mathrm{Nb^*} = \mathrm{Nb_{total}} - \mathrm{Nb(stab)} \quad \text{.....(3.5)}$$

Here, $\mathrm{Ti_{total}}$ and $\mathrm{Nb_{total}}$ represent the amount of titanium and niobium respectively present in the steel composition. A positive value of Ti*(or Nb*) shows that excess amount of Ti(or Nb) is present in steel composition than is required for complete stabilization of interstitials. Similarly, a negative value of Ti*(or Nb*) shows deficiency of Ti(or Nb) in the composition. Table 3.1 presents the chemical composition and other details of the four IFHS steels used in the present work.

3.6 Calculation of A_{c_1} and A_{c_3} temperatures

For the selection of subcritical annealing temperature for all the compositions, there was a need to predict A_{c_1} and A_{c_3} temperatures. Subcritical annealing was to be conducted below the A_{c_1} temperature. A_{c_1} and A_{c_3} temperatures for various chemical compositions were

predicted using 'Thermo-Calc software' (Thermo-Calc 3.0; Thermo-Calc software AB, Stockholm, Sweden) as shown in Fig. 3.2a–d.

Table 3.1: Composition of various IFHS steels along with the calculated minimum alloy addition required for interstitial element stabilization.

Weight percentage of chemical constituents (wt. %) present in various compositions												
Designation for various steels	C	Mn	P	S	Al	N	Nb	Ti	Min Ti (Stab)	Ti*	Min Nb (Stab)	Nb*
C1	0.003	0.45	0.046	0.008	0.045	0.0028	--	0.042	0.0335	0.0084	--	--
C2	0.002	0.62	0.032	0.006	0.035	0.0030	0.016	0.064	0.0272	0.0367	0.0155	0.0005
C3	0.003	0.51	0.048	0.008	0.060	0.0015	0.020	0.022	0.0291	-0.0071	0.0232	-0.0032
C4	0.003	0.50	0.031	0.005	0.120	0.0016	0.014	0.064	0.0277	0.0362	0.0286	-0.0146

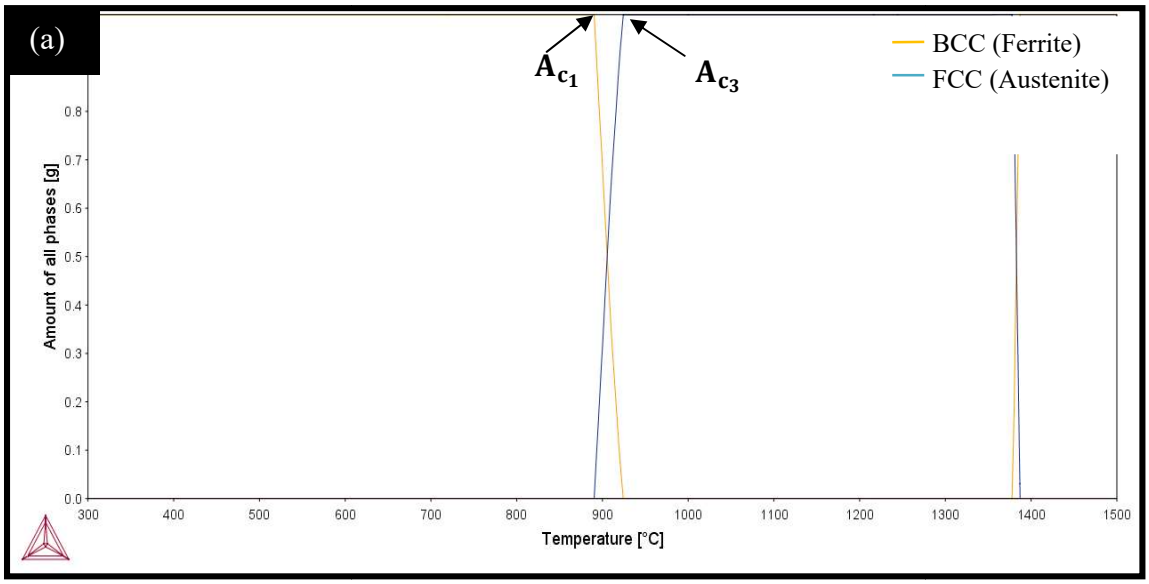

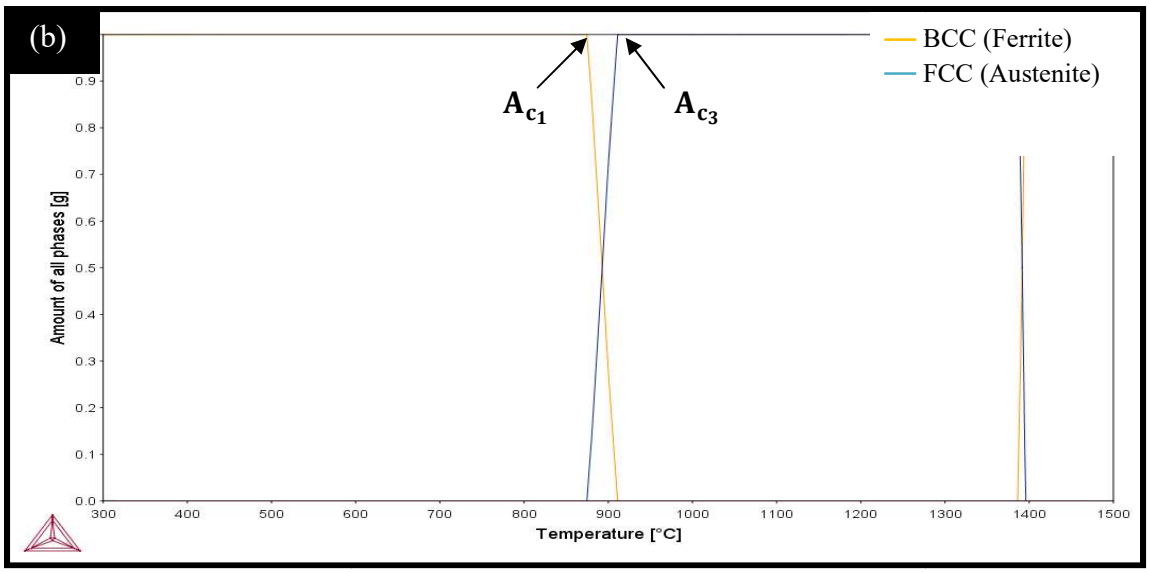

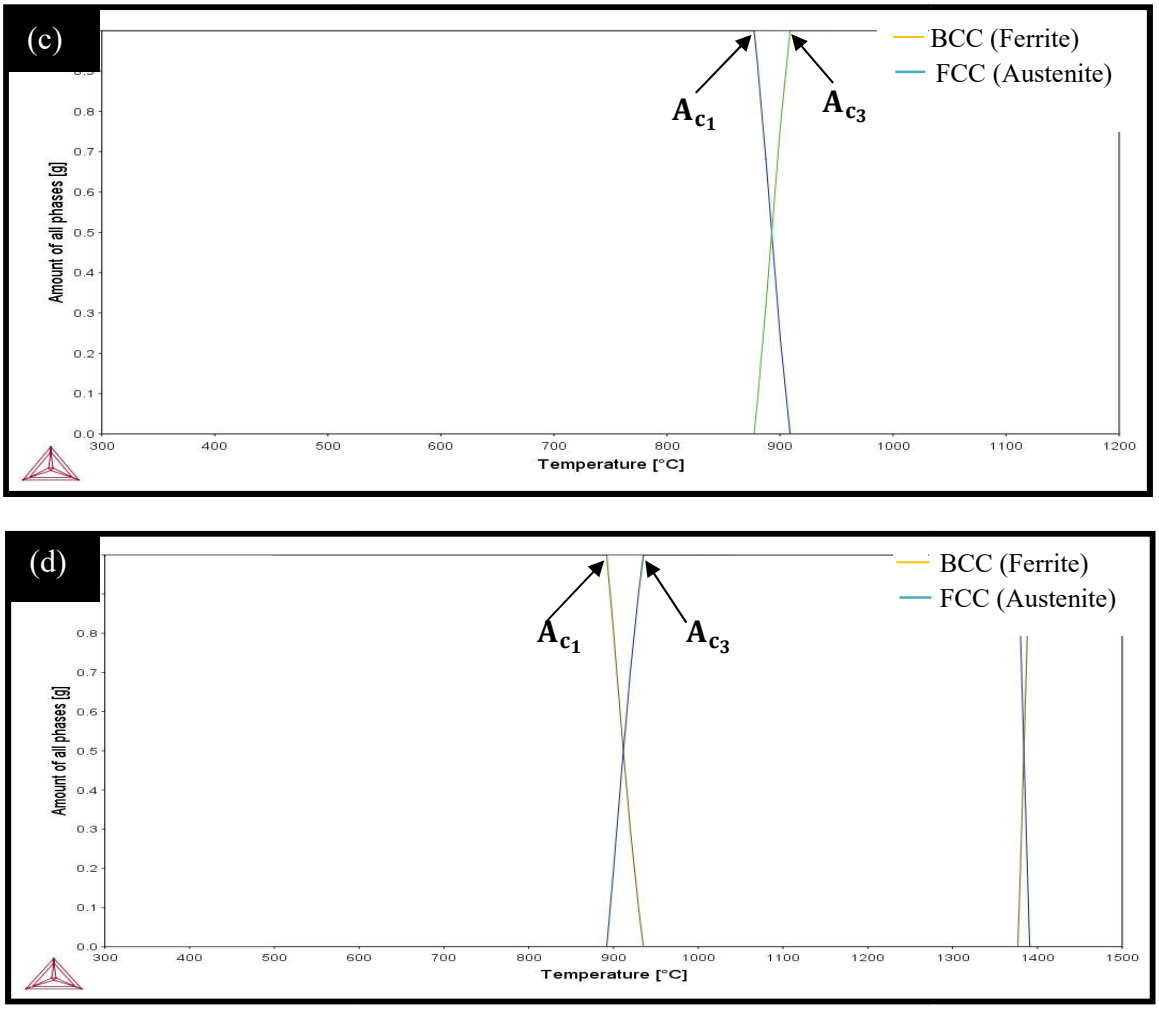

Figure 3.2: Phase fraction diagrams developed using Thermo-Calc for A_{c_1} and A_{c_3} temperatures of (a) C1, (b) C2, (c) C3, and (d) C4 composition.

The predicted A_{c_1} and A_{c_3} temperatures are shown in Table 3.2.

Table 3.2: Values of A_{c_1} and A_{c_3} for C1, C2, C3, and C4 compositions predicted by Thermo-Calc software.

Type of steel	Lower critical temperature, A_{c_1} (°C)	Higher critical temperature, A_{c_3} (°C)
C1	889	921
C2	876	912
C3	877	909
C4	892	935

3.7 Prediction of annealing parameters

Industrially followed BAF and CAL processes were performed on all compositions. Subcritical annealing processes were done, in which annealing temperature remained below A_{c_1} temperature. Batch annealing at 600–800 °C after cold-rolling is a widely used industrial

practice [30, 46]. Bhagat et al. [23] performed BAF process on IFHS steel composition at 710 °C. Banarjee et al [47] showed that BAF process at 700 °C with heating rate of 60 °C/hr and soaking time of 1 h provided better texture and formability in IFHS composition. Similarly, Zhang et al. [48] performed BAF processes at 650, 700, and 750 °C on IFHS composition. Hence the BAF processes were chosen in the range of 600–800 °C on the basis of annealing parameters used by various researchers. The CAL process parameters were chosen on the basis of CAL parameters performed by Kang et al. [19] with the some modifications.

3.7.1 Batch and continuous annealing process

Steel samples of various compositions (C1–C4) were subjected to BAF and CAL process as per the process parameter details presented in Table 3.3. These process parameters represent the typical industrial production process parameters for BAF and CAL processes [19, 23, 30, 46–48]. The schematic illustration of BAF and CAL process simulations are shown in Fig. 3.2a–b.

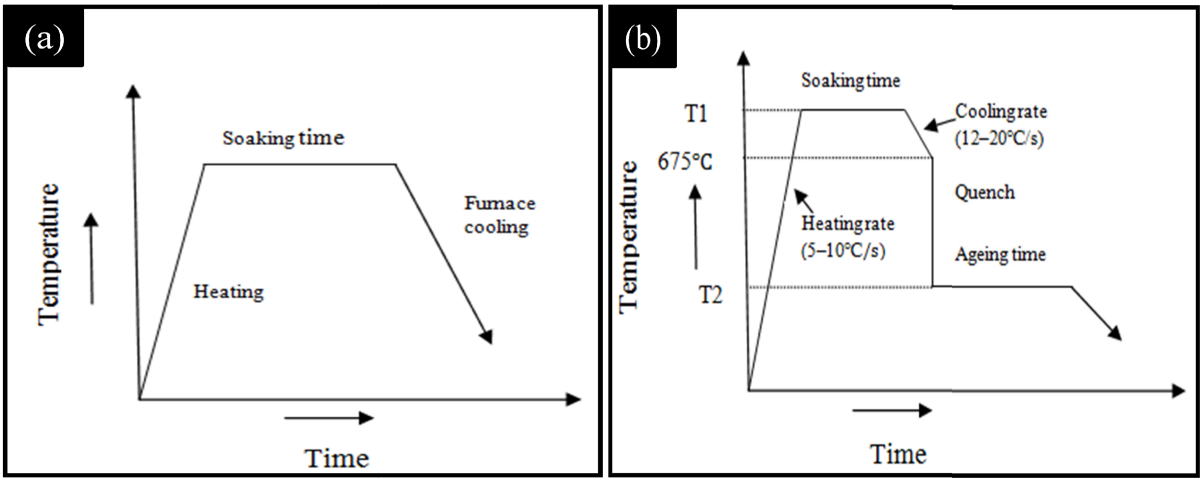

Figure 3.3: Schematic representation of Industrial Annealing process of (a) Batch annealing furnace, and (b) continuous annealing line process used in the present work.

3.8 Machines and equipment used

The section describes the main characteristics and details of the machines and equipment used in the present research work.

3.8.1 Annealing simulator

Annealing simulator is a set-up used for the annealing of samples. This is a custom designed set-up (see Fig. 3.3) developed jointly by CSIR-NML and Tata Steels, Jamshedpur. In this simulator, the samples can be annealed under an inert environment. This inert environment is provided by purging a mixture of N_2 and H_2 gases into the simulator.

Table 3.3: Process parameters for BAF and CAL processes [19, 23, 30, 46–48].

• **Composition: C1 (Ti-stabilized) and C2 (Ti-Nb stabilized) compositions**				
1. Accelerated BAF simulation				
Annealing process	***Heating rate*** *(℃/h)*		***Annealing temperature*** *(℃)*	***Soaking time*** *(min)*
BAF-1	180		710	30
BAF-2	180		740	30
2. CAL process				
Annealing process	***T1****(℃)*	***Soaking Time*** *(s)*	***T2****(℃)*	***Ageing Time*** *(s)*
CAL-1	810	50	330	30
CAL-2	810	50	330	60
• **Composition: C3 (lowTi-lowNb) and C4 (Al added to high Ti-low Nb) compositions**				
1. BAF Industrial simulation				
Annealing process	***Heating rate*** *(℃/h)*		***Annealing temperature*** *(℃)*	***Soaking time*** *(min)*
BAF-3	60		680	60
BAF-4	60		710	60
BAF-5	60		730	60
2. CAL process				
Annealing process	***T1****(℃)*	***Soaking Time*** *(s)*	***T2****(℃)*	***Ageing Time*** *(s)*
CAL-3	810	50/60	330	120
CAL-4	830	60	330	120

This simulator can be used for both types of annealing processes, i.e. batch annealing (BAF) and continuous annealing (CAL). The annealing simulator provides controlled heating and cooling rates. The purging of gas mixture prevents oxidation of samples during heating and also provides controlled and high cooling rates during the cooling step. The annealing simulator consists of following subsystems:

(a) Heating system

The high speed heating system is provided in the annealing simulator. The furnace is provided for heating purpose. The heating can be provided to a maximum temperature of 1200 ℃. The heating chamber is provided in the simulator. This heating chamber is inserted into the furnace for heating to require annealing temperature. For BAF process, the samples are directly placed in the heating chamber and then heating chamber is inserted into the furnace. But in case of CAL cycle, one more chamber has to connect to

the other end of heating chamber. This chamber is known as cooling chamber. In case of CAL cycles, the samples are mounted on the tray in the cooling chamber. This tray can be manually moved in to the heating chamber by sliding on guideways and then the heating chamber is inserted into the furnace. But during cooling, this tray is taken out of heating chamber to the cooling chamber, where cooling is provided by purging the mixture of gases. The temperature is measured by providing two thermocouples, one of which is mounted on the dummy sample surface and the other one is mounted near the sample. In this way the temperature of sample and the temperature of surrounding environment can be determined.

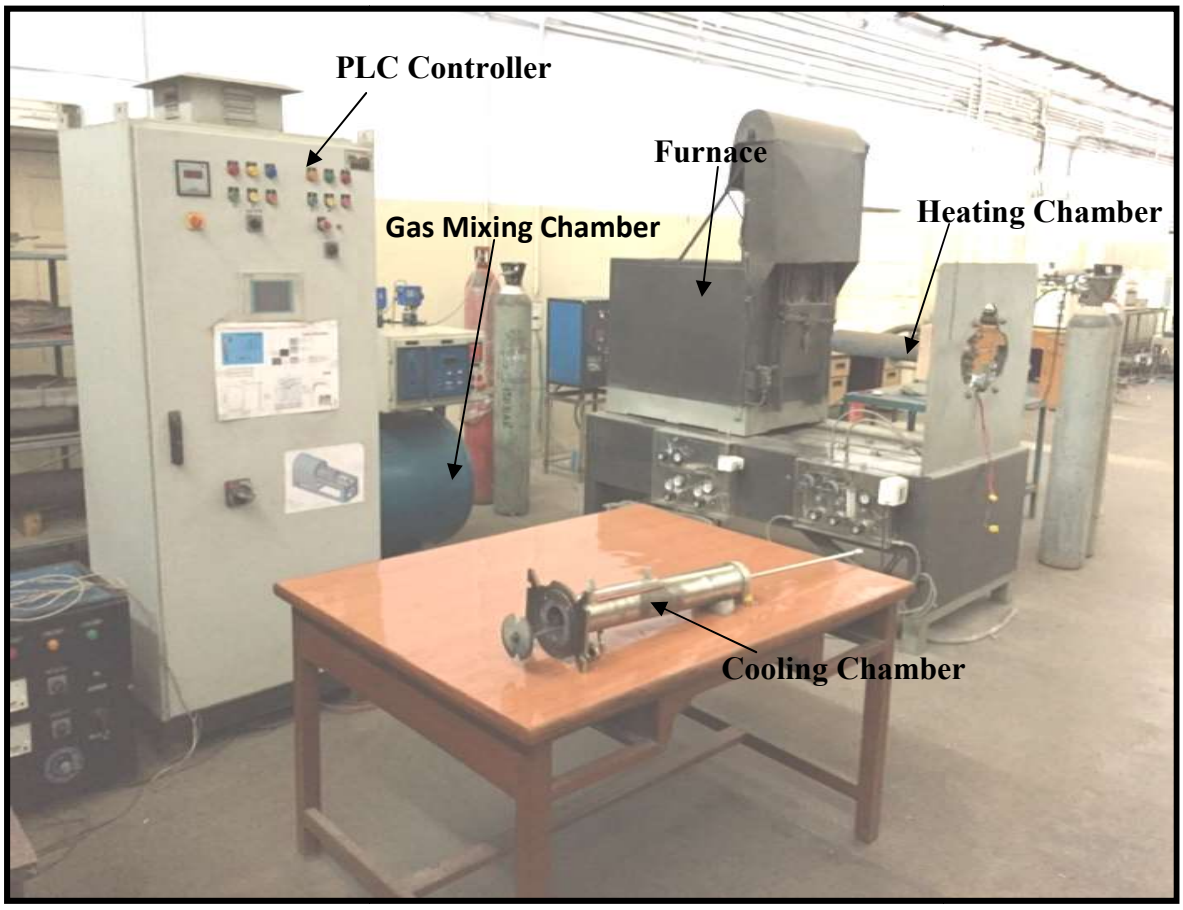

Figure 3.4: Annealing Simulator used for BAF and CAL annealing processes.

(b) Cooling system

The cooling is generally provided by a mixture of 10% H_2 and 90% N_2. These gases are mixed in the mixing chamber. This mixing chamber is connected to cooling chamber by two lines. One line is provided to purge the mixture of gases for the purpose of providing inert atmosphere during heating and also used for slow cooling purpose by controlling the discharge of mixture of gases. The other line is used for quenching purposes. The

different cooling rates can be provided in the annealing simulator by controlling discharge of gases and purging pressure. An exit line is also provided on the cooling chamber which helps in escaping the used gas mixture to the atmosphere.

(c) PLC controller

The furnace parameters in the annealing simulator are controlled by a PLC based digital controller. This is the heart of annealing simulator. Different heating rates, annealing temperatures, and soaking times can be given by using either touch screen provided on PLC or by using computer system connected to the annealing simulator.

3.8.2 Tensile testing machine

After performing various annealing experiments, tensile testing of samples was done as per ASTM standard E8/E8M-09 at a rate of 0.5 mm/min [49]. The extensometer of 50 mm length was used to measure extension produced in samples. Tensile specimens of 50 mm gauge length and 12.5 mm width were cut from as-received steel sheet, were heat treated in annealing simulator, and were subsequently tensile tested using an Instron 8862 system (Instron Engg. Inc., Norwood, USA). Figure 3.5 shows the sample used during tensile testing. The sample was gripped between grips of Instron 8862 system and then extensometer was attached to the tensile sample. The machine gives output in the form of extension values corresponding to different loads. This data is used to obtain stress-strain plots. The tensile stress-strain curves were needed to measure the Lüders strain and yield strength for all the compositions.

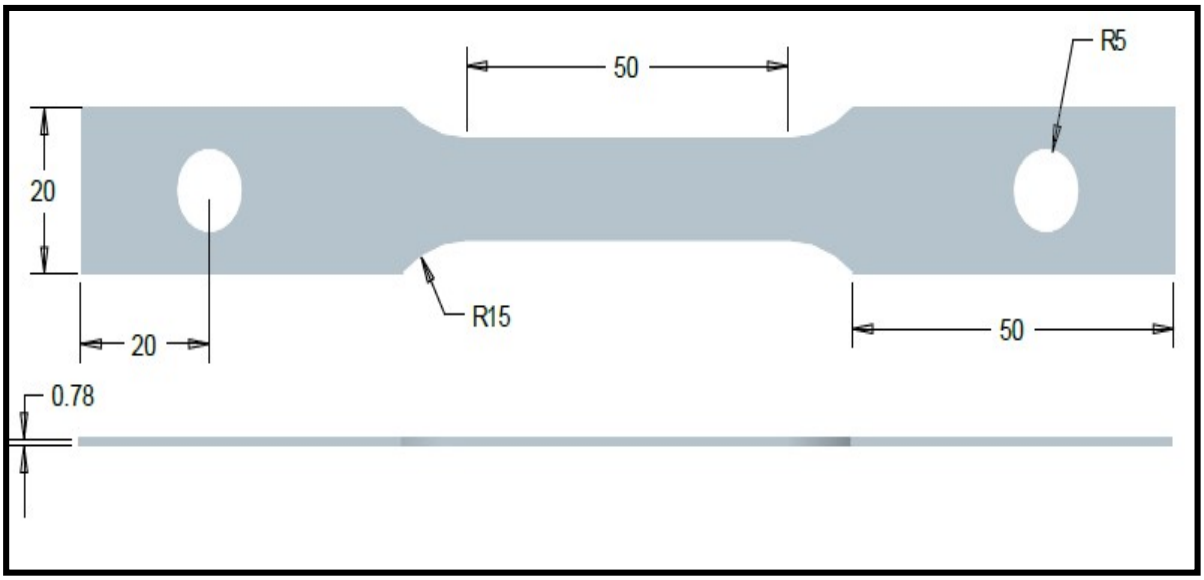

Figure 3.5: Schematic of the tensile testing specimen showing its various dimensions.

Figure 3.5a–b shows the Instron 8862 system used for tensile testing.

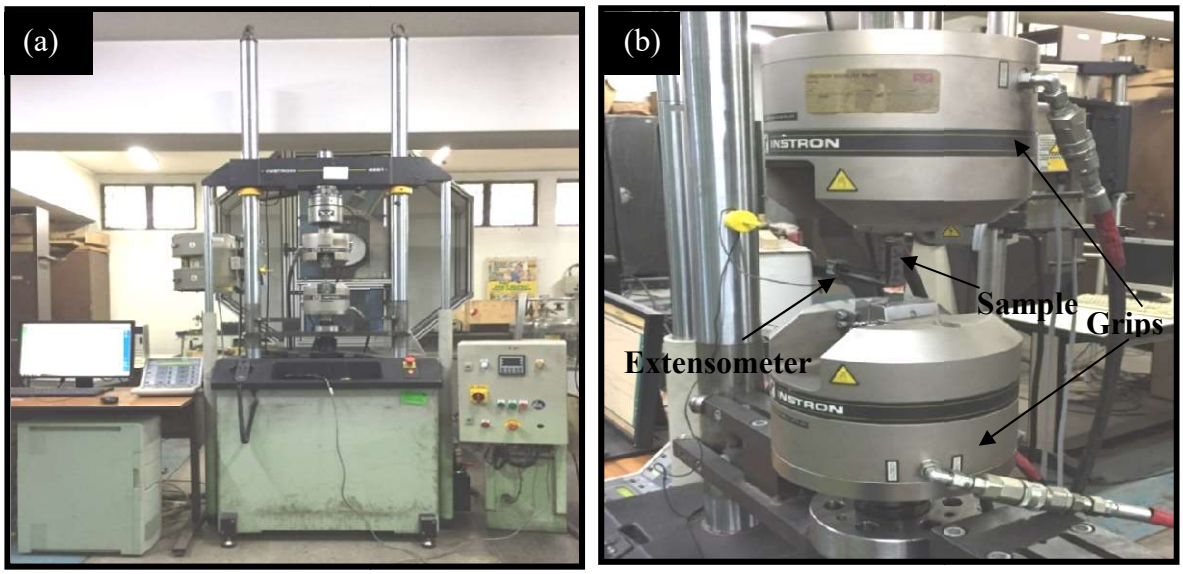

Figure 3.6: (a) Instron 8862 system used for tensile tests, (b) Attachment of extensometer on sample between the grips of Instron 8862 system.

3.8.3 Field Emission Scanning Electron Microscope (FE-SEM)

FE-SEM was used for precipitates analysis of samples subjected to different annealing processes. The different types of precipitates like TiC, TiS, MnS, TiN, NbN etc. were identified in the annealed samples by using FE-SEM (see Fig. 3.6).

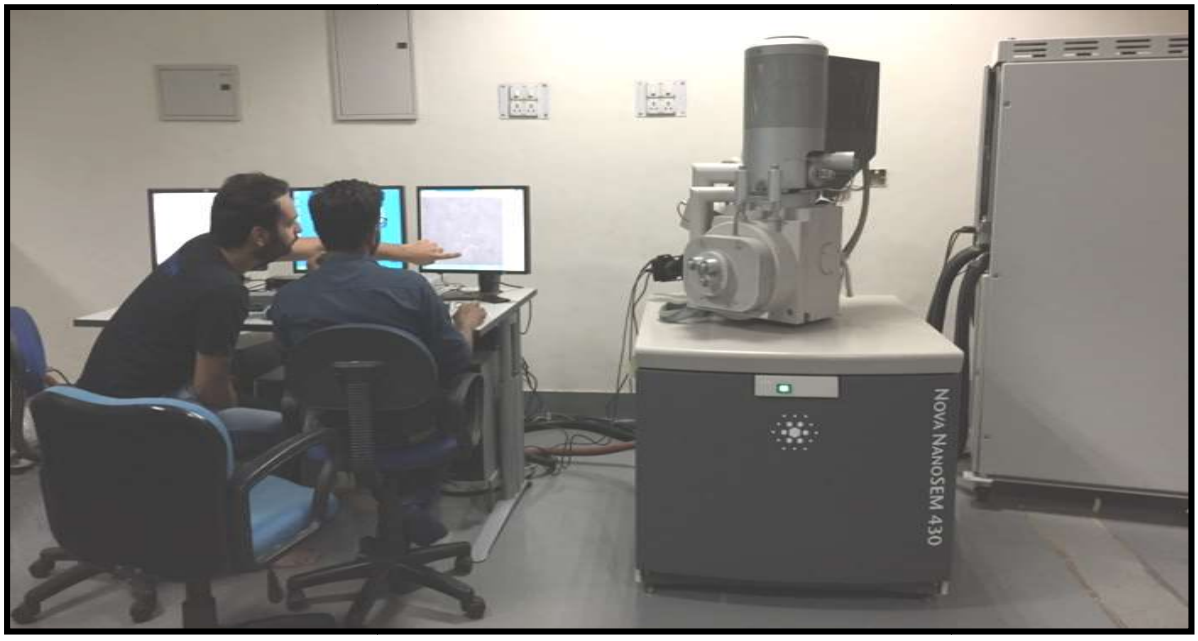

Figure 3.7: FE-SEM and EDS equipment used in the present research work.

In FE-SEM, a focused beam of electrons is made to incident on sample. After striking the sample, the secondary electrons, the diffracted electrons, diffracted back-scattered electrons,

transmitted electrons, visible light, heat and photons are produced. Secondary electrons from the sample are detected by FE-SEM and SEM images are produced. The width of scanning area in FE-SEM varied from 1cm–5μm and maginification varied from 20X–1,00,000X. FE-SEM named Nova Nano SEM 430 (Field Emission Inc., Hillsboro, USA) was used for the research. The composition of observed precipitates in FE-SEM was determined by EDS (Energy dispersive Spectroscopy). In EDS analysis, various peaks of elements were obtained, which indicated the presence of specific precipitates. Also, the weight percent of all elements was also obtained through EDS analysis. From this information, the composition of a particular precipitate can be obtained.

3.8.3.1 Sample Preparation for SEM and EDS characterization

The sample was prepared by using the following steps in order to characterize under SEM and EDS.

(a) Polishing

Firstly, the samples were polished by using SiC emery papers of average grit size of 80, 220, 320, 400, 800, 1000, 1200, 1500, and 2000 (see Fig. 3.7a). The sample was rubbed on one SiC emery paper until all the scratch marks were in one direction only, and then moved to more fine emery paper by changing the direction by 90º until scratch marks were produced in this direction. In this way, the samples were polished from coarse to fine emery papers. After the use of emery paper of average grit size 2000 (i.e. last grade), the one direction scratch marks were remained, which were removed by further polishing on a horizontal rotating wheel. The horizontal rotating wheel (see Fig. 3.7b) has a rotating wheel on which soft cloth of velvet was attached. When this wheel was rotating, the samples were rubbed against this cloth. At the same time, the polishing medium (alumina, colloidal, and water) was provided to remove all the scratches from the sample, which had remained after paper polishing. After polishing on paper, scratch free surface with mirror like surface was obtained. The samples were polished on polishing machine named Banipol Metco PMV018 (Chennai Metco Pvt. Ltd., Chennai, India).

(b) Etching

Revealing the microstructure of a polished sample by chemical attack is known as etching. This is an optional step, as the precipitates can be found with or without etching. The etchant used was 2% nital (a solution of 2 ml ethanol in 100 ml water). After using the etchant, the samples were cleaned by using ethanol and were then dried. Some samples were viewed without etching also.

Figure 3.8: (a) Emery papers of average grit sizes of 80, 220, 320, 400, 800, 1000, 1200, 1500, and 2000, (b) Banipol Metco PMV018 used for polishing purposes.

(c) Levelling

The samples to be viewed under optical microscope should be properly flat and leveled; otherwise there would be problems of focusing. So, to eliminate this problem, the specimen leveling press was used. Figure 3.8a shows leveling equipment used for leveling purpose. Firstly, the clay was placed on the microscope slide plate, and then sample was placed on it and pressed by using specimen leveling press. To avoid scratching, a piece of paper was placed on the sample and then pressing was done.

(d) Visualization of sample under optical microscope

The microscope slide plate having sample on it was placed under optical microscope. If there was any scratch present on the polished sample, then it could be easily identified by using optical microscope. The optical microscope named as Leica DM2500 M (Lieca Microsystems, Wetzlar, Germany) was used for this purpose (see Fig. 3.8b). The microstructure characterization of one sample was also done on optical microscope. This microscope has maximum magnification power of 100X.

3.8.4 TEM (Transmission Electron Microscope)

Transmission electron microscope (TEM) was used in this work only for the detection of FeTiP precipitates in a specific steel composition (called C3 composition in the present work), as this precipitate is so small that SEM is not able to identify it. TEM detects the transmitted electrons from the sample and produces TEM images.

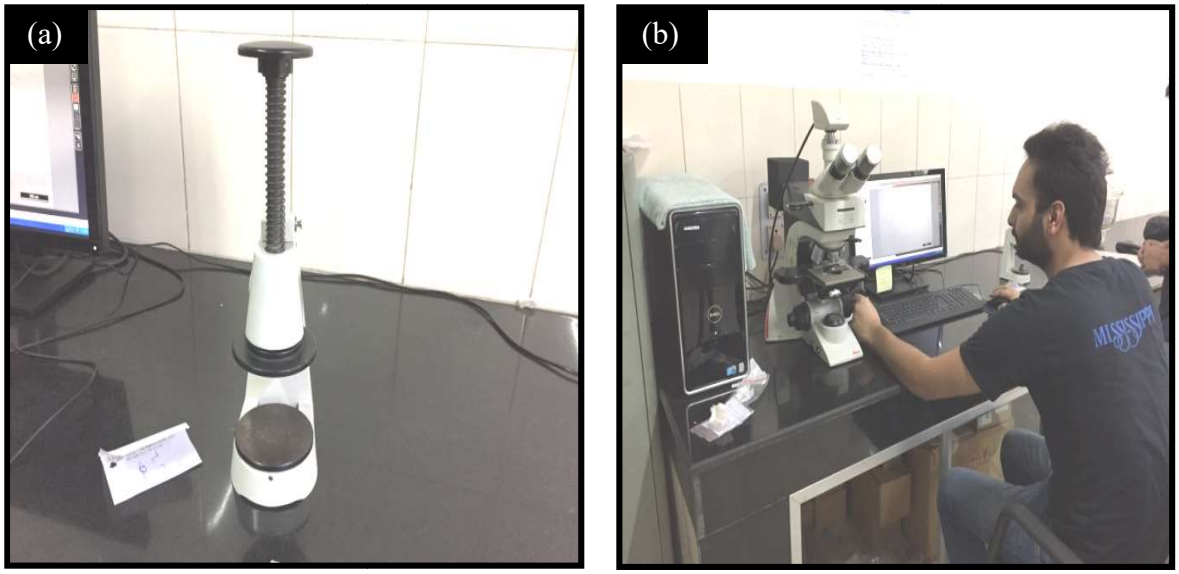

Figure 3.9: (a) Levelling equipment, (b) Optical microscope.

The preparation of samples for TEM was very difficult. For TEM images, the electrons should be transmitted through the sample. Hence, firstly the thickness of sample was reduced from 0.78 mm to 0.06 mm by emery papers. After this puching was done, in which punch is used to remove several 3 mm areas from sample. The punched portion was viewed under TEM after electropolishing. The electropolishing was done by using solution of 10 ml perchloric acid in 90 ml ethanol. The TEM used for this was JEOL JEM 2200FS TEM (JEOL solution of Innovation, USA) shown in Fig. 3.9.

Figure 3.10: TEM equipment used in the present research work.

3.9 Summary of the chapter

This chapter discussed the primary objective of present research. This chapter also discussed the key issues along with the experimental procedure of the current research. Also, this chapter provided information regarding materials, annealing processes parameters, and equipment used in the current research work.

Chapter 4

Results and Discussion

4.1. General

This chapter provides details of various results of the present research work in a sequential manner. The reasons behind the obtained results are also discussed in detail. The chapter provides a proper solution to the present research problem.

4.2. Effect of composition on stabilization of interstitials

4.2.1. C1 composition

C1 was a Ti-stabilized composition in which 0.0084 wt. % of Ti was available in excess (i.e. Ti^{*} = 0.0084 wt. %) as per Eq. 3.4 (see Table 3.1). For this composition, accelerated BAF process was simulated to understand the stabilization effect. Due to the presence of excess of stabilizing element Ti, complete stabilization of all interstitial elements was theoretically anticipated for this composition. However, the tensile stress-strain curves obtained for BAF as well as CAL processed steels exhibited undesirable yield point elongation behaviour as is evident from Fig. 4.1a–b.

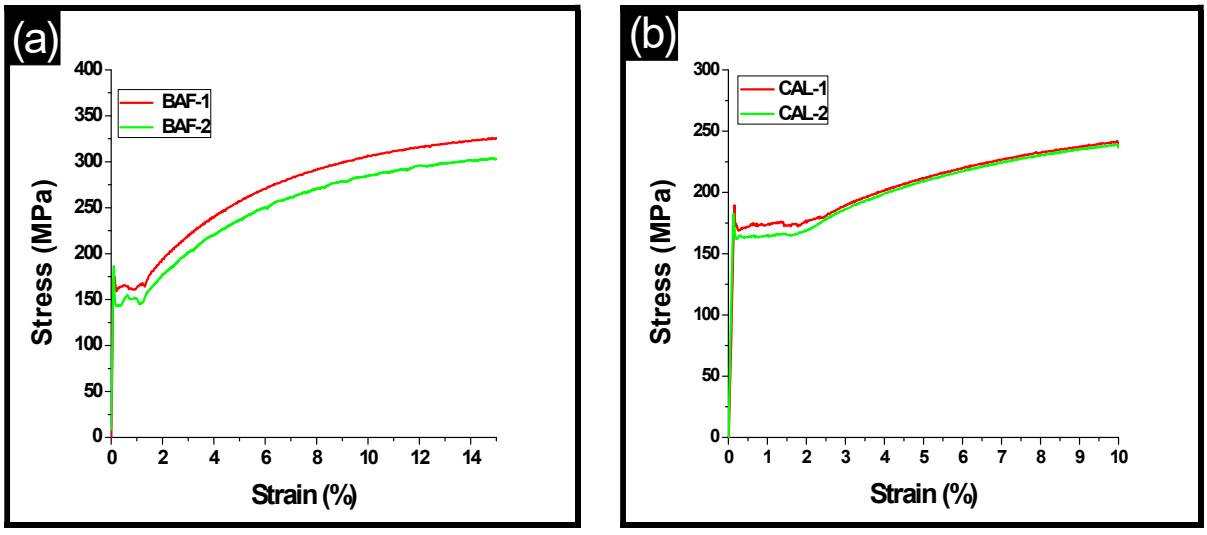

Figure 4.1: Stress-strain curves for C1 composition (Ti-stabilized) for (a) BAF-1 and BAF-2 (b) CAL-1 and CAL-2.

a) Lüders band formation

The magnitude of Lüders strain for various annealing process parameters for C1 composition based IFHS steel is provided in Table 4.1. For all the cases, the Lüders strain was found to be

present in a significant amount (> 1 %), which could have a deleterious effect on surface finish.

Table 4.1: Lüders strain present in C1 composition (Ti-stabilized) subjected to different annealing processes.

Annealing process used for C1 composition	Lüders strain (%)
BAF-1	1.17
BAF-2	1.07
CAL-1	1.69
CAL-2	1.41

b) Precipitate formation characteristics

Lüders bands formation during tensile deformation of C1 composition steel can be correlated with its precipitation behaviour due to the BAF/CAL processes. SEM-EDS analysis of specimens subjected to various annealing processes (as per Table 3.3) was conducted. Results of analysis showed formation of various precipitates. The use of SEM-EDS is well reported in literature for observing various precipitates formed in IFHS steels subjected to annealing process [26, 29, 50, 51].

Figure 4.2a–h shows SEM-EDS spectrum for one typical annealing process of BAF-2. A large fraction of (Ti+Mn)S type precipitates of irregular shape with average size in the range of 0.2–1.0 μm were observed. Figure 4.2a–d shows the typical precipitate nucleation characteristics at grain interior as well as grain boundaries respectively. Further, FeTiP type precipitates (irregular shaped and of size less than 1 μm) were also observed along with (Ti+Mn)S precipitates (Fig. 4.2e–f). Interestingly, TiC precipitate formation was not observed in this steel. This means TiC precipitation was not favored in this specific composition resulting in insufficient stabilization of C atoms. As a result, the free C in the solid solution gave rise to Lüders bands formation. The formation of FeTiP precipitates further hindered the formation of TiC precipitates (since Ti was tied up by FeTiP formation, its availability for TiC formation was limited). Also, presence of TiS precipitates in large amount (i.e. TiS precipitates was most frequently observed) indicated that a substantial fraction of available Ti in steel was consumed by TiS formation. The literature also reports that values of solubility product for FeTiP and TiC are very close [50]. Further, it is well reported that formation of FeTiP precipitates in IFHS compositions mainly occurs in the temperature range between 600–900 ℃ [52]. Hence, the observations agree with the available literature. Further, the yield strength achieved for C1 composition through various annealing process routes was in the range of 150–180 MPa (see Fig. 4.1a–b), which is a reasonably

good value for an IFHS grade [2, 3]. However, the presence of Lüders bands in this Ti-stabilized composition will not render it useful for industrial applications.

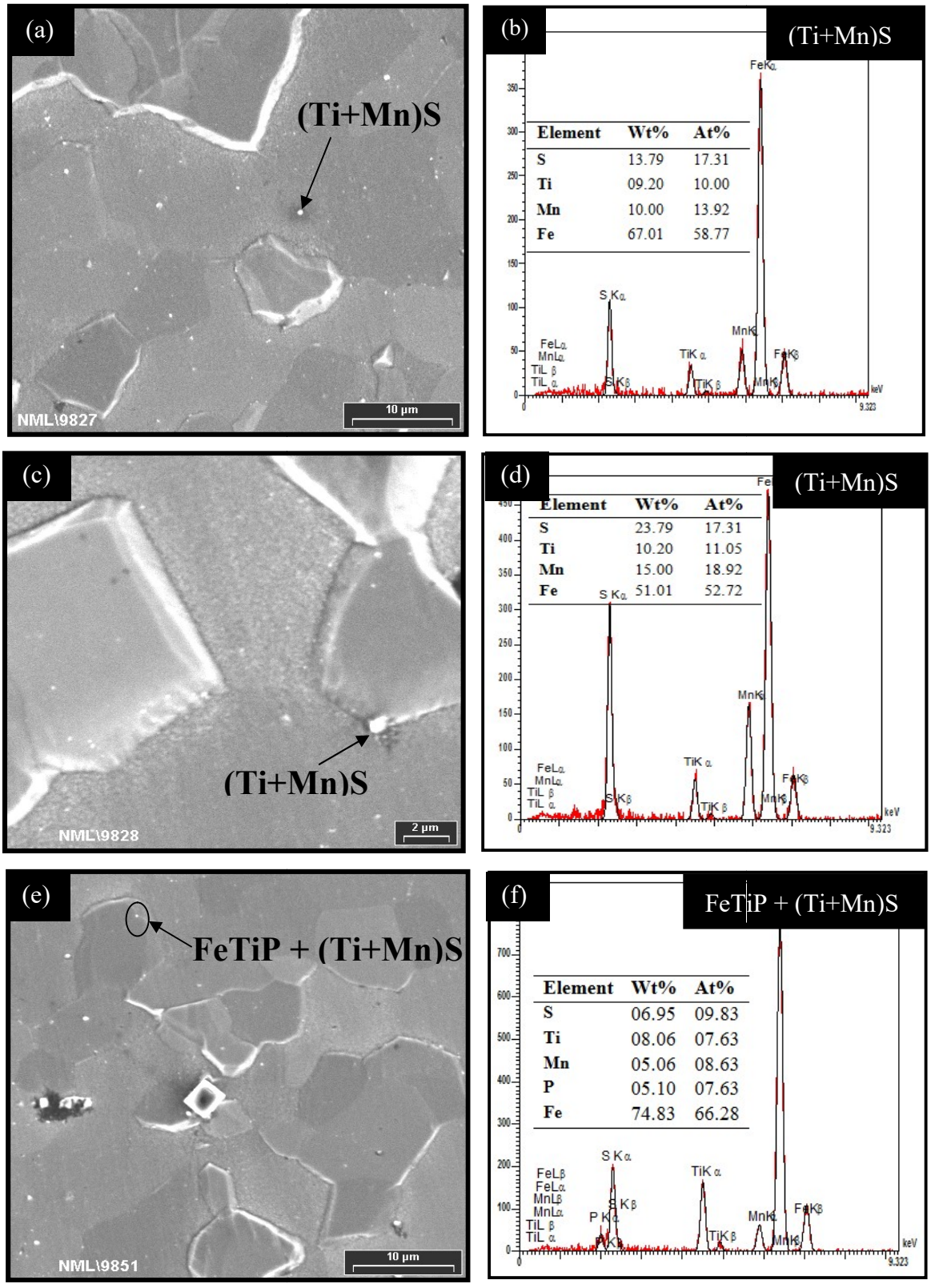

Figure 4.2: Results of SEM-EDS analysis of C1 specimen subjected to BAF-2 process showing precipitate formation of type (a–b) (Ti+Mn)S inside the grain, (c–d) (Ti+Mn)S at grain boundary, (e–f) FeTiP along with (Ti+Mn)S.

4.2.2 C2 composition

C2 composition was Ti stabilized as well as Nb stabilized composition in which 0.03671 wt. % of Ti and 0.0005 wt. % of Nb (i.e. Ti*= 0.03671 wt. %; Nb*= 0.0005 wt.%) were present in excess as per Eq. 3.3–3.4 (see Table 3.1). Complete stabilization of all interstitial elements was theoretically anticipated for this composition.

a) Lüders band formation

The tensile stress-strain curves (Fig. 4.3a–b) obtained for C2 composition based IFHS steel subjected to BAF as well as CAL processes did not show yield point elongation/Lüders bands.

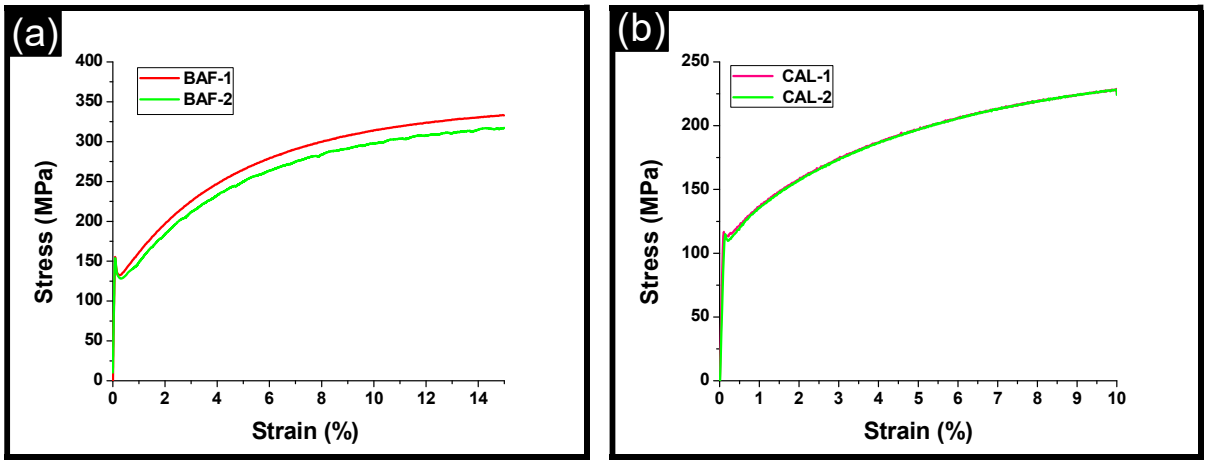

Figure 4.3: Stress-strain curves for C2 composition (Ti-Nb stabilized) for (a) BAF-1 and BAF-2 (b) CAL-1 and CAL-2.

Table 4.2 shows that no Lüders bands and Lüders strain were present in this steel composition after various annealing processes.

Table 4.2: Lüders strain present in C2 composition (Ti-Nb stabilized) subjected to different annealing processes.

Annealing process used for C2 composition	Lüders strain (%)
BAF-1	0.00 (absent)
BAF-2	0.00 (absent)
CAL-1	0.00 (absent)
CAL-2	0.00 (absent)

b) Precipitate formation characteristics

SEM-EDS analysis of C2 composition based IFHS steel subjected to various annealing processes (BAF and CAL processes as shown in Table 3.3) was carried out and the results showed formation of various types of precipitates. Fig. 4.4a–i shows results of SEM-EDS

analysis for a typical annealing process of CAL-2 (i.e. annealing at 810 ℃ with ageing time of 60 s). Precipitates of Ti including TiN (normally observed in rectangular shape; [26, 29]), TiC, and TiS (normally observed in globular shape; [26, 29]) were mainly observed and a few AlN precipitates were also observed as shown in Fig. 4.4a–i.

However, no precipitates of Nb were detected by SEM, may be due to their very fine size. Precipitates obtained for this Ti-Nb stabilized IFHS steel in the present work (i.e. TiN→TiS→TiC) were of the same type as are reported in literature [2, 53, 54]. For C2 composition, since TiC precipitates were frequently observed (see Fig. 4.4a, b, d), therefore, interstitial element C present in the steel could be fully stabilized. Therefore, complete stabilization of interstitial elements present in the steel eliminated Lüders bands formation on the surface of steel.

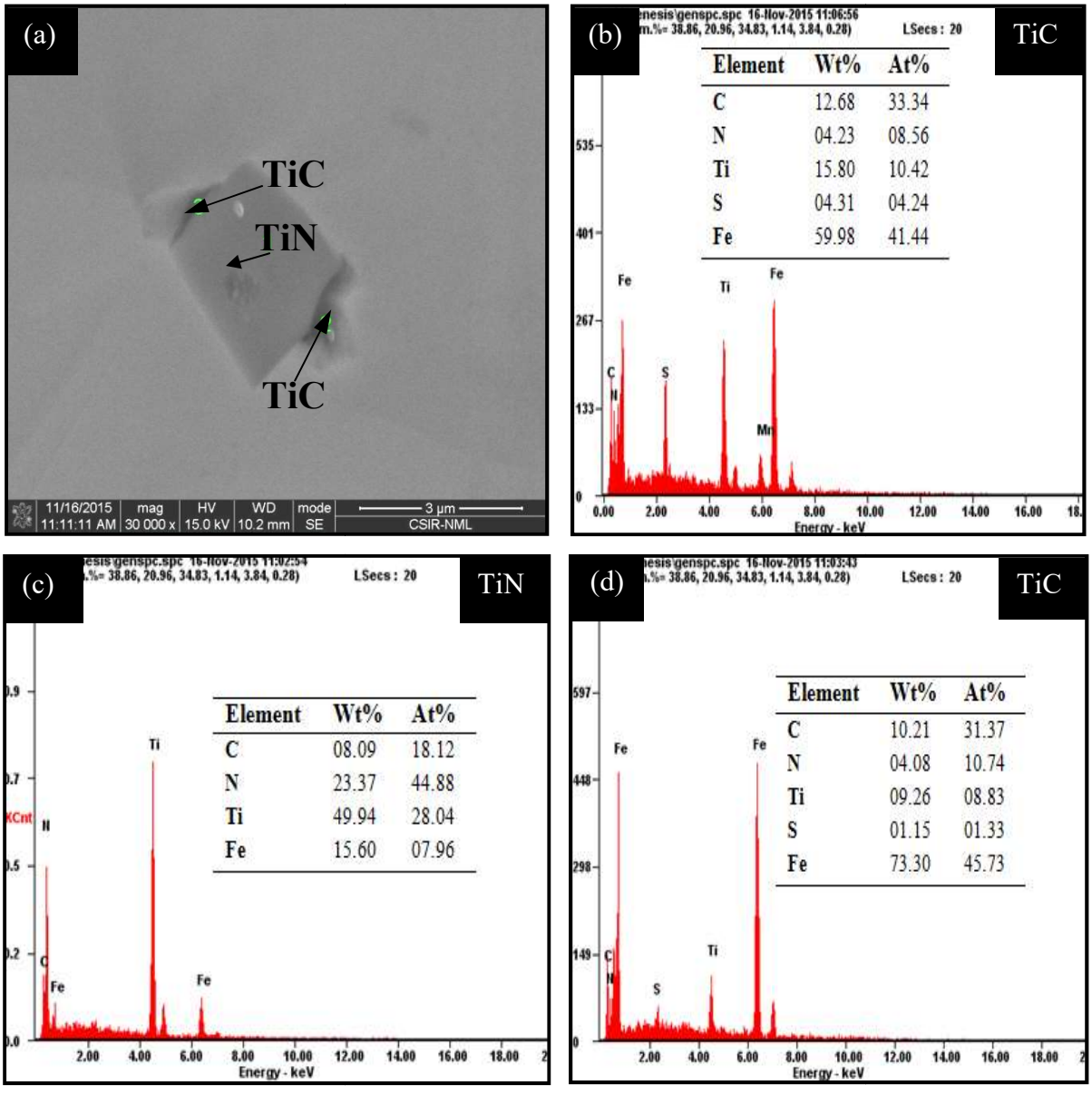

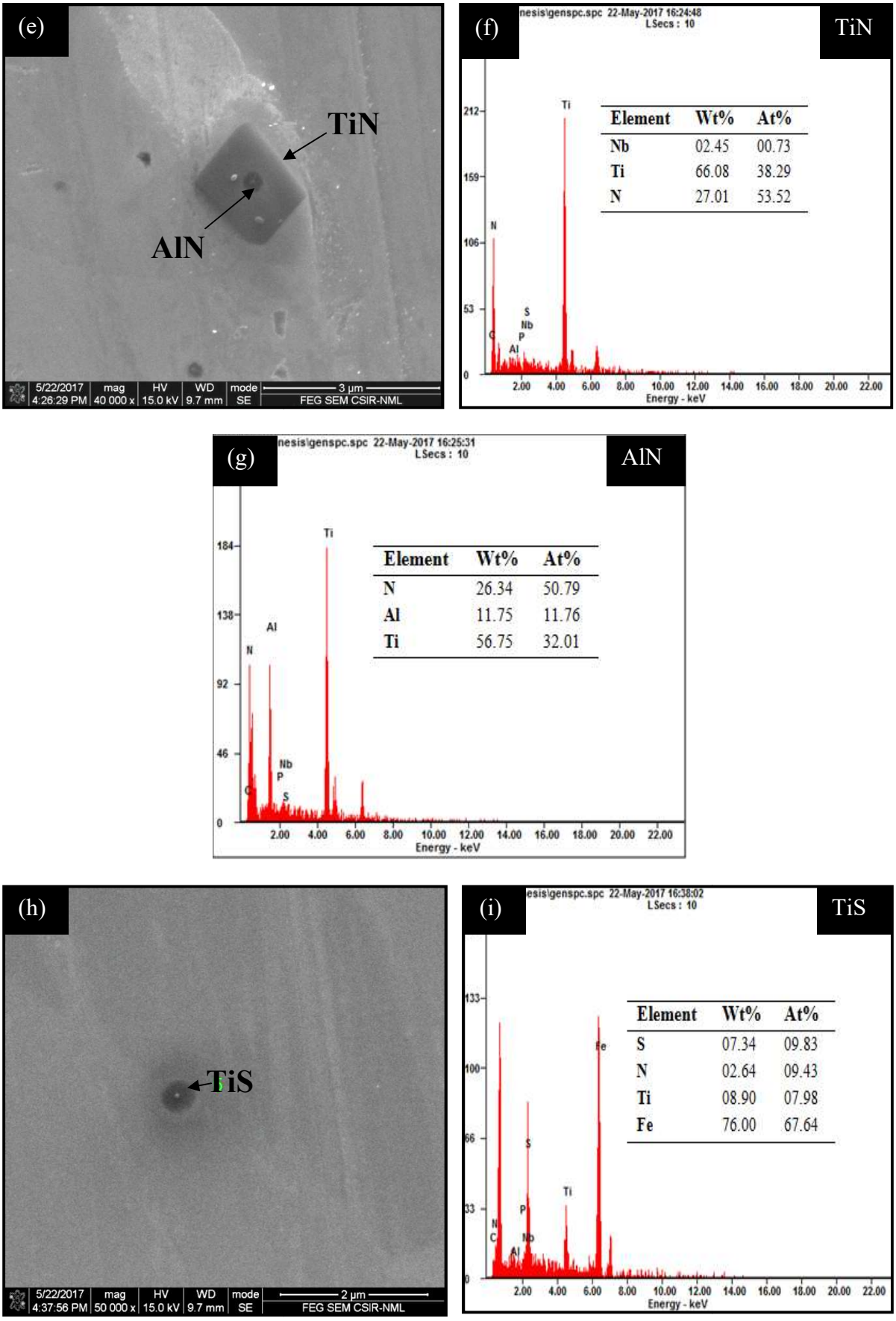

Figure 4.4: Results of SEM-EDS analysis of C2 specimen subjected to CAL-2 process showing precipitate formation of type (a–d) TiC and TiN, (e–g) AlN and TiN, (h–i) TiS

However, despite the absence of Lüders bands and good value of Lanksford parameter (r_m= 1.8–2.1), this IFHS composition is not suitable for automotive panel applications because of its low yield strength (125–150 MPa). The main reason for low strength was small magnitudes of strengthening elements like phosphorous and carbon in this steel. The presence of phosphorous, even in very small amounts, significantly affects the strength of IFHS steels [55].

4.2.3 C3 composition

This was an under-stabilized composition in which Ti and Nb were available in slightly deficient amounts of 0.0071 and 0.0032 wt. % respectively (i.e. Ti*= -0.0071 wt. %; Nb*= -0.0032 wt. %) as per Eq. 3.3–3.4 (see Table 3.1). Theoretically, only partial stabilization of interstitial elements was expected. The stress-strain curves (see Fig. 4.5a–b) for various annealing processes for this composition showed presence of Lüders strain (see Table 4.3) in a significant amount.

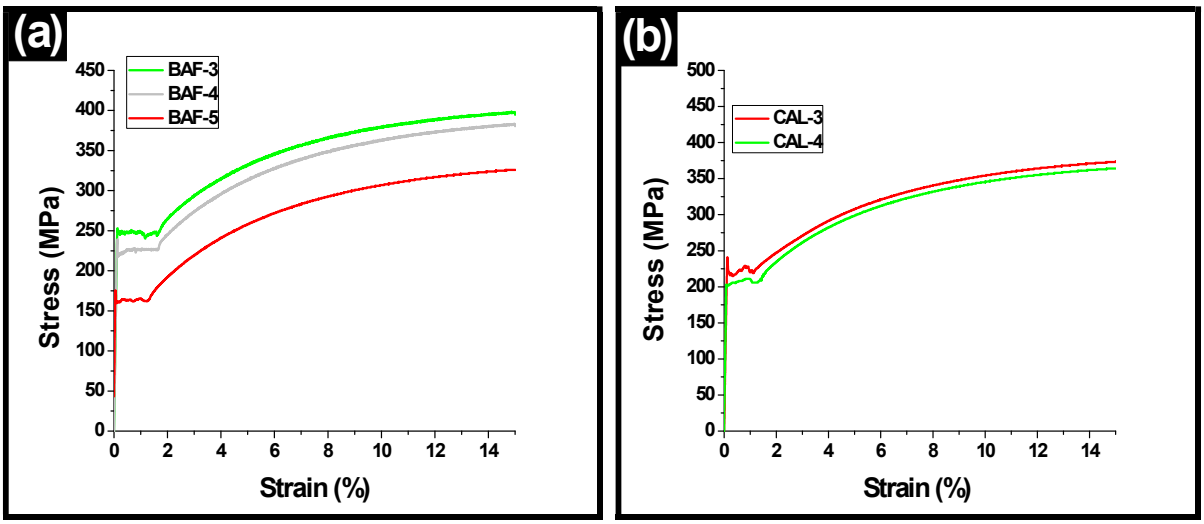

Figure 4.5: Stress-strain curves for C3 composition (low Ti-low Nb) for (a) BAF-3, BAF-4, and BAF-5 (b) CAL-3 and CAL-4.

a) Lüders band formation

The extent of Lüders strain present in C3 composition based IFHS steel is provided in Table 4.3. For all annealing processes, the presence of Lüders strain was in a significant amount (≥ 1 %), which would cause deterioration of surface finish during forming operation.

b) Precipitate formation characteristics

Lüders bands formation during tensile deformation of C3 composition based IFHS steel can be correlated with its precipitation characteristics. SEM-EDS analysis showed formation of various types of precipitates in this steel composition subjected to various annealing routes.

Table 4.3: Amount of Lüders strain present in C3 composition (low Ti-low Nb) subjected to different annealing processes.

Annealing process used for C3 composition	Lüders strain (%)
BAF-3	1.48
BAF-4	1.46
BAF-5	1.21
CAL-3	1.20
CAL-4	1.00

Figure 4.6a–e shows the results of SEM-EDS analysis for one typical annealing cycle of BAF-5 provided to C3 composition. In addition to SEM studies, TEM-EDS analysis was also used for this composition to study the sub-micron size precipitates. For TEM-EDS analysis, one typical case i.e. BAF process at 730 ℃ for C3 composition is discussed.

Nitrides of Al, Nb, Ti and sulphides of Mn were observed (Fig. 4.6a–e). The precipitates of (Al+Nb)N were observed to have needle like shape with size close to 1 μm. Further, precipitates of MnS and TiN were observed together frequently with sizes in the range of 0.5–1 μm.

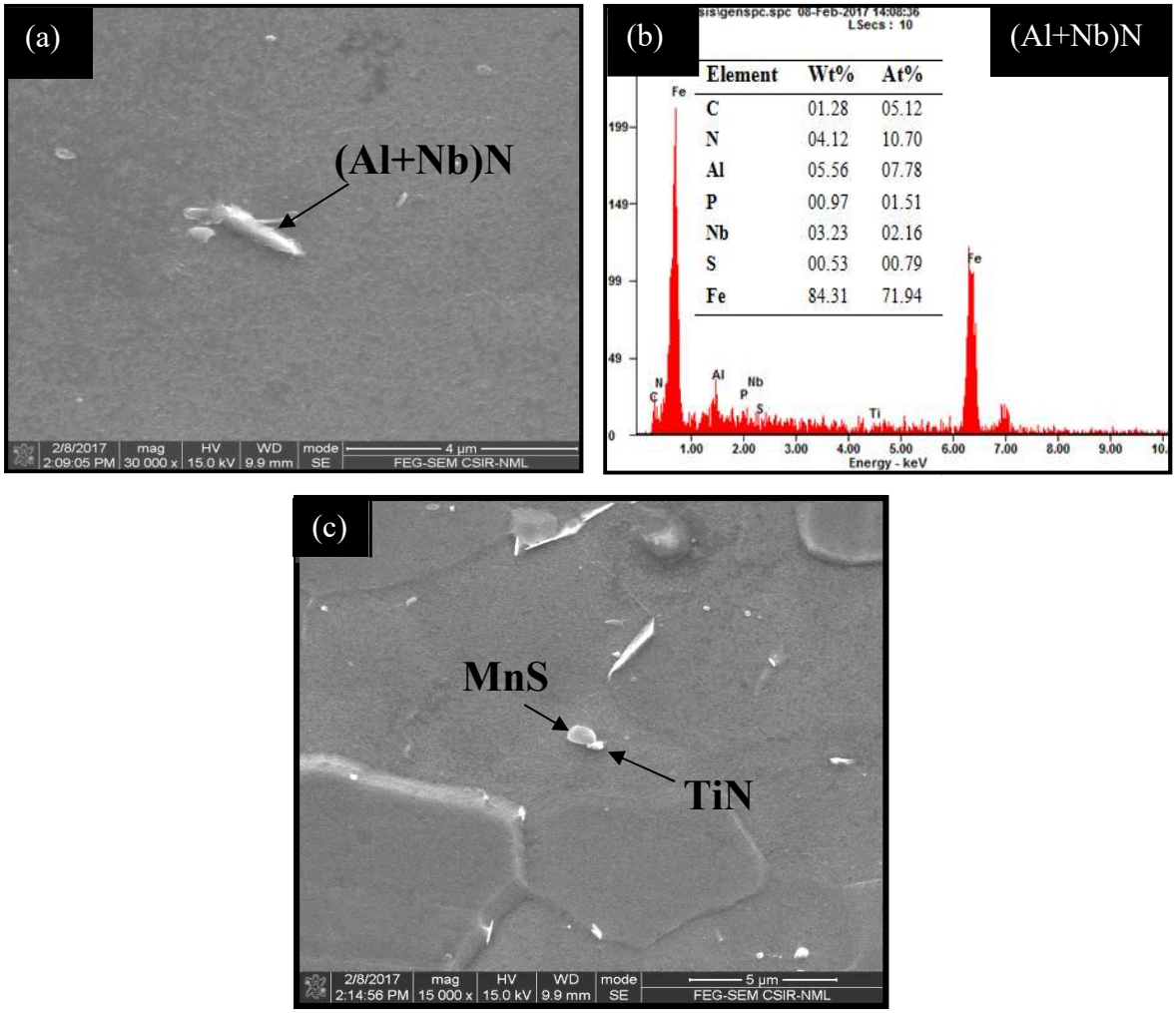

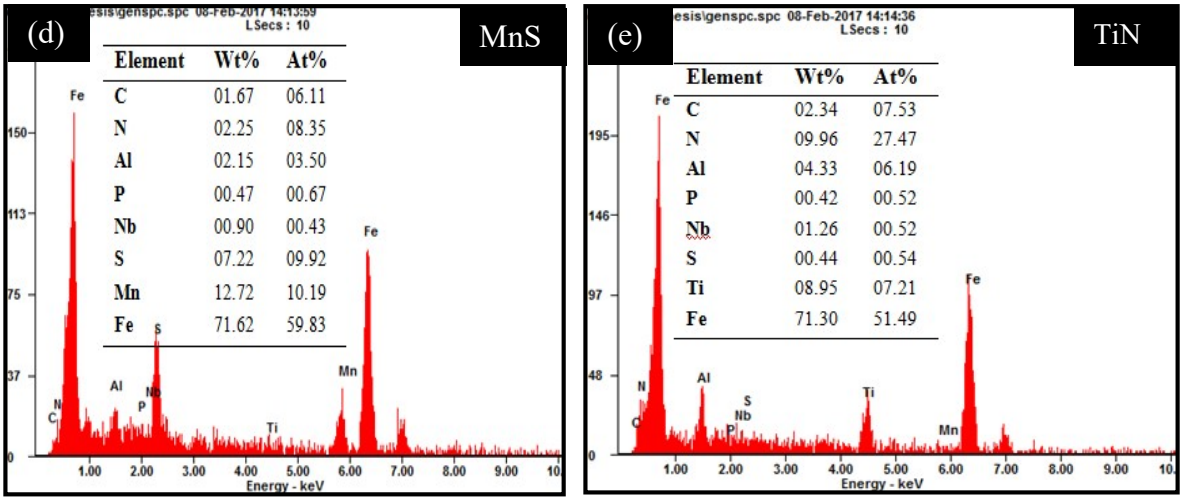

Figure 4.6: Results of SEM-EDS analysis of C3 specimen subjected to BAF-5 process showing precipitate formation of type (a–b) (Al+Nb)N, (c–e) MnS and TiN.

The results showed that N was effectively stabilized by Al, Nb, and Ti, whereas, Mn was tied up with S for this IFHS. However, precipitation of TiC was not observed in this IFHS composition. The absence of TiC precipitation was attributed to formation of a few FeTiP precipitates. TEM-EDS analysis was used to confirm presence of FeTiP precipitates because these are generally not observed through SEM-EDS owing to their very fine size. The results of TEM-EDS analysis confirmed presence of FeTiP precipitates (Fig. 4.7a–b) with average size in the range of 15–25 nm.

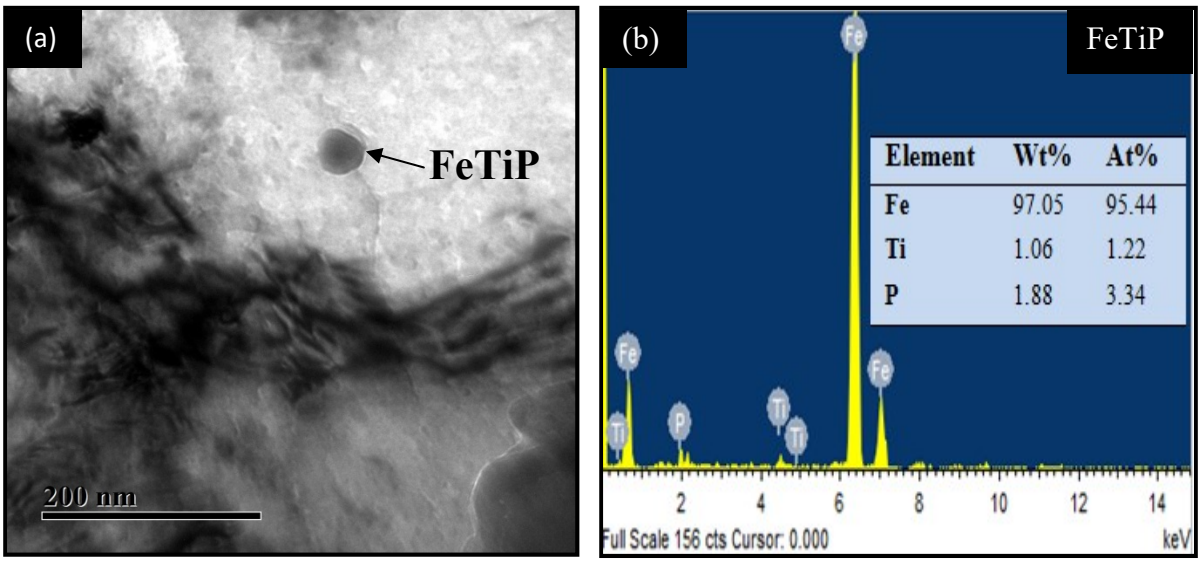

Figure 4.7: Results of TEM-EDS analysis of C3 specimen subjected to BAF-5 process showing precipitate formation of type FeTiP through (a) TEM micrograph, (b) EDS spectrograph.

Ghosh et al. also reported that frequency of formation of FeTiP precipitates was more in IFHS steels with higher P content, and in the present work, C3 composition contained the

highest P content [50]. Further, C3 composition had low Ti content, out of which some amount (of Ti) was taken up by FeTiP precipitate formation. Hence, stabilization of C was not complete in this composition under all types of annealing processes causing Lüders band formation.

4.2.4 C4 composition

This was a Ti-over-stabilized but Nb-under-stabilized composition in which 0.0362 wt. % of Ti was available in excess and -0.0146 wt. % of Nb was available in deficient amount (i.e. Ti^*= -0.0362 wt. %; Nb^*= -0.0146 wt. %) as per Eq. 3.3–3.4 (Table 3.1). Further, this composition contained very high amount of Al (0.12 wt. %). Jeong et al. [56] reported that addition of Al in IF steels in amounts greater than 0.10 wt. % results in scavenging of N from the ferrite matrix by formation of coarse AlN precipitates. Kang et al. [19] reported that addition of Al in IFHS steels in amounts excess of 0.10 wt. % increases their formability. Due to these reported advantages of high Al content, C4 composition based IFHS was investigated. The C4 composition was considered as a stabilized composition, in which the small amount of Nb present in steel was for stabilization of some fraction of C atoms, and the remaining C atoms were to be mainly stabilized by Ti. Further, stabilization of N was anticipated by presence of both Al and Ti present in this composition.

a) Lüders band formation

The stress-strain curves (Fig. 4.8a) obtained for C4 composition based IFHS steel subjected to various BAF processes did not display Lüders bands (Table 4.4).

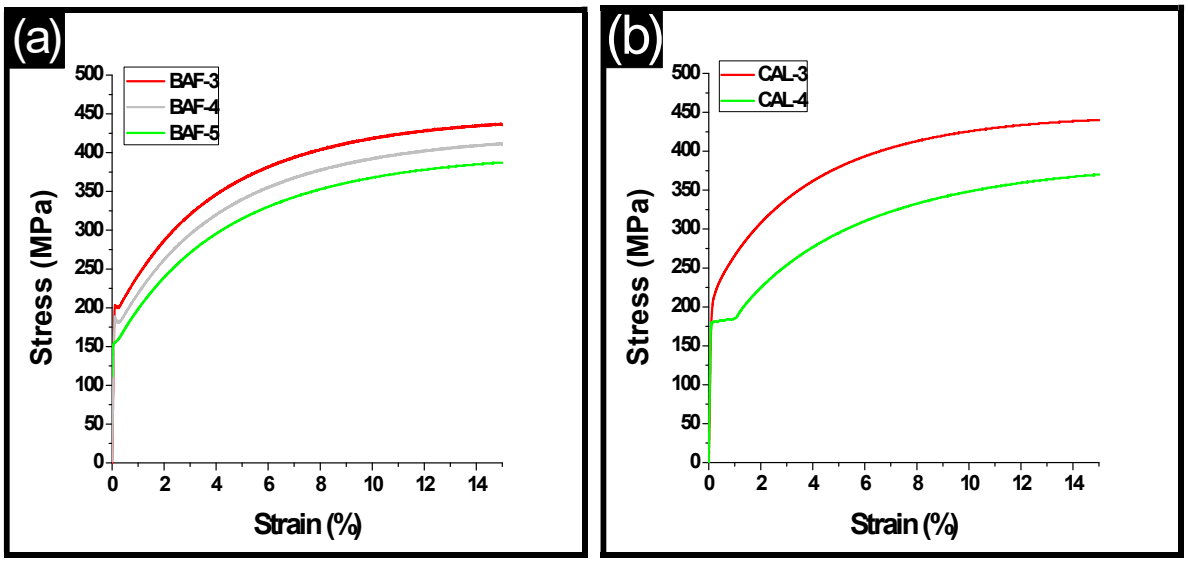

Figure 4.8: Stress-strain curves for C4 composition (high Al-high Ti) for (a) BAF-3, BAF-4, and BAF-5 (b) CAL-3 and CAL-4.

Though yielding phenomena occurred for less than 0.2% strain, but no yield point elongation was present. This indicated that BAF processes for C4 composition were effective in stabilization of interstitial elements (C, N) by means of favourable precipitation kinetics. However, IFHS steels of C4 composition processed by CAL-4 route resulted in Lüders bands formation (Fig. 4.8b and Table 4.4).

Table 4.4: Amount of Lüders strain present in C4 composition (high Al-high Ti) subjected to different annealing processes.

Annealing process used for C4 composition	Lüders strain (%)
BAF-3	0.00 (absent)
BAF-4	0.00 (absent)
BAF-5	0.00 (absent)
CAL-3	0.00 (absent)
CAL-4	1.00

b) Precipitate formation characteristics

SEM-EDS analysis of C4 based IFHS steel composition subjected to BAF processes (shown in Table 3.3) showed formation of various precipitates. N was stabilized by Al in the form of AlN precipitates. Further, any residual N and C elements were stabilized by Ti and Nb as TiC, TiN, and NbC etc. Also, S was stabilized by Ti by formation of TiS precipitates. Figure 4.9a–f presents the results of SEM-EDS analysis for one typical BAF process (BAF-3 process at 680 ℃) which revealed presence of several AlN, TiC type precipitates and some TiN precipitates. It may be noted that due to the preferential formation of AlN over TiN in BAF processed IFHS, Ti was largely available for formation of TiC, thus locking the free C and providing continuous yielding behaviour. Table 4.4 shows that no Lüders bands were present in this steel composition after various BAF processes.

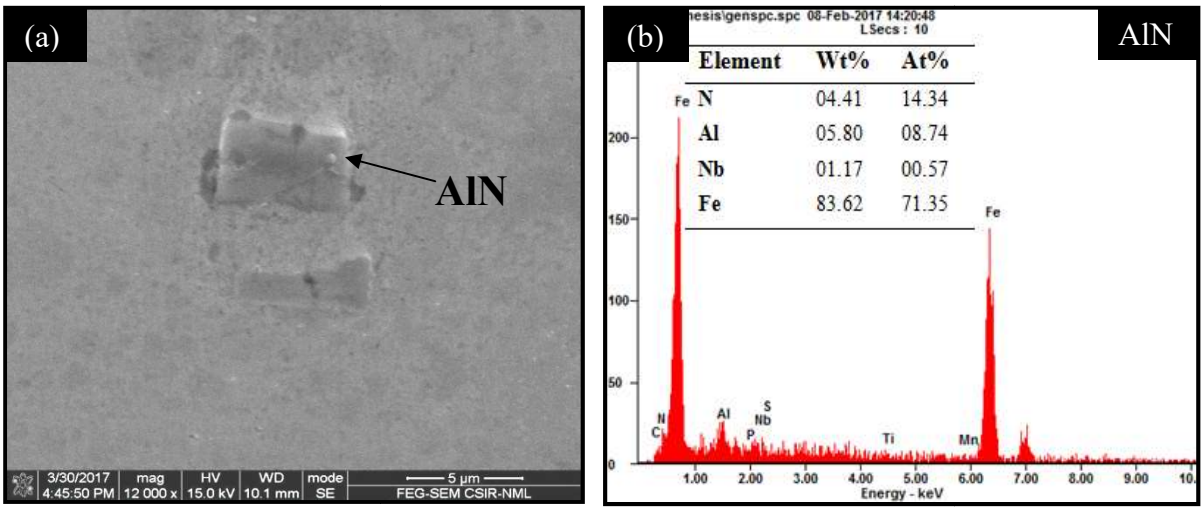

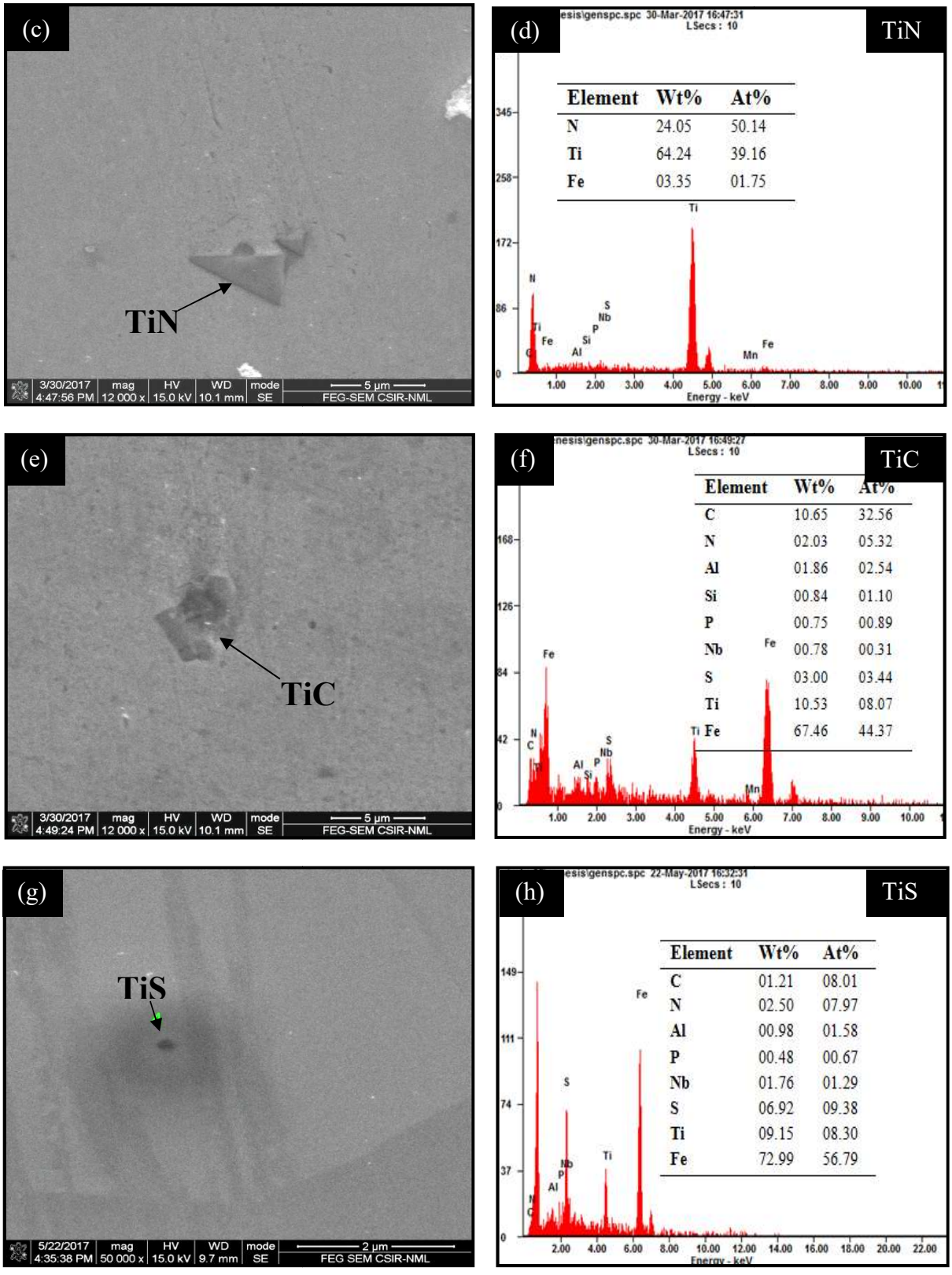

Figure 4.9: Results of SEM-EDS analysis of C4 specimen subjected to BAF-3 process showing precipitate formation of type (a–b) AlN, (c–d) TiN, (e–f) TiC, (g–h) TiS.

Figure 4.8b shows the stress-strain curve (for tensile loading in rolling direction) for C4 composition based IFHS steel subjected to CAL-3 processing route. Though, the stress-strain

curve showed good mechanical properties for C4 composition based IFHS steel, but the r_m value could not be computed for this steel. This was because the tensile samples for the transverse as well as diagonal directions failed miserably (fracture at very low strains of even less than 10%) under tensile testing (see Fig. 4.10 showing stress-strain curve for specimen in transverse direction). This unusual typical behaviour shown by the steel under the given processing conditions not related to its precipitation behaviour and was further investigated. Optical micrograph of the C4 composition based steel subjected to CAL-3 showed incomplete recrystallization (see Fig. 4.11). Thus, the continuous yielding shown (in the rolling direction) by this composition-processing condition combination was traced to incomplete recrystallization.

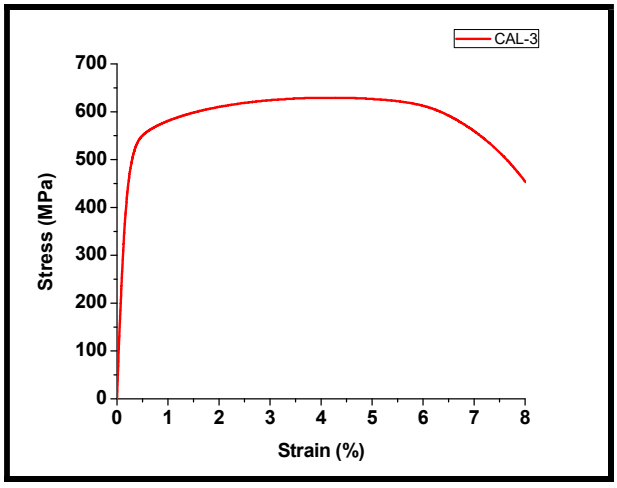

Figure 4.10: Stress-strain curve for C4 composition (high Al-high Ti) in transverse direction for CAL-3 processing route showing fracture before 10%.

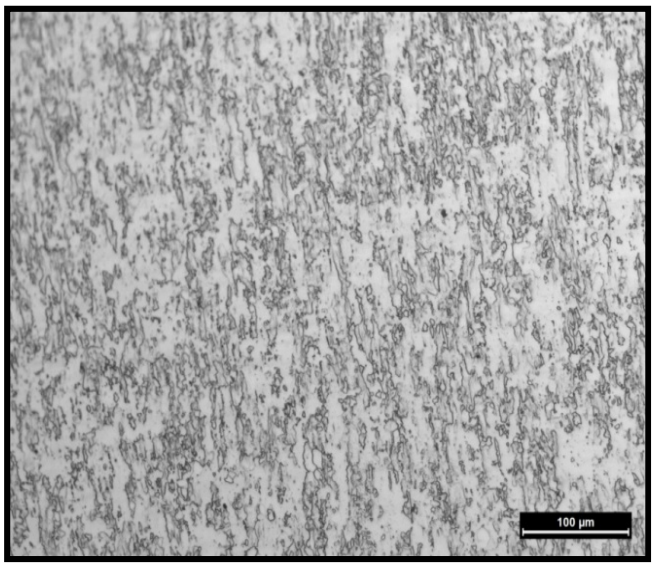

Figure 4.11: Optical micrograph of C4 composition after CAL-3 process (CAL at 810°C with 50 s soaking) showing incomplete recrystallization.

Further, for obtaining complete recrystallisation, CAL process at 810 ^{o}C was repeated with increased soaking time from 50 to 60 sec. Despite increase in time, complete recrystallisation was not achieved. Cottrell and Bilby [57] reported that discontinuous yielding mainly occurs due to locking of dislocations, generated during deformation, by the interstitial atoms (i.e. due to formation of Cottrell atmosphere). Due to incomplete recrystallisation, wherein dislocations are present in abundance, efficacy of dislocation locking is not adequate.

On the other hand, a reasonable fraction of TiN precipitates in addition to AlN precipitates were found in CAL simulated IFHS (see Fig. 4.12a–c). This was contrary to what was observed for BAF process, wherein presence of TiN was limited and the loss of Ti in nitride formation was less. Thus, absence of Lüders bands formations for the CAL process was primarily because of incomplete recrystallization and not related to precipitation behaviour.

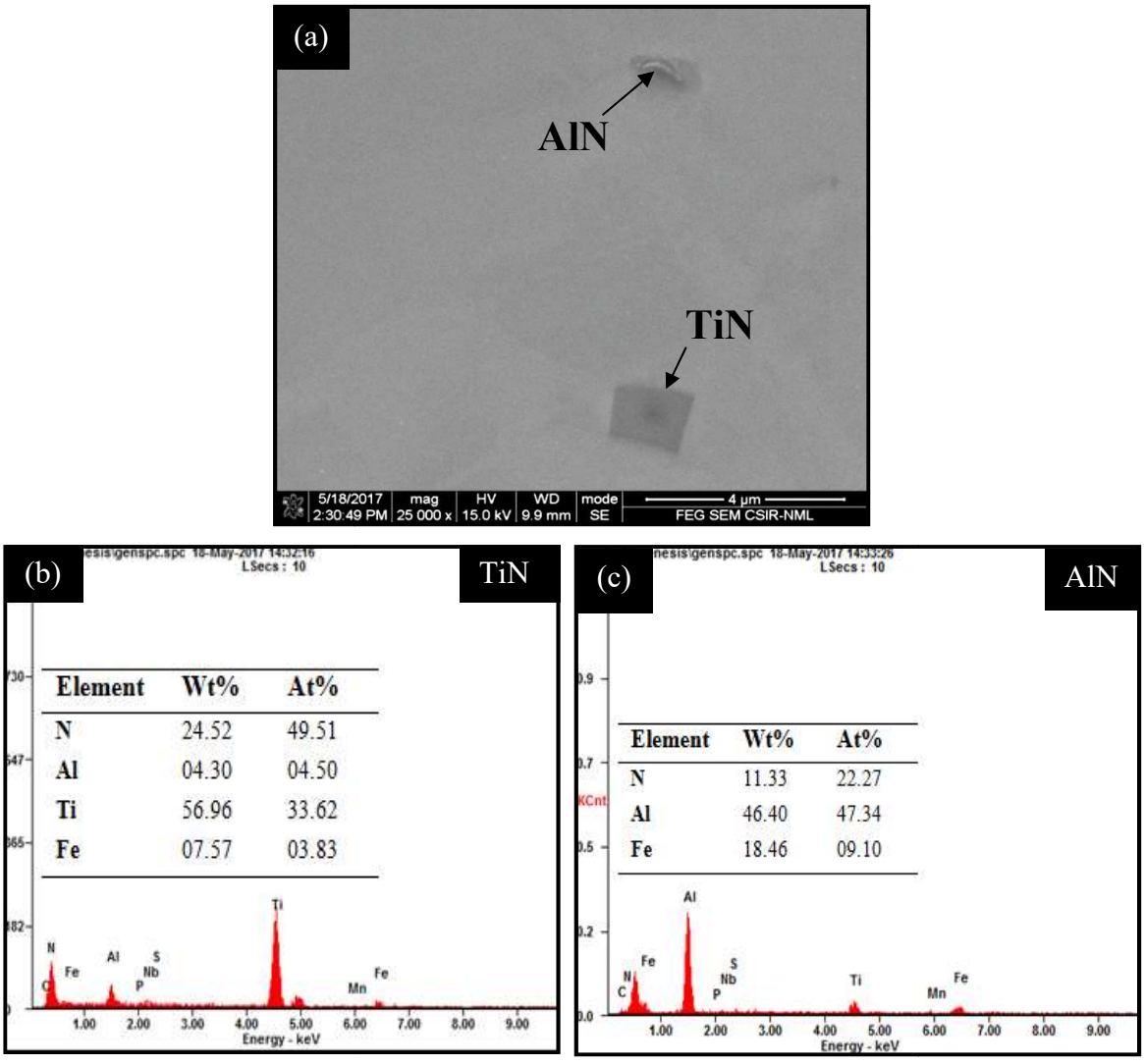

Figure 4.12: Results of SEM-EDS analysis of C4 specimen subjected to CAL-3 process (a) SEM micrograph showing TiN and AlN precipitates, and EDS spectrographs showing (b) TiN and (c) AlN precipitates.

Further, the second CAL process (CAL-4) conducted at a relatively higher temperature of 830 ℃ led to complete recrystallization but resulted in appearance of Lüders bands as is evident from the tensile stress-strain curve shown in Fig. 4.8b. Results of SEM-EDS analysis shown in Fig. 4.13(a–f) clearly exhibited formation of TiN precipitates in abundance while formation of AlN precipitates was almost negligible. Thus, increasing the annealing temperature (to 830 ℃) had an adverse effect on precipitation kinetics resulting in lesser tendency of Al in consuming N (for the formation of AlN). Almost entire Ti was used in formation of TiN, and so availability of Ti for TiC formation was less in this case. Moreover, TiS precipitation was also frequently observed, which further limited the formation of TiC precipitates. All this resulted in incomplete stabilization of carbon and thus formation of Lüders bands.

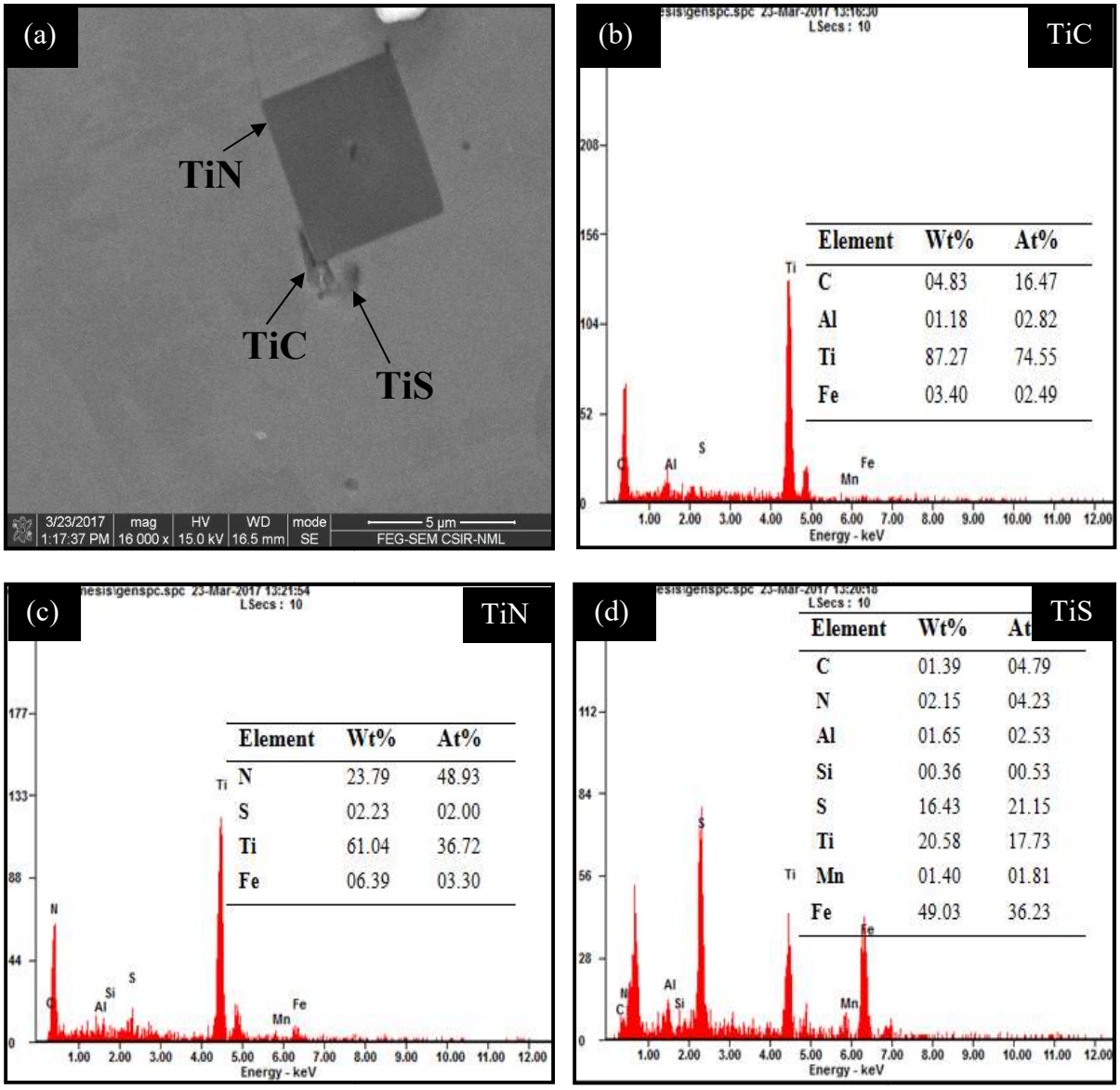

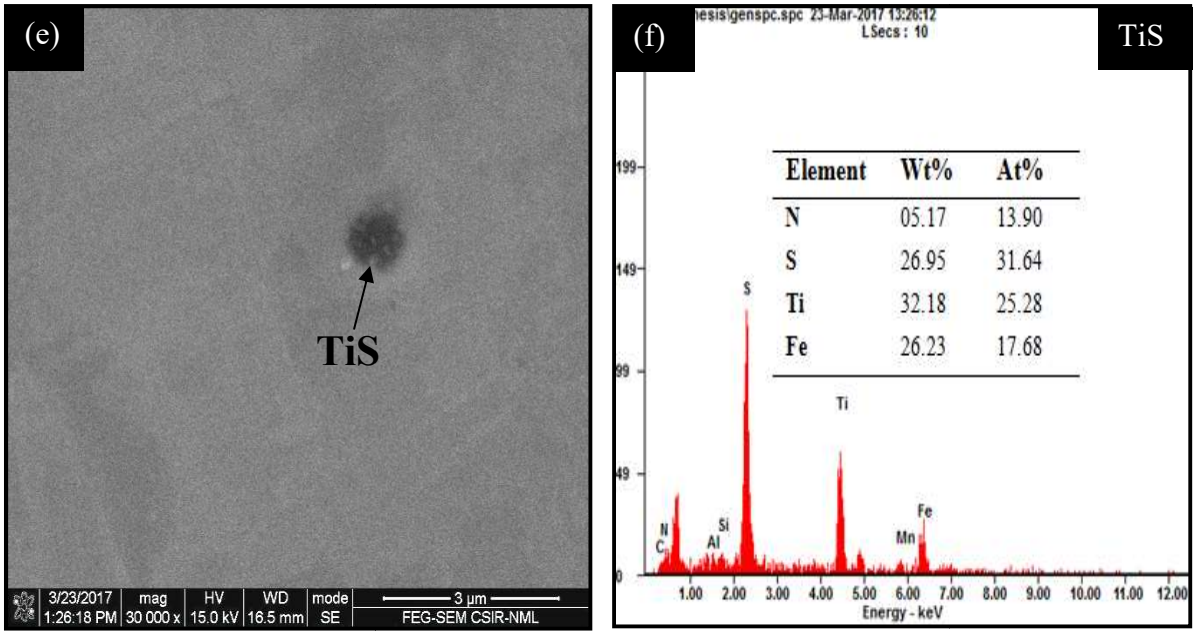

Figure 4.13: Results of SEM-EDS analysis of C4 specimen subjected to CAL-4 process showing precipitate formation of type (a–d) TiC, TiN, TiS and (e–f) TiS.

Therefore, the above results showed that C4 composition can be effective with BAF and not with CAL process. This composition did not provide desirable results with CAL process in stabilizing interstitial element.

The mechanical properties of C4 IFHS specimens subjected to various BAF processes are shown in Table 4.5. It can be observed that BAF process provide good combination of mechanical properties for C4 IFHS composition. BAF process conducted at a higher temperature resulted in decrease in yield strength but increase in value of Lankford parameter. BAF at 710 ^{o}C (BAF-5) appear to be an optimum process condition for C4 composition, as this process provided best combination of properties (YS= 190 MPa; $\bar{r}$-value= 1.57; Δr-value= 0.25).

Table 3.5: Mechanical properties obtained in C4 steel specimens after BAF processes.

Batch process	Yield Strength (MPa)	r̄- value	Δr
BAF-3	203	1.25	-0.27
BAF-4	190	1.57	0.25
BAF-5	160	1.95	-0.82

The detail of various precipitates (type, morphology, average size, and frequency of occurance) observed in the four IFHS compositions subjected to different annealing processes is summarized in Table 4.6 for easy references.

Table 4.6: Detail of precipitates observed in different IFHS compositions after various annealing processes.

IFHS Composition	Type of precipitates	Morphology of precipitates	Average size	Frequency of occurrence
C1	(Ti+Mn)S	Irregular	0.2–1 μm	High
	FeTiP	Irregular	<1 μm	Low
C2	TiN	Rectangular	1–3 μm	High
	TiC	Irregular	1–2 μm	High
	AlN	Globular	0.2–0.5 μm	Low
	TiS	Globular	0.2–1.5 μm	High
C3	TiN	Rectangular	0.3–1.5μm	High
	(Al+Nb)N	Needle	2 μm	Only one
	MnS	Globular	0.5–1μm	High
	FeTiP	Globular	15–25 nm	Low
C4	AlN	Rectangular, Needle	0.5–5 μm	High
	TiN	Square	1.5–5μm	High
	TiS	Globular	0.2–0.8μm	High
	TiC	Irregular	0.5–3 μm	High

Chapter 5

Conclusions

5.1 General

This chapter reveals the major findings and main conclusions obtained from the results of the present research work. These findings and conclusions provide solution to the one of the problems related to industrial processing of IFHS steels i.e. Lüders bands formation. This chapter concludes the major results in a systematic manner and also provides future scope of the research.

5.2 Major results and findings

5.2.1 Results for C1 composition

- C1 based IFHS steel composition contained excess Ti content as was theoretically required for complete stabilization of all interstitials elements (C, N), but still this composition showed Lüders strain or yield point elongation (YPE) of magnitudes of greater than 1% during tensile deformation after annealing (through industrially followed BAF and CAL processes). Hence, this composition is not considered good for processing of automobile panels and components due to presence of Lüders bands which tends to deteriorate the surface finish of material.
- The main precipitates observed by SEM-EDS characterization in this composition were (Ti+Mn)S and FeTiP. No TiC precipitate was observed. The formation of Lüders bands was mainly due to the incomplete stabilization of interstitial element carbon (C). The stabilizing element Ti mainly got consumed in the formation of TiS and FeTiP precipitates and hence no TiC precipitate was observed. As a result, Lüders band problems occured in this composition.

5.2.2 Results for C2 composition

- C2 based IFHS steel composition contained excess of both Ti and Nb elements as were theoretically required for complete stabilization of all interstitial elements and showed no Lüders strain or yield point elongation (YPE) during tensile deformation after BAF and CAL processes. As a result, this steel did not suffer from Lüders bands problem.

- The main precipitates observed in this composition included TiN, TiC, AlN, and TiS. As a result, complete stabilization of C took place and hence no Lüders bands formation occurred. Though this composition does not show surface finish problems, but still is not rendered useful for industrial applications because of its low strength (125–150 MPa). The low yield strength was because of lack of adequacy of solid solution strengthening elements in this composition.

5.2.3 Results for C3 composition

- C3 based IFHS steel composition contained slightly deficient amount of both Ti and Nb as were theoretically required for complete stabilization of all interstitial elements and showed Lüders strain or yield point elongation (YPE) of greater than 1% during tensile deformation after annealing (through each BAF and CAL process).
- The main precipitates observed in this composition were TiN, (Al+Nb)N, MnS, and FeTiP during SEM and EDS characterization. No TiC precipitate was observed in this composition. Mainly FeTiP precipitate formation scavanged most of the Ti element with it and hence less Ti was available for the formation of TiC precipitates. Further, formation of TiN took the remaining Ti and thus TiC precipitates were not formed. Also, the formation of TiN formation took remaining Ti and hence no TiC precipitates was observed and Lüders bands problem was present in this composition.

5.2.4 Results for C4 composition

- C4 based IFHS composition contained Ti in excess and Nb in deficient amount as was theoretically required for complete stabilization of all interstitial elements and also contained high Al content than other compositions and showed no Lüders strain or yield point elongation (YPE) during tensile deformation after any BAF process, but showed presence of Lüders strains during tensile deformation after annealing through CAL cycle.
- The main precipitates observed in this composition were AlN, TiN, TiS, and TiC. During BAF processes, AlN was mainly formed but TiN was formed in limited amount. This made Ti element available for TiC formation. However, in case of CAL process, AlN dissolved due to high temperature and TiN formation again started, which decreased availability of Ti element for formation of TiC and hence Lüders Bands formation. Thus, for this composition, BAF process routes provided better results as compared to CAL processes. This composition is mainly used in BAF processes only due to Lüders Bands problem in CAL processes.

- The best combination of properties (YS= 190 MPa; $\bar{r}$-value= 1.57; Δr-value= 0.25) obtained from this composition after BAF process at 710 ℃ with heating rate of 60 ℃/h and cooling by furnace.

5.3 Major conclusions

The present work brought forth a new research finding that IFHS steels which are generally reported not to show Lüders bands formation during tensile deformation can show discontinuous yielding behaviour and hence Lüders bands formation under tensile deformation depending upon the chemical composition and precipitation behaviour of steel during industrially used annealing treatment.

The main conclusions to be drawn from the present work are as follows:

a) For a particular steel composition subjected to a given annealing cycle, the presence/absence of Lüders bands is strongly dependent on the precipitation behaviour of steel during heat treatment. It was observed that steel compositions in which TiC precipitates was either absent or formed in limited quantity showed problem of Lüders bands formation. This situation occurred either because of lack of Ti content in steel or when Ti available in the steel composition extensively formed precipitates with non-interstitial atoms (viz. FeTiP, TiS, etc.) rather than forming precipitates of interstitials viz. TiC, TiN.

b) The presence of Al in steel composition showed a profound effect on precipitation behavior and mechanical properties of the processed IFHS steels. High Al content in IFHS steel resulted in preferential formation of AlN precipitates over TiN precipitates. As a result, Ti present in the steel remained available for formation of TiC precipitates, thus resulting in locking of free C atoms and hence elimination of Lüders bands.

c) Though chemical composition of IFHS steels and their precipitation behaviour during heat treatment emerged as the significant factors affecting Lüders bands formation and mechanical properties of IFHS steels, but complete ferrite recrystallization (during annealing) along with these factors is important for good combination of surface finish-mechanical properties in IFHS steels.

5.4 Future scope of the present research

The present research is very helpful in deciding the chemical composition and annealing process parameters for eliminating the problem of Lüders bands formation in IFHS steels. This research work has some limitations also, which can be worked upon in future. First of

all, the frequency of occurrence of various precipitates in a given composition-annealing route was determined by repeated observations on a sample at various locations. However, a more advanced technique can be used in future work for determining the volume fraction of various precipitates. Secondly, the traditional marking method was used for measurement of Lankford parameter (r_m value) in the present work. Ultrasonic measurement is available which gives direct measurement of r_m value. So, ultrasonic measurement of r_m value is recommended for future work. Next, as Lüders bands formation deteriorates the surface finish, there is a need to measure the surface roughness values after annealing cycles.

References

1. P.K. Mallick, Materials, Design and Manufacturing for Lightweight Vehicles, 1st ed., Woodhead Publishing Limited, 2010.
2. B. Bhattacharya, Physical Metallurgy of Interstitial Free Steels, A monograph, Tata Steel Press, 2009.
3. S. Hoile, Processing and properties of mild interstitial free steels, Materials Science and Technology 16(10) (2013) 1079–1093.
4. Engineering & Manufacturing Services for Automotive Products, Rear Floor Pan, http://emsautomotive.com/index.php?route=product/product&product_id=149, (accessed on 26/11/2016).
5. NK Group Innovation, Service and Quality, Car Soundproofing Full Kit, http://www.nkgroup.co.uk/product/car-soundproofing-full-kit-no-engine-blanket/, (accessed on 26/11/2016).
6. H. Takechi, Metallurgical Aspects on Interstitial Free Sheet Steel from Industrial Viewpoints, ISIJ International 34(1) (1994) 1–8.
7. R.I.L. Guthrie, J.J. Jonas, Steel Processing Technology, ASM International 1 (1990) 107–127.
8. N.D.A. Sardinhaa, I.C.D. Santosa, B.V. Andradea, R.A. Botelhoa, R.V.D. Oliveiraa, S.B. Diniza, A.D.S. Paula, L.P. Brandao, Mechanical properties and crystallographic texture of symmetrical and asymmetrical cold rolled IF steels, Materials Research 19(5) (2016) 1042–1048.
9. R.K. Ray, J.J. Jonas, R.E. Hook, Cold rolling and annealing textures in low carbon and extra low carbon steels, International Materials Reviews 39(4) (1994) 129–172.
10. K. Banerjee, Evaluation of annealing texture in IF and EDD steel sheets, Materials and Manufacturing Processes 22(4) (2007) 462–468.
11. S.K. Paul, Effect of anisotropy on ratcheting: An experimental investigation on IFHS steel sheet, Materials Science and Engineering A 538 (2012) 349–355.
12. I. Mohanty, S. Datta, D. Bhattacharjee, Composition–processing–property correlation of cold-rolled IF steel sheets using neural network, Materials and Manufacturing Processes 24(1) (2008) 100–105.
13. D.W. Beardsmore, J.Q. Fonseca, J. Romero, C.A. English, S.R. Ortner, J. Sharples, A.H. Sherry, M.A. Wilkes, Study of Lüders phenomena in reactor pressure vessel steels, Materials Science and Engineering A 588 (2013) 151–166.
14. D. Akama, N. Nakada, T. Tsuchiyama, S. Takakia, A. Hironakac, Discontinuous yielding induced by the addition of nickel to interstitial-free steel, Scripta Materialia 82 (2014) 13–16.
15. University of Cambridge, Plane stress, https://doitpoms.admin.cam.ac.uk/tlplib/metal-forming-3/plane_stress.php, (accessed on 16/6/2017).
16. W. Hoffelner, Materials for Nuclear Plants: From Safe Design to Residual Life Assessments, Springer Science & Business Media, 2012.

17. J. Shi, D. Cui, On optimizing batch annealing for the production of IF steels, Materials and Manufacturing Processes 18(1) (2003) 51–66.

18. J. Jia, W. Zhu, X. Song, Z. Yuan, Precipitation behavior of FeTiP in Ti-added interstitial free high strength steels, Journal of Iron and Steel Research International 23(7) (2016) 692–698.

19. H. Kang, C.I. Garcia, K. Chin, A.J. Deardo, Effect of aluminum content on the mechanical properties of dual stabilized Ti–Nb interstitial free high strength steel (IF-HSS), ISIJ International 47(3) (2007) 486–492.

20. S.K. Nath, G.P. Chaudhari, M. Singla, Effect of thermomechanical treatment on the microstructure and mechanical properties of an IF steel, ASM International 19 (2010) 1325–1329.

21. S. Gao, M. Chen, M. Joshi, A. Shibata, N. Tsuji, Yielding behavior and its effect on uniform elongation in IF steel with various grain sizes, Journal of Materials Science 49(19) (2014) 6536–6542.

22. D. Akama, N. Nakada T. Tsuchiyama, S. Takakia, A. Hironakac, Discontinuous yielding induced by addition of nickel to interstitial free steel, Scripta Materialia 82 (2014) 13–16.

23. A. N. Bhagat, Avtar Singh, N. Gope, T. Venugopalan, Development of cold-rolled high-strength formable steel for automotive applications, Materials and Manufacturing Processes 25 (2010) 202–205.

24. R. Rana, W. Bleck, S.B. Singh, O.N. Mohanty, Development of high strength interstitial free steel by copper precipitation hardening, Materials Letters 61(2007) 2919–2922.

25. J.S. Rege, M.Hua, C.I. Garcia, A.J. Deardo, The segregation behavior of phosphorus in Ti and Ti-Nb stabilized interstitial-free steels, ISIJ International 40(2) (2000) 191–199.

26. P. Ghosh, C. Ghosh, R.K. Ray, Precipitation in interstitial free high strength steels, ISIJ International 49(7) (2009) 1080–1086.

27. S. Ghosh, A.K. Singh, S. Mula, P.Chanda, V. V. Mahashabde, T.K. Roy, Mechanical properties, formability and corrosion resistance of thermomechanically controlled processed Ti-Nb stabilized IF steel, Materials Science & Engineering A 684 (2017) 22–36.

28. R. Zheng, R. Song, W. Fan, Effects of annealing cooling rates on mechanical properties, microstructure and texture in continuous annealed IF steel, Journal of Alloys and Compounds 692 (2017) 503–514.

29. W. Guo, Z. Wang, Y. Li, N. Xu, J Shi, Effect of phosphorus content on properties of warm-rolled interstitial-free steel sheets, Metallography, Microstructure, and Analysis 2(4) (2013) 249–256.

30. S. Majumdar, D. Bhattacharjee, K.K. Ray, Mechanism of fatigue failure in interstitial-free and interstitial-free high-strength steel sheets, Scripta Materialia 64 (2011) 288–291.

31. P. Ghosh, R.K. Ray, D. Bhattacharjee, Determination of the crystal structure of FeTiP-type precipitates in a few interstitial-free high-strength steels, Scripta Materialia 57 (2007) 241–244.

32. P. Ghosh, R.K. Ray, C. Ghosh, D. Bhattacharjee, Comparative study of precipitation behavior and texture formation in continuously annealed Ti and Ti + Nb added interstitial-free high-strength steels, Scripta Materialia 58 (2008) 939–942.

33. R. Saha, R.K. Raya, D. Bhattacharjee, Attaining deep drawability and non-earing properties in Ti+Nb interstitial-free steels through double cold rolling and annealing, Scripta Materialia 57 (2007) 257–260.
34. C. Capdevila, V. Amigo, F.G. Caballero, C.G.D. Andres, M.D. Salvador, Influence of microalloying elements on recrystallization texture of warm-rolled interstitial free steels, Materials Transactions 51(4) (2010) 625–634.
35. J.Y. Choi, B.S. Seong, S.C. Baik, H.C. Lee, Precipitation and recrystallization behavior in extra low carbon steels, ISIJ International 42(8) (2002) 889–893.
36. X. Song, Z. Yuan, J. Jia, D. Wang, P. Li, Z. Deng, Effect of phosphorus grain boundaries segregation and precipitations on mechanical properties for Ti-IF steel after recrystallization annealing, Journal of Materials Science & Technology 26(9) (2010) 793–797.
37. K.P. Ajit, A. Gautam, P.K. Sarkar, Ductile behaviour characterization of low carbon steel: a CDM approach, Journal of Mechanical Engineering 62(5) (2016) 299–306.
38. S. Gao, A. Shibata, M. Chen, N. Park, N. Tsuji, Correlation between continuous/discontinuous yielding and Hall-Petch slope in high purity iron, Materials Transactions 55(1) (2014) 69–72.
39. J. R. Davis (Ed.), Alloying: understanding the basics, ASM International, 2001.
40. L.E. Samuels, Light microscopy of carbon steels, ASM International, 1999.
41. F.E. Sesen, O.S. Ozgen, A study of electrochemical boronizing of an IF steel, Sigma Journal of Engineering and Natural Sciences 32 (2014) 334–337.
42. D.K. Nayak, R.K.Palai, To study the effect of strain rate on tensile properties and high cycle fatigue behaviour of IF steel, B. Tech Project Report, National Institute of Technology, Rourkela, 2013.
43. R.K. Ray, P. Ghosh, D. Bhattacharjee, Effects of composition and processing parameters on precipitation and texture formation in microalloyed interstitial free high strength (IFHS) steels, Materials Science and Technology 25(9) (2009) 1154–1167.
44. R. Yoda, I. Tsukatani, T. Inoue, T. Saito, Effect of chemical composition on recrystallization behavior and $\bar{r}$-value in Ti-added ultra low carbon sheet steel, ISIJ International 34(1) (1994) 70–76.
45. K. Banerjee, Physical metallurgy and drawability of extra deep drawing and interstitial free steels, Intech Open Access Publisher, 2012.
46. R. Pradhan, Metallurgy of Vacuum-degassed Steel Products, The Minerals, Metals and Materials Society, Warrendale, PA, 2011.
47. K. Banerjee, T. Venugopalan, Heating rate effect on the drawability of titanium stabilized interstitial free high strength steel, Tata Steel Report, 1–24.
48. J. Zhang, Y. Cao, G. Jiang, H. Di, Effect of annealing temperature on the precipitation behavior and texture evolution in a warm-rolled P-containing interstitial-free high strength steel, Acta Metallurgica Sinica (English Letters) 27(3) (2014) 395–400.
49. G. Anand, A. Sinha, P.P. Chattopadhyay, On the plasticity of interstitial-free steel subjected to cryogenic rolling followed by annealing, Materials and Manufacturing Processes 28(3) (2013) 242–248.

50. P. Ghosh, C. Ghosh, R.K. Ray, Thermodynamics of precipitation and textural development in batch-annealed interstitial-free high-strength steels, Acta Materialia 58 (2010) 3842–3850.
51. P. Ghosh, R.K. Ray, B. Bhattacharya, S. Bhargava, Precipitation and texture formation in two cold rolled and batch annealed interstitial-free high strength steels, Scripta Materialia 55 (2006) 271–274.
52. R.K. Ray, P. Ghosh, An overview on precipitation and texture formation in IF and IFHS steels during processing, Materials and Manufacturing Processes 25 (2010) 195–201.
53. D. Llewellyn, R. Hudd, Steels: Metallurgy and Applications, Butterworth-Heinemann, 1998.
54. R.K. Ray, A. Haldar, Texture development in extra low carbon (ELC) and interstitial free (IF) steels during warm rolling, Materials and Manufacturing Processes 17(5) (2002) 715–729.
55. R. Rana, S.B. Singh, Automotive Steels: Design, Metallurgy, Processing and Applications, Elsevier Science & Technology, 2016.
56. W.C. Jeong, Role of aluminium in hot-rolled ultra-low carbon Nb-interstitial-free steels, Metallurgical and Materials Transactions A 37(12) (2006) 3737–3739.
57. A.H. Cottrell, B.A. Bilby, Dislocation theory of yielding and strain ageing of iron, Proceedings of the Physical Society A 62 (1949) 49–62.